学位論文

Theoretical Study on Universal Few-Body Effects in Ultracold Atomic Gases

（冷却原子気体における普遍的な少数多体効果の理論研究）

平成２９年１２月 博士（理学） 申請

東京大学大学院理学系研究科
物理学専攻

吉田　周平

Abstract

Universality is a crucial concept in modern physics, which allows us to describe phenomena without referring to microscopic details of systems. The unitary Fermi gas is a prime example, where universal relations among physical observables and a universal equation of state have been developed and studied in detail. In this thesis, we extend these notions beyond the paradigm of the unitary Fermi gas and investigate universal effects of few-body correlations in resonantly interacting ultracold atomic gases. In particular, we discuss (i) universal relations in a spinless Fermi gas with an anisotropic p-wave resonance and (ii) universality of the few-body spectra and the ground-state properties of an impurity-boson system.

Firstly, we investigate the universal relations in a spinless Fermi gas with an anisotropic p-wave resonance. We show that the high-momentum distribution and the short-range density-density correlation have characteristic power laws, whose coefficients define the p-wave contact tensor. We derive the adiabatic sweep theorem, which relates the p-wave contact tensor to the total energy. We also discuss the experimental scheme to measure the p-wave contact tensor and test our results.

Secondly, we examine the ground states and lower excited states of an impurity resonantly interacting with one, two, and three non-interacting bosons. We calculate the energy spectra of this few-body system with two different models. The overall scale of length depends on the models. However, we find that once we fix the three-body parameter, which is a critical scattering length of the ground-state Efimov trimer, the few-body spectrum is independent of a specific choice of the models. This finding is corroborated by comparing our numerical results with the one obtained by Ardila and Giorgini [Phys. Rev. A **92**, 033612 (2015)].

Thirdly, we investigate the case in which the mass of an impurity is infinite. In this limit, we show that the model of a Feshbach resonance can be mapped to a bosonic extension of Anderson's single impurity model, which can be used to analytically solve the three-body problem. We find that the ground-state energy with a Feshbach resonance is drastically different from that in a potential-interaction system, and that the former approaches the latter logarithmically as the unitarity limit is taken. We argue

that this logarithmic correction is a universal consequence of an effective three-body repulsion.

Lastly, we address the universality of the ground-state properties of a Bose polaron, which is an impurity immersed in a weakly interactinng Bose-Einstein condensate. We employ a variational wave function that takes into account three Bogoliubov excitations on top of the background Bose-Einstein condensate. By calculating the ground-state energy with two different models and comparing the results with those obtained by Ardila and Giorgini [Phys. Rev. A **94**, 063640 (2016)], we argue that the ground-state energy is a universal function of the three-body parameter, even when the density is high enough to smear out well-defined Efimov trimers. We also calculate other observables and discuss their universality. In particular, we find that the quasi-particle residue is strongly suppressed in the limit of $a_{\mathrm{B}} \to 0$, where the background Bose gas is non-interacting. This is consistent with the perturbation theory, in which an infrared divergence leads to the vanishing residue. On the other hand, both the variational calculation and the perturbative calculation show that the residue is finite for $a_{\mathrm{B}} > 0$.

Acknowledgements

This thesis would not have been possible without the help and support of many people.

I would like to express my gratitude to my supervisor, Professor Masahito Ueda, for his guidance and sincere encouragement over the period of my PhD program. He was a great teacher; he taught me a lot of things, from the way of a good scientist to a key to happy married life. I would also like to thank my secondary supervisors, Professor Tetsuo Hatsuda and Professor Junji Yumoto, for valuable advice on my study, and sometimes on job hunting. They also organized meetings where I could learn studies of other students.

Much of the work in this thesis started during my stay at Quantum Matter group in Monash University, where I greatly benefited from fruitful collaboration with the group members. I am deeply grateful to Professor Meera M. Parish and Dr. Jesper Levinsen for letting me stay at Monash University and giving me helpful advice and warm encouragement. I also appreciate fruitful discussions with Dr. Shimpei Endo and Dr. Zheyu Shi, whose profound knowledge and thought on physics were extremely helpful. Mr. Thomas Kirk kindly gave me useful advice on numerical techniques, and also taught me a proper way of making a cup of milk tea that makes life more enjoyable.

I would like to thank Dr. Luis A. Peña Ardila for the quantum Monte Carlo data of his Bose polaron study. I gratefully acknowledge fruitful discussions with Professor Shunsuke Furukawa, Professor Yusuke Nishida, and Dr. Yusuke Horinouchi. I also appreciate discussions and feedback offered by the thesis committee members, Professor Masaki Oshikawa, Professor Hosho Katsura, Professor Naoki Kawashima, Professor Yoshio Torii, and Professor Kosuke Yoshioka.

I wish to thank my parents, Minoru and Chie, for their supports and understanding, which were truly indispensable to complete the PhD course. My wife, Saki, has supported me and has been a great source of motivation for me; I thank her always.

Finally, I greatly acknowledge financial supports from the Japan Society for the Promotion of Science through Program for Leading Graduate Schools "Advanced Leading Graduate Course for Photon Science" (ALPS) and Grant-in-Aid for JSPS Research Fellow (JPSJ KAKENHI Grant No. JP16J06706). I would like to thank the ALPS for covering my visit to Monash University through its overseas dispatch program.

List of Publications

This thesis is based on the following publications:

1. Shuhei M. Yoshida and Masahito Ueda, *p-wave contact tensor: Universal properties of axisymmetry-broken p-wave Fermi gases*, Physical Review A **94**, 033611 (2016).

2. Shuhei M. Yoshida, Shimpei Endo, Jesper Levinsen, and Meera M. Parish, *Universality of an impurity in a Bose-Einstein condensate*, accepted for publication in Physical Review X [preprint, arXiv:1710.02968].

3. Shuhei M. Yoshida, Zheyu Shi, Jesper Levinsen, and Meera M. Parish, *Static impurity in a Bose-Einstein condensate*, in preparation.

The following publication is not directly related to this thesis:

4. Shuhei M. Yoshida and Masahito Ueda, *Universal High-Momentum Asymptote and Thermodynamic Relations in a Spinless Fermi Gas with a Resonant p-Wave Interaction*, Physical Review Leters **115**, 135303 (2015).

Contents

Chapter 1

Introduction

1.1 Universality in quantum few-body systems

Few-body problems have played fundamental roles since the early days of classical and quantum mechanics. For example, studies of the celestial few-body motion fostered the development of classical mechanics and its derivative areas. Kepler's laws, which concerns the two-body problem of a planet and the sun, finally led Issac Newton to the discovery of the law of universal gravitation. The gravitational three-body problem has also been a rich source of concepts in dynamical systems theory. On the other hand, the Coulombic few-body problems, namely atomic and molecular systems, drove the development of quantum mechanics.

In quantum mechanics, few-body systems can display emergent *universality*, which is absent in classical few-body problems. Classical particles can interact with each other only when two particles are within the range of an interaction, and their motion follows the detailed structure of the interaction potential. In quantum mechanics, on the other hand, owing to the wave nature of matter, a particle can affect the motion of another particle far beyond the interaction range. When this happens, the particle motion becomes insensitive to microscopic details of an interaction because in most of the time particles are outside the interaction range and do not feel the interaction potential itself.

A two-body problem already provides a nontrivial example. For a short-range potential[1], unless the two particles are identical fermions, two-particle collisions are predominantly of the s-wave type, which has the scattering amplitude with the following

[1] A "short-range" potential need not be exponentially decaying in the discussions below. For example, atomic interactions have the long-range tail of the van der Waals potential C/r^6. In that case, the function $r(k^2)$ introduced below has non-analyticity, which is, however, irrelevant for the low-energy physics [1].

low-energy expansion [1, 2]:

$$f(k) = -\frac{1}{a^{-1} + ik + k^2 r(k^2)}, \tag{1.1}$$

where k is the magnitude of the incoming momentum, a is the s-wave scattering length, and $r(k^2)$ is a real function of k^2, which is analytic at $k^2 = 0$. The s-wave scattering length can, in general, take any real value, depending on interactions. Suppose that a is positive and much larger than the range of the interaction. Then the scattering amplitude $f(k)$ has a pole at $k \simeq ia^{-1}$, regardless of the detailed form of $r(k^2)$. This implies that there is a two-body bound state, whose energy is $-\hbar^2/2m_{\rm r}a^2$, where $m_{\rm r}$ is the reduced mass of the two particles, and that its radius a is much larger than the radius of the interaction potential. Remarkably, the energy of the shallowest dimer is determined by the s-wave scattering length a and is independent of any other details of the interaction when a is large. The low-energy scattering also becomes universal as the scattering cross section can be approximated by

$$\sigma(k) \equiv |f(k)|^2 \simeq \frac{1}{a^{-2} + k^2}. \tag{1.2}$$

Of particular interest is the limit of $|a| \to \infty$, which is called the *unitarity limit*. Here, the scattering cross section is

$$\sigma(k) = \frac{1}{k^2}, \tag{1.3}$$

which saturates the constraint imposed by the unitarity of the S-matrix [1]. This limit realizes the strongest possible interaction, which is clearly scale-invariant and independent of any microscopic details.

Three-body systems at the unitarity limit are even more nontrivial. Vitaly N. Efimov showed for three identical bosons and three distinguishable particles with arbitrary mass ratios that there are an infinite number of three-body bound states if at least two of the three pairwise interactions are at the unitarity limit, and that they dissociate into three atoms at a negative scattering length and into a pair of a dimer and an atom at a positive scattering length [3–6][2]. The Efimov effect in multicomponent systems was also discussed by Amado and Noble almost simultaneously [7]. The presence of the bound states indicates a breakdown of the scale invariance, which we have at the two-body level for unitarity-limited interactions. However, Efimov found that there is a remnant discrete scale invariance. In particular, the binding energy of the nth-excited trimer for

[2]Although it is not explicitly mentioned in Ref. [6], the discussion there also includes the possibility of the Efimov trimers in the system of one light particle that resonantly interacts with two heavy identical fermions.

large n is written as

$$E_n = \lambda^{-2n} E_0, \tag{1.4}$$

where λ is determined by the configuration of the resonating pairs and the mass ratios, and is independent of microscopic details of interactions. This universal three-body phenomenon has driven much theoretical effort to investigate a diversity of universal few-body clusters [8–10] such as two-component fermion systems [11–15], four or more identical boson systems [16–21], one particle interacting with three or more identical bosons [22, 23], three identical fermions in three [24, 25] and two dimensions [26–30].

Traditionally, these universal few-body phenomena have been investigated mainly in nuclear physics. Efimov originally had the ^{12}C nucleus (or three α particles) and three ^{4}He atoms in mind [3]. Today, however, ultracold atomic gases offer ideal experimental test beds for studies on the universal few-body and many-body physics. As we detail in Chapter 2, one can control the s-wave scattering length to an arbitrary value by using a magnetic Feshbach resonance [31–34]. This has enabled us to study universal phenomena that emerge near the unitarity limit. One can also make various mass ratios of particles by preparing mixtures of different atomic species. This unprecedented controllability of ultracold atomic gases enables us to systematically examine a wide variety of few-body phenomena. The Efimov effect has been experimentally explored in various setups. For identical boson systems, not only the resonance of the Efimov trimer [35–37], but also those associated with a tetramer [38, 39] and a pentamer [40] have been experimentally observed. Experimentalists have also investigated mixtures of different atomic species [41–45] and of atoms in different spin states [46–48].

1.2 Universality in the unitary Fermi gas

The universality in few-body systems has huge implications for many-body physics. A prime example is the unitary Fermi gas, which is a gas of spin-1/2 fermions with a unitarity-limited interaction between a spin-↑ particle and a spin-↓ particle and no interaction between the same spin particles. Here, let us focus on the mass-balanced case, where the ↑-particle and the ↓-particle have the same mass. Then no three-body subsystem of the unitary Fermi gas has Efimov states [6]. The unitary few-body Fermi systems with more than three particles have also been examined, and to date, breaking of the scale invariance has not been found [9, 10]. These evidence suggests that the unitary Fermi gas has a strictly scale-invariant interaction, which saturates the unitarity bound of the scattering cross section.

One of the most important consequences of the scale invariance is the universal thermodynamics [49]. Owing to the absence of any interaction length scale, the free energy is completely determined only by the number of particles N, the volume V, the temperature times the Boltzmann constant $k_{\mathrm{B}}T$, the mass of particles m, and Planck's constant $\hbar$. The dimensional analysis then allows one to write down the following expression of the free energy:

$$F(N, V, k_{\mathrm{B}}T; m, \hbar) = \frac{3}{5}\varepsilon_{\mathrm{F}} N f\left(\frac{k_{\mathrm{B}}T}{\varepsilon_{\mathrm{F}}}\right), \tag{1.5}$$

where $\varepsilon_{\mathrm{F}} \equiv \frac{\hbar^2}{2m}\left(3\pi^2 N/V\right)^{2/3}$ is the Fermi energy and $f(x)$ is a universal dimensionless function[3]. Once $f(x)$ is determined, either theoretically or experimentally, all the thermodynamics quantities are derived from this single function and its derivative. Also the ground-state properties are determined by a set of dimensionless numbers, among which $\xi \equiv f(0)$ is particularly called the Bertsch parameter [50, 51].

Another important aspect of the universality in the unitary Fermi gas is a set of universal relations that relate short-range correlations to thermodynamic properties [52–60]. Such relations do not rely on perturbation expansions, and hold true even in the strongly correlated regime. Moreover, they are very general; a fermionic system in the unitarity regime is constrained by those relations whether it is a few-body or many-body system, in the superfluid or normal fluid phase, at zero or finite temperatures. For example, the density-density correlation function diverges as

$$g_{\uparrow\downarrow}(\boldsymbol{r}) \equiv \langle \hat{n}_{\uparrow}(\boldsymbol{r})\hat{n}_{\downarrow}(0)\rangle \simeq \frac{16\pi^2 C}{V r^2} \tag{1.6}$$

for $r \ll k_{\mathrm{F}}^{-1}$, where k_{F} is the Fermi wave number, $\hat{n}_{\sigma}$ is the density operator for the spin-σ particles, V is system's volume, and C is Tan's contact, which plays a central role in the universal relations. The origin of this divergence is the one that appears in two-body subsystems of the unitary Fermi gas. One can show [61–63] that a relative wave function of a two-body system composed of an $\uparrow$-particle and a $\downarrow$-particle is

$$\psi(\boldsymbol{r}) = \frac{1}{kr} - \frac{1}{ka} + O(kr), \tag{1.7}$$

for $r/r_0 \ll kr \ll 1$, where $k \equiv \sqrt{m|E|/\hbar^2}$, a is the s-wave scattering length, and r_0 is the range of an interaction. For the unitarity regime, where $ka \gtrsim 1$, the first term in $\psi(\boldsymbol{r})$ dominates over the other terms, leading to the r^{-2}-divergence in the density-density correlation. The singularity in Eq. (1.6) mirrors this short-range behavior in the two-body

[3]The prefactor 3/5 is chosen in order that $f(0) = 1$ for the free Fermi gas at zero temperature.

subsystems in the many-body unitary Fermi gas, and Tan's contact C encapsulates all the other many-body effects. The momentum distribution [52] and dynamical quantities such as the radio-frequency spectrum [64–67], the dynamic structure factor [68–71], and the viscosity spectral function [69, 72], have similar factorization of power-low behaviors originating from two-body physics and many-body effects represented by the contact. The contact is also related to thermodynamic quantities. A representative example is the adiabatic sweep theorem [53]:

$$C = \frac{4\pi m}{\hbar^2} \frac{\partial E}{\partial(-1/a)}. \tag{1.8}$$

This means that the contact represents the response to the change of the s-wave scattering length. This interpretation is consistent with Eq. (1.6). As the interaction is short-ranged, only pairs of two particles that are close to each other are responsible for the energy change when the s-wave scattering length is shifted. Equation (1.6), on the other hand, clearly shows that the number of such small pairs is characterized by C. These universal relations have been extended to bosonic systems [73–75], Bose-Fermi mixtures [73], and lower dimensions [58, 59, 76–78] with an s-wave resonance. They are also extended to p-wave [79–82] and d-wave [82, 83] resonances. The present author contributed to one of the first studies on the universal relations for a p-wave resonance.

Experimental development of ultracold atomic gases has boosted the search for universal phenomena in the unitary Fermi gas, in spite of the fact that Bertsch, after whom the Bertsch parameter is named, posed the theoretical challenge on the unitary Fermi gas originally as a parameter-free model of dilute neutron matter [50, 51, 84]. A number of experimental groups have studied the unitary Fermi gas. They have measured the universal equation of state [85–87] and transport properties [88–92]. The universal relations in the unitary Fermi gas have also been tested by many experiments through the measurement of Tan's contact from correlation functions and thermodynamic quantities [93–97].

1.3 Outline of this thesis

Inspired by the progress in the Efimov physics and the unitary Fermi gas, we investigate effects of universal few-body correlations in strongly interacting ultracold atomic gases in this thesis. In particular, we discuss the universal relations in an anisotropic p-wave Fermi gas and the universality of the few-body spectra and the ground-state properties of an impurity-boson system.

We begin with reviewing the physics of Feshbach resonances and the derivation of the two-channel model, which is the effective-field theory for the resonance physics. It enables us to discuss universal features of resonant interactions without referring to microscopic details of systems; indeed, the resulting two-channel model has also been used to describe low-energy nuclear systems[98–100].

From Chapter 3 to Chapter 6, we present our original contributions.

Chapter 3 is devoted to addressing what kind of universal relations are associated with interactions beyond the conventional s-wave interactions. For this, we previously found universal relations for a p-wave Fermi gas and introduced the notion of a p-wave contact, which was, however, restricted to systems with rotational symmetry [79, 80]. Compared with an s-wave resonance, a new feature of a p-wave resonance is the possibility of anisotropy in ultracold atomic experiments; due to an external magnetic field to control a Feshbach resonance, the three-fold degeneracy of the p-wave resonance can be lifted [101, 102]. This can cause, for example, a novel superfluid phase, where the axisymmetry is spontaneously broken [103–105]. In Chapter 3, we present the universal relations in an anisotropic p-wave Fermi gas with anisotropy fully taken into account. We derive the asymptotic behavior of the momentum distribution and the density-density correlation function, from which we define the notion of a p-wave contact tensor. It has nine components, in contrast to Tan's contact, which is a scalar quantity. We show the adiabatic sweep theorem for the p-wave contact tensor, which relates the contact to the derivative of the energy with respect to the generalized p-wave scattering volume. We also argue that our results can be experimentally tested with the Λ configuration of the Raman lasers.

The other issue is related to the universal equation of state: do unitary Bose systems have universal equations of state, and if so, what do they look like? We address these questions for the ground state of an impurity-boson system, where a mobile impurity interacts via a unitarity-limited interaction with a weakly interacting Bose gas. Such a system has recently been realized using a mixture of atomic species, and found to be relatively stable and amenable to detailed investigations [106, 107].

The impurity-boson system is the simplest bosonic system that may display universality in its ground state. Two bosons resonantly interacting with a single impurity are known to support an infinite tower of Efimov states [5–7]. Remarkably, even the ground Efimov state is extremely loose in the impurity-boson system; the radius of the ground state trimer is $O(10^3)$ times larger than microscopic length scales such as the effective range associated with an interaction between the impurity and a boson [108]. One can expect that this huge separation of the scales makes the system insensitive to the short-range details of interactions if the density of bosons is sufficiently low. This

situation should be contrasted with the scalar Bose system in which bosons interact via a unitarity-limited interaction. There, the three-body ground state has the radius comparable to the range of the interaction. As a result, its properties depend on specific interactions, and the scaling factor between the ground state and the first-excited state deviates from its universal value [3] by 10-20% [9]. On the other hand, the excited states are exponentially loose and asymptotically follow the universal discrete scale invariance. The impurity-boson system is, therefore, a good candidate to explore for a universality in the ground state.

In Chapter 4, we consider an impurity and a few non-interacting bosons, where the mass of the impurity is equal to that of a boson. When bosons are heavier than the impurity, the four-body spectrum has been calculated [23, 109]. We calculate the energy spectra of the impurity with up to three bosons within two different models of interactions, which we call the r_0-model and the Λ-model. We show that the spectra, including the ground states, have a universal shape with high accuracy, which is independent of the choice of the models. This finding is corroborated by comparing the ratio of the three-body and four-body ground-state energies with the one calculated previously within yet another model [110]. Note that the universality found in this chapter is different from the universality of the discrete scale invariance in Eq. (1.4), which generally holds only for excited states [8–10].

In Chapter 5, we discuss an infinite-mass impurity interacting with a few non-interacting bosons. This limit no longer supports excited Efimov states, and only the ground state survives, because the scaling factor (λ in Eq. (1.4)) becomes infinite. This implies that the scale invariance of the unitarity limit is recovered. We show by analytically solving the 2+1 problem within the r_0-model that an effective three-body repulsion in a Feshbach resonance results in a bound-state spectrum that is drastically different from that in potential-interaction systems. We find that as the unitarity limit is approached, the result of the r_0-model converges logarithmically to that of potential-interaction systems. By comparing the analytical result with the numerical calculation within the Λ-model, we argue that the logarithmic correction is a universal consequence of the effective three-body repulsion.

In Chapter 6, we discuss the ground-state properties of the many-body impurity-boson system, that is, an impurity immersed in a finite-density Bose gas, which we call a Bose polaron [108, 110–125]. There is a study based on a renormalization-group approach, which, however, has omitted the three-body interaction [121]. To examine the universality of ground-state properties of the Bose polaron and take the Efimov effect into account, we employ a variational approach that incorporates three Bogoliubov excitations on top of the background condensate. Similar wave functions have been

used to describe the Bose polaron [108, 114], an impurity in a Fermi sea [126, 127], and an impurity in a Fermi superfluid [128]. We also note that a similar method has been known for long as the Tamm-Dancoff method [129, 130], which is used to discuss elementary excitations in nuclear systems. Here, by comparing the ground-state energies determined within the r_0-model and the Λ-model, we argue that for a sufficiently low density of the Bose gas, the ground-state energy is a universal function of the three-body parameter, which is a characteristic length scale of the ground-state Efimov state. This universality is carried over to the density which is high enough to smear out the well-defined Efimov states. The universal function corresponds to the Bertsch parameter in the unitary Fermi gas, although in a Bose polaron, it is no longer a pure number but a function. We also calculate other observables, the quasi-particle residue, the effective mass, and Tan's contact, and discuss their universality.

Finally, Chapter 7 is devoted to the summary of this thesis and makes some remarks on the future prospect.

In the following dissussions, we adopt the unit in which $\hbar = 1$.

Chapter 2

From atomic properties to effective-field theories

To discuss universal aspects of dilute atomic gases, it is essential to be equipped with effective-field theories that correctly reproduce low-energy few- and many-body physics. In particular, the two-channel model has been successfully employed in the field of ultracold atoms interacting via a Fano-Feshbach resonance, or a Feshbach resonance [34, 131–134], especially in describing atomic Bose-Einstein Condensates (BEC) [135, 136], fermionic superfluids [103, 105, 137–141], and few-body physics [25, 142–144]. In Section 2.1, we review atomic physics underlying a Feshbach resonance [145]. In Section 2.2, we describe this phenomenon and construct the two-channel model [138, 139]. The approach in this chapter is bottom-up; we start from microscopic description of a Feshbach resonance and arrive at its effective model. On the other hand, the same field theory can be reached by a top-down approach, where one retains all the terms that are allowed by symmetry and important for low-energy physics. This approach has been taken to describe low-energy properties of nuclear systems [98–100]. This fact displays the power of the two-channel model that it can describe a variety of phenomena near a scattering resonance in a unified manner regardless of microscopic details.

2.1 Microscopic description of atomic interactions

Feshbach resonances occur because atoms have rich internal structures. Therefore, in the first subsection, we explain one-atom properties. In the next subsection, we describe the basic coupled-channel picture of two-atom interactions.

2.1.1 Atomic properties

In cold-atom experiments, we can safely assume that atoms are in their electronic ground state unless one intentionally excites them. This is because the energy scale of the electronic excitation is of the order of 10^4K while the typical temperatures of atomic gases are μK to nK. For alkali atoms, all but one electron form closed shells, and the remaining valence electron occupies the s orbital. Therefore, an atom has the total electronic spin $S = 1/2$ and the electronic orbital angular momentum $L = 0$. The other component of an atom, a nucleus, also has a spin degree of freedom. The nuclear spin I depends on atomic species and isotopes.

In the absence of an external magnetic field, the nuclear spin of an alkali atom couples to the electronic spin by the hyperfine interaction of the form

$$\hat{H}_{\mathrm{hf}} = A\hat{\boldsymbol{I}} \cdot \hat{\boldsymbol{S}}, \tag{2.1}$$

where A is a hyperfine coupling constant, and $\hat{\boldsymbol{I}}$ and $\hat{\boldsymbol{S}}$ are the nuclear spin and the electronic spin[1], respectively. By using the total atomic angular momentum $\hat{\boldsymbol{F}}$ and the identity $\hat{\boldsymbol{I}} \cdot \hat{\boldsymbol{S}} = \frac{1}{2}(\hat{\boldsymbol{F}}^2 - \hat{\boldsymbol{I}}^2 - \hat{\boldsymbol{S}}^2)$, the eigenstates of the hyperfine interaction is those of $\hat{\boldsymbol{F}}^2$ for a fixed pair of I and S. Therefore, the eigenvalue $E_{F,I,S}$ of $\hat{H}_{\mathrm{hf}}$ for a given combination of F, I, and S is,

$$E_{F,I,S} = \frac{A}{2}\left[F(F+1) - I(I+1) - S(S+1)\right]. \tag{2.2}$$

As alkali atoms have $S = 1/2$, the addition rule of angular momenta gives $F = I \pm 1/2$. This leads to the zero-field hyperfine splitting,

$$\Delta E_{\mathrm{hf}} \equiv E_{I+1/2,I,1/2} - E_{I-1/2,I,1/2} = A\left(I + \frac{1}{2}\right). \tag{2.3}$$

Each of the two levels has $(2F+1)$-fold degeneracy as in any spherically symmetric systems with the angular momentum F.

When an external magnetic field $\boldsymbol{B}$ is applied, this degeneracy is lifted due to the symmetry-breaking Zeeman coupling,

$$\hat{H}_{\mathrm{Z}} = \left(g_{\mathrm{e}}\mu_{\mathrm{B}}\hat{\boldsymbol{S}} - \frac{\mu}{I}\hat{\boldsymbol{I}}\right) \cdot \boldsymbol{B} = \left(g_{\mathrm{e}}\mu_{\mathrm{B}}\hat{S}_z - \frac{\mu}{I}\hat{I}_z\right) B. \tag{2.4}$$

Here, $g_e \simeq 2$ is the electronic g factor, $\mu_{\mathrm{B}} \equiv e\hbar/2m_{\mathrm{e}}$ is the Bohr magneton, and μ is the magnetic moment of the nucleus. For simplicity, we assume $\boldsymbol{B} = B\boldsymbol{e}_z$ where $\boldsymbol{e}_z$ is the unit

[1] In general, we need to use $\hat{\boldsymbol{J}}$, the total electronic angular momentum, instead of $\hat{\boldsymbol{S}}$, because the orbital angular momentum can also couple to the nuclear spin. Here, $\hat{\boldsymbol{J}} = \hat{\boldsymbol{S}}$ because an alkali atom in the electronic ground state does not have orbital angular momentum.

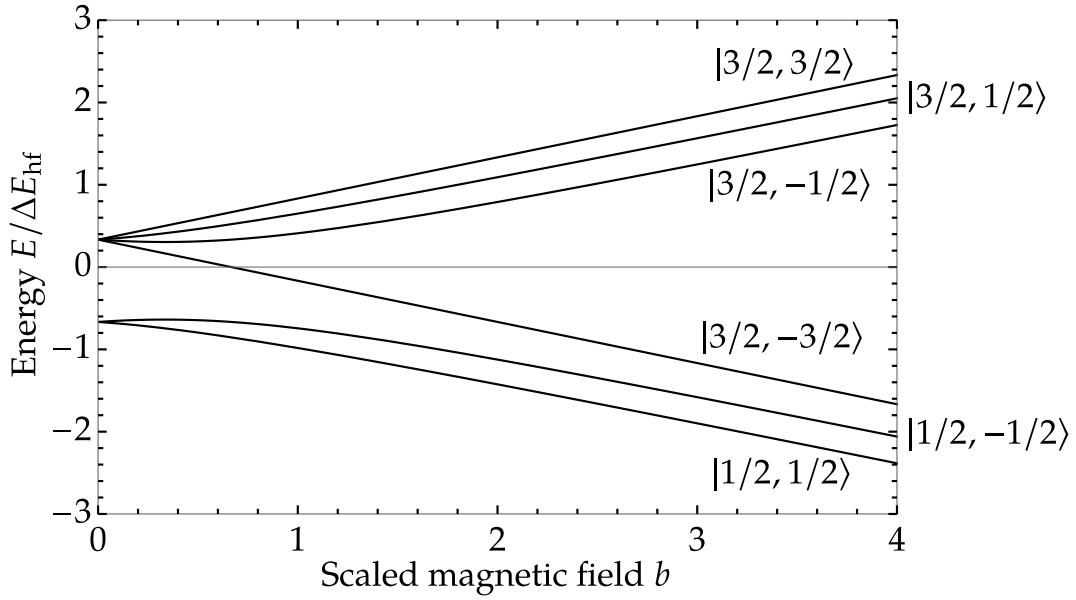

Figure 2.1: Energies of an alkali atom with $I = 1$ under a magnetic field, where $\Delta E_{\rm hf} = \frac{3}{2}A$. We assume that the hyperfine coupling A is positive, and adopt a scaled magnetic field $b = g_{\rm e}\mu_{\rm B}B/\Delta E_{\rm hf}$. The labels $|F, m_F\rangle$ show the corresponding zero-field states, while the actual eigenstates are not eigenvectors of $\hat{\boldsymbol{F}}^2$.

vector parallel to the z axis. As this term is still symmetric with respect to rotation around the z axis, the z component m_F of $\hat{\boldsymbol{F}}$ remains to be a good quantum number. Therefore, the fully polarized states $|F = I + 1/2, m_F = \pm(I + 1/2)\rangle$ are the eigenvectors of $\hat{H}_{\rm hf} + \hat{H}_{\rm Z}$ because the subspace specified by $m_F = I + 1/2$ or $-I - 1/2$ is one-dimensional, while the other states with $-I + 1/2 \le m_F \le I - 1/2$ are mixed by $\hat{H}_{\rm Z}$ within the two-dimensional subspace specified by m_F. Each eigenstate is continuously connected to $|F, m_F\rangle$ when the magnetic field is turned off.

As a specific example, we show in Fig. 2.1 the energy eigenvalues of an alkali atom with $I = 1$ as a function of the magnetic field[2]. In this case, the hyperfine splitting at the zero magnetic field is given by $\Delta E_{\rm hf} = \frac{3}{2}A$. For small magnetic fields, with which $\hat{H}_{\rm Z}$ can be regarded as a perturbation, the eigenstates are well approximated by $|F, m_F\rangle$, and their energies deviate linearly from $E_{F,1,1/2}$. In the opposite limit of strong fields, $\hat{H}_{\rm Z}$ dominates over $\hat{H}_{\rm hf}$, and now not only $m_F = m_I + m_S$ but also m_I and m_S become good quantum numbers. In particular, as $\mu/\mu_{\rm B} = O(10^{-3})$, the Zeeman shift due to the electronic spin gives a major contribution to the energies, with a small splitting $A/2$ due to the hyperfine coupling.

[2]The nuclear spin $I = 1$ is realized in a ^{6}Li atom.

2.1.2 Coupled-channel interaction

Now consider two atoms prepared in the internal states labeled as α and β, which are referred to as the entrance channel. In general, they can be of two different atomic species. Suppose that a collision with a relative momentum $\boldsymbol{k}$ produces two scattered atoms in the internal states α' and β', referred to as the exit channel, with an outgoing relative momentum $\boldsymbol{k}'$. The energy conservation then reads

$$\frac{k'^2}{2m_\mathrm{r}} + \varepsilon_{\alpha'} + \varepsilon_{\beta'} = \frac{k^2}{2m_\mathrm{r}} + \varepsilon_\alpha + \varepsilon_\beta, \tag{2.5}$$

where m_r is the reduced mass of the two atoms, and ε_α is the one-atom energy of the state α. The exit channel $\alpha'\beta'$ is said to be closed if the collision energy (given by the right-hand side of Eq. (2.5)) is less than a threshold energy $E_\mathrm{th}(\alpha'\beta')$ defined as

$$E_\mathrm{th}(\alpha'\beta') = \varepsilon_{\alpha'} + \varepsilon_{\beta'}. \tag{2.6}$$

There is no real transition to such closed channels, and it can occur only as a virtual process, because the atoms do not have a sufficient energy. On the other hand, if the pair of atoms can scatter into a channel $\alpha'\beta'$ as a real process, the channel is said to be open. Note that the definition of "open" and "close" depends on the incident energy. In a thermal atomic gas, the hyperfine splitting is of the order of GHz, which implies that the inelastic scattering into a channel $\alpha'\beta'$ with $E_\mathrm{th}(\alpha'\beta') > E_\mathrm{th}(\alpha\beta)$ is negligible at temperatures less than mK. Therefore, the channels with larger threshold energies than that of the entrance channel can generally be regarded as closed.

An interaction potential, in the most general form, has the indices of the entrance and exit channels, $U_{\alpha'\beta',\alpha\beta}(\boldsymbol{r})$. For alkali atoms in their electronic ground states with $S = 1/2$, the dominant part of the interaction is spherically symmetric and diagonal with respect to the total electronic spin of the two atoms:

$$U_{\alpha'\beta',\alpha\beta}(\boldsymbol{r}) = U_\mathrm{s}(r)\hat{\mathcal{P}}_\mathrm{s} + U_\mathrm{t}(r)\hat{\mathcal{P}}_\mathrm{t} \tag{2.7}$$

$$= \frac{U_\mathrm{s}(r) + 3U_\mathrm{t}(r)}{4} + [U_\mathrm{t}(r) - U_\mathrm{s}(r)]\hat{\boldsymbol{S}}_1 \cdot \hat{\boldsymbol{S}}_2, \tag{2.8}$$

where $\hat{\mathcal{P}}_\mathrm{s} = 1/4 - \hat{\boldsymbol{S}}_1 \cdot \hat{\boldsymbol{S}}_2$ and $\hat{\mathcal{P}}_\mathrm{t} = 3/4 + \hat{\boldsymbol{S}}_1 \cdot \hat{\boldsymbol{S}}_2$ are the projection operators onto the electronic-spin singlet and triplet states, respectively. It is clear from Eq. (2.8) that the inter-channel coupling is of the electronic-spin exchange type, which conserves the two-atom total electronic spin and the projection of the total angular momentum on the quantization axis. Other processes such as the magnetic dipole-dipole interaction and three-body collisions can lead to other forms of channel couplings; they are not too

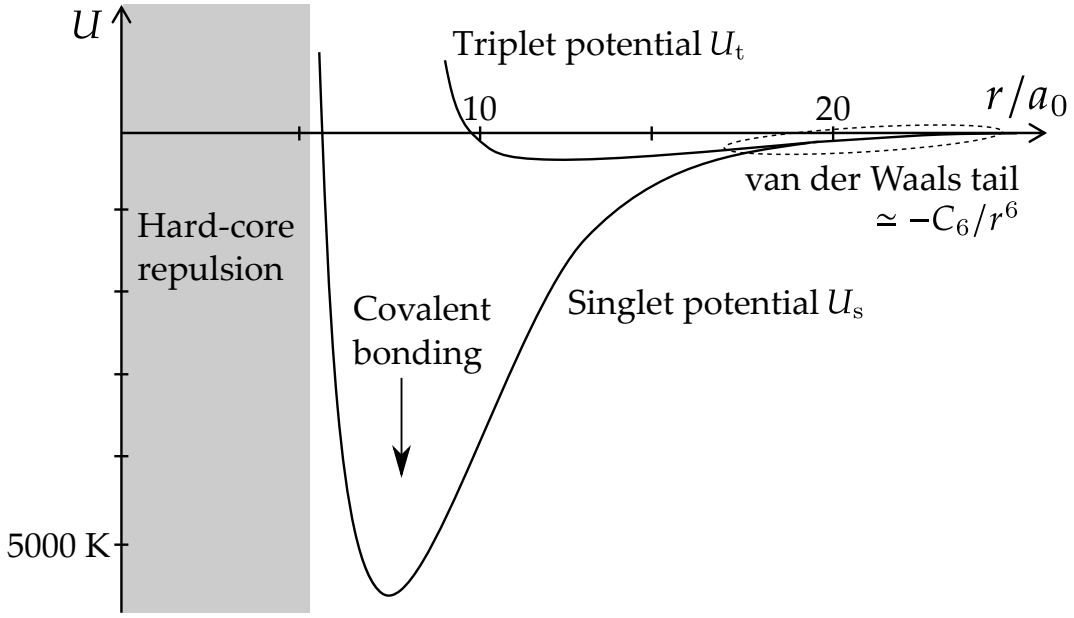

Figure 2.2: Schematic plot of the singlet and triplet potentials for two Rubidium atoms in the orbital ground state, where a_0 is the Bohr radius. Both potentials share the same long-range van der Waals tail $\propto r^{-6}$ and the hard-core repulsive part. Between them, the singlet potential has a deep minimum due to the covalent bonding, while the triplet potential does not have such a pronounced dip.

strong for alkali atoms, but often impose limitations on experimental time scales. Here, we focus on the time scales which are sufficiently short compared to such limitations but long enough for the spherically symmetric part to cause collisions and eventually make the system thermalize.

Figure 2.2 shows a schematic plot of U_s and U_t. For large separations, the tails of the interaction potentials are given by the van der Waals interaction. It is an attractive interaction of the form $-C_6/r^6$, where C_6 is a constant and r is the separation between two atoms. The van der Waals interaction originates from the second-order process of the electric dipole-dipole interaction and is independent of the spin states. For smaller separations, we can see a strong repulsive core due to the overlap of the electron clouds. Just before the core, the singlet potential has a pronounced minimum with a depth of nearly 6000K for Rubidium atoms, while the minimum of the triplet potential is much shallower, of a few hundred kelvin. This can be understood as the presence or absence of the covalent bonding. When two atoms possess opposite spins, the two valence electrons can reduce the energy by sharing the same orbital. By contrast, two polarized electrons cannot occupy the same orbital, and no energy reduction from the covalent bonding can be made.

In experiments, we prepare atoms in some selected hyperfine state(s). The entrance channel of a collision in such an atomic gas may or may not be the electronic spin

singlet or triplet. If both of the colliding atoms are in the same fully polarized state, the two-electron spin state is triplet, and therefore no spin exchange occurs during the collision. In other words, within the approximate potential of Eq. (2.8), the interaction between such pairs is of single-channel nature. On the other hand, other channels are superpositions of electronic-spin singlet and triplet, and subject to the spin exchange interaction. This implies that a pair of atoms in such a channel can undergo inelastic scattering if there is an open channel coupled to the entrance channel by the exchange interaction. If there is no available open channel, two atoms interact only elastically. This process may also be drastically affected by the presence of the channel coupling, which is a Feshbach resonance.

2.2 Feshbach resonance and the two-channel models

A major qualitative difference between single-channel potential interactions and coupled-channel interactions is that the latter can support inelastic two-body scattering. In atomic gas experiments, however, such processes are not so important since we usually prepare atoms in low-lying hyperfine states so that no open channel is available for inelastic two-body collisions. On the other hand, the channel coupling can strongly affect an elastic process via a so-called Feshbach resonance [34, 131–134]. It is a resonant enhancement of elastic scattering caused by coupling to a virtual bound state in a closed channel.

A Feshbach resonance occurs when a pair of atoms collides with the incoming energy near that of a bound state in a closed channel. One open and one closed channel are enough to describe this phenomenon, which is called a two-channel picture. In this model, the interaction potential in the closed channel has bound states, one of which lies near the threshold energy of the open channel, as illustrated in Fig. 2.3. An intuitive, though somewhat oversimplified, understanding is then obtained by considering the second-order Born approximation of the T-matrix in terms of the coupling between the open channel and the closed-channel bound state. It gives a shift to the on-shell T-matrix at the threshold energy, or equivalently the s-wave scattering length a,

$$\delta T(0) \equiv \frac{2\pi\delta a}{m_{\mathrm{r}}} = -\sum_{n} \frac{\left|\left\langle n \left| \hat{H}_{\mathrm{ex}} \right| 0 \right\rangle\right|^2}{E_n} \simeq -\frac{\left|\left\langle b \left| \hat{H}_{\mathrm{ex}} \right| 0 \right\rangle\right|^2}{E_{\mathrm{b}}}, \tag{2.9}$$

where m_{r} is the reduced mass of the colliding atoms, $\hat{H}_{\mathrm{ex}}$ is an inter-channel Hamiltonian (here "ex" represents the exchange interaction for concreteness), $|0\rangle$ is an unperturbed open-channel state at threshold, and $|n\rangle$ is an unperturbed closed-channel state with an energy E_n measured from the open-channel threshold. In the last approximate equality

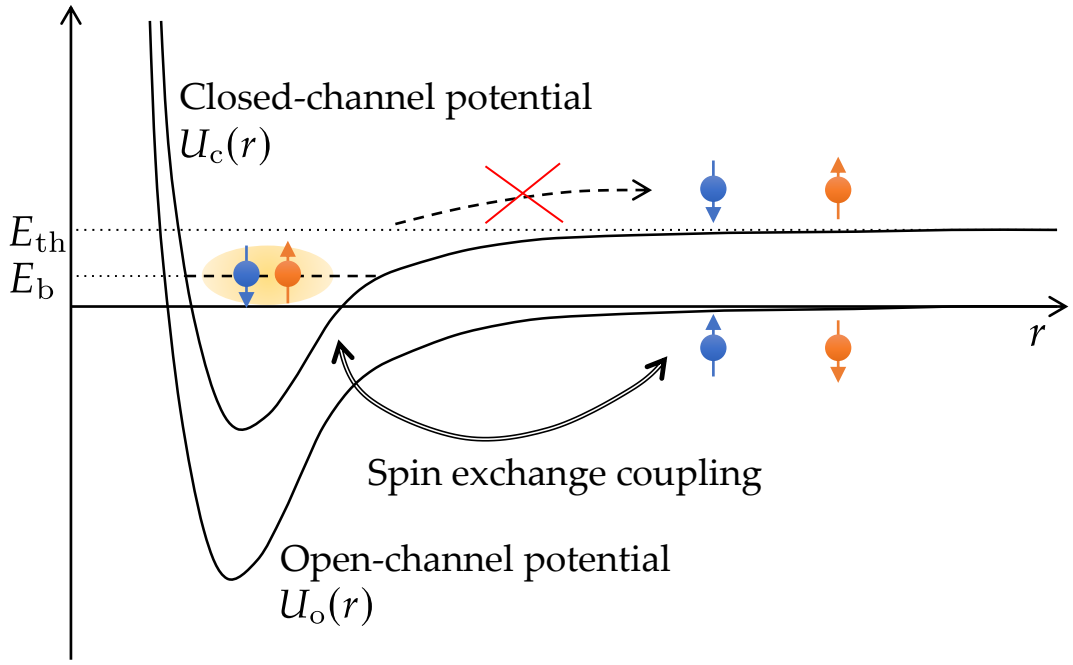

Figure 2.3: Sketch of a mechanism of a Feshbach resonance. The low-energy incoming atoms are coupled via the spin-exchange interaction to a bound state in the closed channel near the open-channel threshold. Since the incident energy is not enough for the atoms to scatter into the continuum above $E_{\rm th}$, the bound state eventually dissociate back into the entrance channel.

in Eq. (2.9), we only retain the contribution from the bound state lying closest to the zero energy. Equation (2.9) implies that the coupling gives an effective attraction if $E_{\rm b} > 0$ while it gives a repulsion if $E_{\rm b} < 0$. Another important implication is that if we can control $E_{\rm b}$, it amounts to controlling the s-wave scattering length in the open channel. This is indeed possible in atomic systems, where a pair of atoms in a closed channel may have the magnetic moment $\mu_{\rm c}$ that is different from $\mu_{\rm o}$ in the open channel. In the presence of an external magnetic field, the bound-state energy $E_{\rm b}$ is

$$E_{\rm b} = (\mu_{\rm o} - \mu_{\rm c})(B - B_0) \equiv \delta\mu(B - B_0), \tag{2.10}$$

where B_0 is the threshold magnetic field at which $E_{\rm b}$ vanishes. Therefore, by changing the strength of the applied magnetic field, we can control the strength and even the sign of the effective interaction. Note, however, that the Born approximation breaks down just in the vicinity of the resonance $E_{\rm b} \simeq 0$. A discussion beyond this approximation is given later.

To discuss many-body physics involving a Feshbach resonance, we now derive an effective-field theory that encapsulates the essence of this phenomenon [138, 139]. To this end, first consider the general coupled Schrödinger equations for the relative motion

of two atoms,

$$(E - \hat{H}_{PP}) |\Psi_P\rangle = \hat{H}_{PQ} |\Psi_Q\rangle , \tag{2.11}$$

$$(E - \hat{H}_{QQ}) |\Psi_Q\rangle = \hat{H}_{QP} |\Psi_P\rangle , \tag{2.12}$$

where P and Q denote the spaces of the states in the open and closed channels, respectively. Here again, we can eliminate the far-off-resonant states in the closed channel such as the continuum. To do this, let us introduce a projection operator $\mathcal{P} = \mathbb{I}_P \oplus \mathcal{P}_Q$, where $\mathbb{I}_P$ is the identity operator in the space of the open channel and $\mathcal{P}_Q = \sum_i |i_Q\rangle \langle i_Q|$ is a projector from the closed-channel space onto the unperturbed bound state(s) $|i_Q\rangle$ of $\hat{H}_{QQ}$ that is resonant to the open channel. By restricting the Hilbert space by $\mathcal{P}$, we obtain a pair of approximate Schrödinger equations,

$$(E - \hat{H}_{PP}) |\Psi_P\rangle = \sum_i \hat{H}_{PQ} |i_Q\rangle \langle i_Q|\Psi_Q\rangle , \tag{2.13}$$

$$(E - \nu_i) \langle i_Q|\Psi_Q\rangle = \langle i_Q| \hat{H}_{QP} |\Psi_P\rangle , \tag{2.14}$$

where ν_i is the unperturbed energy of $|i_Q\rangle$ given by $(\nu_i - \hat{H}_{QQ}) |i_Q\rangle = 0$. In Eq. (2.14), we do not have summation over the index i because of the orthogonality of $|i_Q\rangle$. It is important to note that we no longer need the degrees of freedom of the relative motion of two atoms in $|i_Q\rangle$, because Eq. (2.13) and (2.14) contain just the amplitude $\langle i_Q|\Psi_Q\rangle$. The equations for a set of $|\Psi_P\rangle$ and $\langle i_Q|\Psi_Q\rangle$ are naturally expressed in terms of a Hamiltonian constructed from the field operator(s) $\hat{\psi}_\alpha(\boldsymbol{r})$ representing atoms and the molecular field operator $\hat{\phi}_i(\boldsymbol{r})$, where the index α denotes the hyperfine state and the atomic species. If we assume for simplicity that the open channel consists of two atoms in the same hyperfine state and that only one closed-channel molecular state is resonant, the indices can be dropped, and the Hamiltonian reads

$$\hat{H}_{\mathrm{PP}} = \int d\boldsymbol{r}\, \frac{1}{2m} \nabla\hat{\psi}^\dagger \cdot \nabla\hat{\psi} + \frac{1}{2} \int d\boldsymbol{r}\, d\boldsymbol{r}'\, U_{\mathrm{o}}(\boldsymbol{r} - \boldsymbol{r}') \hat{\psi}^\dagger(\boldsymbol{r}) \hat{\psi}^\dagger(\boldsymbol{r}') \hat{\psi}(\boldsymbol{r}') \hat{\psi}(\boldsymbol{r}), \tag{2.15}$$

$$\hat{H}_{PQ} = \hat{H}_{QP}^\dagger = \frac{1}{2} \int d\boldsymbol{r}\, d\boldsymbol{r}'\, g(\boldsymbol{r} - \boldsymbol{r}') \hat{\psi}^\dagger(\boldsymbol{r}) \hat{\psi}^\dagger(\boldsymbol{r}') \hat{\phi} \left(\frac{\boldsymbol{r} + \boldsymbol{r}'}{2} \right), \tag{2.16}$$

$$\hat{H}_{QQ} = \int d\boldsymbol{r} \left(\frac{1}{4m} \nabla\hat{\phi}^\dagger \nabla\hat{\phi} + \nu \hat{\phi}^\dagger \hat{\phi} \right). \tag{2.17}$$

Here, m is the mass of an atom, U_{o} is the interaction potential within the open channel, and $g(\boldsymbol{r} - \boldsymbol{r}') \equiv \langle \boldsymbol{r}\boldsymbol{r}'_P | \hat{H}_{PQ} | i_Q \rangle$. This so-called two-channel model gives us a natural starting point of analyzing many-body systems with a Feshbach resonance. We can easily generalize this for systems with multiple hyperfine states or multiple closed-channel molecular states.

We can restrict the form of $g(\boldsymbol{r})$ by symmetry. Suppose that the inter-channel coupling is induced by the spherically symmetric exchange interaction, as discussed in the previous section. In this case, the orbital angular momentum in the relative motion of two colliding atoms is a conserved quantity. Therefore, if the rotational motion of a closed-channel molecule has the angular momentum l and its projection m, the associated Feshbach resonance occurs in the scattering processes with the same quantum numbers. Correspondingly, the angular dependence of $g(\boldsymbol{r})$ is given by the spherical harmonic function $Y_l^m(\hat{\boldsymbol{r}})$. This implies that in spherically symmetric systems, a Feshbach resonance in the lth partial wave has $(2l+1)$-fold degeneracy, which reflects the degeneracy of the closed-channel molecule. In practice, an external magnetic field is applied to a gas to control the Feshbach resonance. This may result in multiplet structures of an lth-wave Feshbach resonance for $l > 0$, which have been observed in p-wave [101] and d-wave [102] resonances.

In dilute, low-temperature atomic gases described by the Hamiltonian (2.15-2.17), many-body properties are expectedly independent of the detailed profiles of $g(\boldsymbol{r})$ and $U_{\mathrm{o}}(\boldsymbol{r})$, as typical length scales such as the interparticle spacing and the thermal de Broglie length are much larger than the range of these functions. Therefore, one can choose a convenient function suitable for one's needs.

We would like to emphasize again that Eqs. (2.15-2.17) are the Hamiltonian that corresponds to the Lagrangians in Refs. [98–100] if one truncates the Taylor expansion of the Fourier transform of $g(\boldsymbol{r})$. This indicates that the use of the two-channel model is not restricted to atomic systems with a Feshbach resonance, and that results that follow from the two-channel model are potentially relevant not only to ultracold atomic gases but also to low-energy nuclear systems.

Now, let us discuss specific examples of the two-channel models that are relevant to our research.

2.2.1 s-wave resonance in a two-component Bose gas

Consider a mixture of two atomic species labeled 1 and 2, each of which is prepared in a single hyperfine state. For definiteness and later use, we assume the atoms are bosons, although in this section we only discuss a two-body system consisting of one atom for each species. If there is an s-wave Feshbach resonance between the two species, the two-channel Hamiltonian reads

$$\begin{aligned}\hat{H} = \int d\boldsymbol{r} \Bigg(& \frac{1}{2m_1}\nabla\hat{\psi}_1^\dagger \cdot \nabla\hat{\psi}_1 + \frac{1}{2m_2}\nabla\hat{\psi}_2^\dagger \cdot \nabla\hat{\psi}_2 + U_0\hat{\psi}_1^\dagger\hat{\psi}_2^\dagger\hat{\psi}_2\hat{\psi}_1 \\ & + \frac{1}{2M}\nabla\hat{\phi}^\dagger \cdot \nabla\hat{\phi} + \nu_0\hat{\phi}^\dagger\hat{\phi} + g_0\hat{\psi}_1^\dagger\hat{\psi}_2^\dagger\hat{\phi} + g_0\hat{\phi}^\dagger\hat{\psi}_2\hat{\psi}_1 \Bigg),\end{aligned} \tag{2.18}$$

where m_i is the mass of an atom of the ith species ($i = 1, 2$), $M \equiv m_1 + m_2$ is the mass of a closed-channel molecule, and we adopt $U_o(\boldsymbol{r}) = U_0\delta(\boldsymbol{r})$ and $g(\boldsymbol{r}) = g_0\delta(\boldsymbol{r})$.

The parameters, U_0, ν_0, and g_0, are determined so that they reproduce low-energy scattering data, especially the scattering amplitude. To this end, we need to solve the two-body problem beyond the Born approximation. Let us consider a two-body state whose total momentum is zero, and write down the coupled Schrödinger equations in the momentum representation:

$$\left(E - \frac{k^2}{2m_\mathrm{r}}\right)\Psi_\mathrm{o}(\boldsymbol{k}) = U_0 \int \frac{d\boldsymbol{k}'}{(2\pi)^3}\Psi_\mathrm{o}(\boldsymbol{k}') + g_0\Psi_\mathrm{c} \equiv T(E), \tag{2.19}$$

$$(E - \nu_0)\,\Psi_\mathrm{c} = g_0 \int \frac{d\boldsymbol{k}'}{(2\pi)^3}\Psi_\mathrm{o}(\boldsymbol{k}'). \tag{2.20}$$

Here, $\Psi_\mathrm{o}(\boldsymbol{k})$ is the wave function for the relative motion of the open-channel atoms, Ψ_c is the amplitude of the closed-channel molecule, and m_r is the reduced mass of the two particles. Note that the right-hand side of Eq. (2.19), which is actually a T-matrix element, is independent of $\boldsymbol{k}$ but implicitly depends on E. This is because we have taken the zero-range limit of the interaction.

The solutions consists of continuous scattering states with $E \geq 0$, and if any, discrete bound states with $E < 0$ [1, 2]. To find the scattering state, we need to specify a boundary condition because otherwise the value of $\Psi_\mathrm{o}(\boldsymbol{k})$ for $|\boldsymbol{k}| = \sqrt{2m_\mathrm{r}E}$ would not be uniquely determined. Here, we require the wave function to be a superposition of an incoming plane wave and an outgoing scattered wave. In the momentum representation, a solution for $\Psi_\mathrm{o}(\boldsymbol{k})$ reads

$$\Psi_\mathrm{o}(\boldsymbol{k}) = (2\pi)^3\delta(\boldsymbol{k} - \boldsymbol{k}_0) + \frac{T(E + i0)}{E + i0 - k^2/2m_\mathrm{r}}, \tag{2.21}$$

where $\boldsymbol{k}_0$ is the momentum of the incoming plane wave that satisfies $E = k_0^2/2m_\mathrm{r}$, and the imaginary part of the energy is set to be the positive infinitesimal to ensure that the scattered wave is outgoing [2]. Solutions of this form constitute a continuous spectrum, which is physically a set of the scattering states labeled by $\boldsymbol{k}_0$. By substituting this and Eq. (2.20) into the T-matrix, we obtain

$$T(E + i0) = \left(U_0 + \frac{g_0^2}{E - \nu_0}\right)\left[1 + T(E + i0)\int \frac{d\boldsymbol{k}}{(2\pi)^3}\frac{1}{E + i0 - k^2/2m_\mathrm{r}}\right] \tag{2.22}$$

$$= \left[\left(U_0 + \frac{g_0^2}{E - \nu_0}\right)^{-1} - \int \frac{d\boldsymbol{k}}{(2\pi)^3}\frac{1}{E + i0 - k^2/2m_\mathrm{r}}\right]^{-1}. \tag{2.23}$$

This expression contains an ultraviolet divergence in the $\boldsymbol{k}$-integration. However, it can be absorbed into the definition of the bare interaction parameters so that the resulting T-matrix becomes finite. If we impose an ultraviolet cutoff at the momentum Λ, the momentum integral above is calculated as

$$\int_{|\boldsymbol{k}|<\Lambda} \frac{d\boldsymbol{k}}{(2\pi)^3} \frac{1}{E + i0 - k^2/2m_\mathrm{r}} = -\frac{m_\mathrm{r}\Lambda}{\pi^2} - \frac{im_\mathrm{r}}{2\pi}\sqrt{2m_\mathrm{r}E}. \tag{2.24}$$

The linear divergence is cancelled by setting

$$U_0(\Lambda) = Z(\Lambda)U, \quad g_0(\Lambda) = Z(\Lambda)g, \quad \nu_0(\Lambda) = \nu - [1 - Z(\Lambda)]\frac{g^2}{U}, \tag{2.25}$$

where $Z(\Lambda) = (1 - m_\mathrm{r}U\Lambda/\pi^2)^{-1}$. Therefore, U and g are subject to multiplicative renormalization, while the closed-channel molecular energy ν is additively shifted. The resulting T-matrix is

$$T(E + i0) = \frac{2\pi}{m_\mathrm{r}} \left[\frac{2\pi}{m_\mathrm{r}} \left(U + \frac{g^2}{E - \nu} \right)^{-1} + i\sqrt{2m_\mathrm{r}E} \right]^{-1}, \tag{2.26}$$

which is now cutoff-independent and implies that the s-wave scattering length a is

$$a = \frac{m_\mathrm{r}}{2\pi} T(0) = \frac{m_\mathrm{r}}{2\pi} \left(U - \frac{g^2}{\nu} \right). \tag{2.27}$$

This expression results from the exact solution of the two-body problem within the two-channel model, without relying on the Born approximation. It is therefore applicable even when a diverges. In particular, the higher-order interaction modifies the condition for the resonance from $\nu_0 = 0$ to $\nu = 0$. Experimentally, if we approximate $\nu \simeq \delta\mu(B - B_0)$ near the resonance and once $\delta\mu$ and B_0 are known, one can determine U and g by, for example, locating the zero crossing of a and measuring a at the zero magnetic field.

We can also find the closed-channel amplitude Ψ_c. It is obtained by substituting Eq. (2.21) into Eq. (2.20),

$$\Psi_\mathrm{c} = \frac{g_0 T(E + i0)}{E - \nu_0} \int \frac{d\boldsymbol{k}}{(2\pi)^3} \frac{1}{E + i0 - k^2/2m_\mathrm{r}} \tag{2.28}$$

$$\to \frac{gT(E + i0)}{U(E - \nu) + g^2} \quad (\Lambda \to \infty). \tag{2.29}$$

When taking the infinite cutoff limit, we used the expressions of the bare parameters in Eq. (2.25). Near the resonance $E \simeq \nu \simeq 0$, the expression of the T-matrix as given in

Eq. (2.26) reduces to

$$T(E) \simeq \frac{2\pi}{i m_{\mathrm{r}} \sqrt{2 m_{\mathrm{r}} E}}, \tag{2.30}$$

and the closed-channel amplitude is

$$\Psi_{\mathrm{c}} \simeq \frac{2\pi}{i m_{\mathrm{r}} g \sqrt{2 m_{\mathrm{r}} E}}. \tag{2.31}$$

This indicates that for a given energy, the inter-channel coupling g controls the closed-channel amplitude. In particular, if $g \to \infty$, the closed-channel amplitude vanishes, which implies that the two-channel model behaves like a single-channel interaction in the limit of the large g.

When the detuning crosses the open-channel threshold $\nu \simeq 0$, the low-energy form of the T-matrix does not change if one takes the limit $U \to 0$. This limit is equivalent to the effective-range approximation, where the T-matrix takes the form

$$T(E + i0) = \frac{2\pi}{m_{\mathrm{r}}} \left[a^{-1} - m_{\mathrm{r}} r_0 E + i\sqrt{2 m_{\mathrm{r}} E} \right]^{-1}. \tag{2.32}$$

Here, r_0 is the effective range. In this case, the renormalization factor $Z(\Lambda)$ is identically unity, and therefore, the inter-channel coupling g is not renormalized. On the other hand, the detuning is again additively renormalized,

$$\nu_0(\Lambda) = \nu + \frac{m_{\mathrm{r}} g^2 \Lambda}{\pi^2}. \tag{2.33}$$

These couplings give a and r_0 as follows:

$$a^{-1} = -\frac{2\pi\nu}{m_{\mathrm{r}} g^2}, \quad r_0 = -\frac{2\pi}{m_{\mathrm{r}}^2 g^2}. \tag{2.34}$$

In this limit, the effective range r_0 is directly related to the inter-channel coupling g_0. In particular, when g_0 is sufficiently large, r_0 may be negligible. This implies that a system with a large g_0 looks like a single-channel system, which is consistent with the observation for the finite U model. Note that the effective range r_0 is always negative within the two-channel model as long as the coupling constant is a real number. It is realistic for Feshbach resonances, while if we consider more general interactions, the effective range can take an arbitrary real number.

In addition to the continuous scattering states, the complete energy spectrum may contain discrete bound states. They are found as poles of the T-matrix. Here, we focus on the case of $U \to 0$, which is relevant to the later discussion. The equation for

the bound-state energy $T(-E_\mathrm{B})^{-1} = 0$ can be easily solved, where $E_\mathrm{B} > 0$. Note that the imaginary part of $\sqrt{E}$ for a negative energy should be positive for physical bound states [2]. If the scattering length is negative, it has no bound-state solution that has a real energy. By contrast, for positive scattering lengths, there is a single bound state, whose binding energy is given by

$$E_\mathrm{B} = \frac{(\sqrt{1 - 2r_0/a} - 1)^2}{2m_\mathrm{r} r_0^2}. \tag{2.35}$$

The wave function of this bound state is immediately obtained if we set $\Psi_\mathrm{c} = Z^{1/2}$ and use Eq. (2.19):

$$\Psi_\mathrm{o}(\boldsymbol{k}) = -\frac{g_0 Z^{1/2}}{E_\mathrm{B} + k^2/2m_\mathrm{r}}. \tag{2.36}$$

Note that a discrete negative-energy state does not have a term corresponding to an incident plane wave. One can also find the closed-channel amplitude $Z^{1/2}$ from the normalization condition:

$$Z^{1/2} = \frac{\sqrt{2m_\mathrm{r} r_0^2 E_\mathrm{B}}}{1 + \sqrt{2m_\mathrm{r} r_0^2 E_\mathrm{B}}}. \tag{2.37}$$

Note that for $r_0 \to 0$, Z is always zero while E_B remains finite. This indicates that this physical bound state is totally different from the bare closed-channel molecule. The bound state in this limit is composed of two atoms in the open channel.

One can confirm by direct calculations that the solutions found here constitute the complete orthonormal basis of the Hilbert space representing the relative motion, as we expect for physical Hamiltonian.

2.2.2 p-wave resonance in a spinless Fermi gas

Collisions of identical particles are subject to symmetry restriction. In particular, for spinless fermions, where s-wave interactions are prohibited, the p-wave scattering gives the dominant contribution. Here, the word "spinless" means that we prepare atoms in a single hyperfine state, in which case we can formally drop the spin index from the fermionic field operator because there is no remaining internal degree of freedom in an atom. In ultracold collisions, effects of the p-wave scattering are usually negligible. However, Feshbach resonances have been utilized to realize atomic gases with strong p-wave interactions.

The two-channel model of a p-wave resonance has at least three closed-channel molecules corresponding to three different projections of the relative angular momentum:

$$\begin{aligned}\hat{H} = &\int d\boldsymbol{r}\left[\frac{1}{2M}\nabla\hat{\psi}^\dagger\cdot\nabla\hat{\psi} + \sum_{m=-1}^{1}\left(\frac{1}{4M}\nabla\hat{\phi}_m^\dagger\cdot\nabla\hat{\phi}_m + \nu_0^{(m)}\hat{\phi}_m^\dagger\hat{\phi}_m\right)\right] \\ &+ \frac{1}{2}\int d\boldsymbol{r}\,d\boldsymbol{r}'\sum_{m=-1}^{1}\left[g_m(\boldsymbol{r}-\boldsymbol{r}')\hat{\psi}^\dagger(\boldsymbol{r})\hat{\psi}^\dagger(\boldsymbol{r}')\hat{\phi}_m\left(\frac{\boldsymbol{r}+\boldsymbol{r}'}{2}\right) + \text{H. c.}\right].\end{aligned} \tag{2.38}$$

Here, we use the upper-case M for the mass of an atom and the lower-case m for the projection of angular momentum. In the spherically symmetric system, the energies of the closed-channel molecules are degenerate. However, in cold-atom experiments, we apply a magnetic field to control a Feshbach resonance, which breaks the rotational symmetry into the axisymmetry around the direction of the applied field. This is why the detuning $\nu_0^{(m)}$ has explicit dependence on m. We drop the off-resonant interaction in the open channel because the p-wave interaction in the absence of the Feshbach resonance is negligibly small. The coupling function $g_m(\boldsymbol{r})$ is proportional to $Y_1^m(\hat{\boldsymbol{r}})$ and kept finite-ranged. This is necessary if we want the Hamiltonian to be a Hermitian, all the states to have positive norms, and the inner product to be defined as a usual Hermitian inner product [25, 98–100, 146–150][3]. Instead of taking the zero-range limit, we assume that $g_m(\boldsymbol{r})$ is sufficiently smooth so that its Fourier transform $\tilde{g}_m(\boldsymbol{k})$ is also analytic and sufficiently smooth. This implies that $\tilde{g}_m(\boldsymbol{k})$ can be written as

$$\tilde{g}_m(\boldsymbol{k}) = g_0 k Y_1^m(\hat{\boldsymbol{k}})\chi(k^2), \quad \chi(0) = 1, \tag{2.39}$$

where $\chi(k^2)$ is an analytic function of k^2. If $g_m(\boldsymbol{r})$ has a radius R, outside of which the coupling is negligible, a simple dimensional analysis suggests that $\chi(k^2)$ also has a radius of $O(R^{-1})$ unless $g_m(\boldsymbol{r})$ has a short-range structure of the size $R' \ll R$. Here, we assume $g_m(\boldsymbol{r})$ is well-behaved in this sense. An important consequence of this assumption is that at low momenta, $g_m(\boldsymbol{k})$ grows linearly with $\boldsymbol{k}$ before it is cut off at $k \sim R^{-1}$.

Similarly to the s-wave resonance, we can perform the renormalization of this p-wave model. For this model, the two-body coupled Schrödinger equations are

$$\left(E - \frac{k^2}{M}\right)\Psi_{\text{o}}(\boldsymbol{k}) = \sum_{m=-1}^{1}\tilde{g}_m(\boldsymbol{k})\Psi_m \equiv \sum_{m=-1}^{1} 4\pi k k_0 Y_1^m(\hat{\boldsymbol{k}})Y_1^{m*}(\hat{\boldsymbol{k}}_0)T_m(E+i0;k,k_0), \tag{2.40}$$

[3] An alternative approach is to make the range of the coupling function $g(\boldsymbol{r})$ arbitrarily small at the cost of the positivity of the norm. This is done in Refs. [98–100]. In that case, we can no longer interpret the ϕ-field as the closed-channel molecule because it is an unphysical state. The ϕ-field is then called a ghost field.

$$\left(E - \nu_0^{(m)}\right)\Psi_m = \frac{1}{2}\int \frac{d\boldsymbol{k}}{(2\pi)^3}\tilde{g}_m^*(\boldsymbol{k})\Psi_o(\boldsymbol{k}). \tag{2.41}$$

In contrast to the previous s-wave case, the T-matrix depends on both $\boldsymbol{k}$ and the incident momentum $\boldsymbol{k}_0$, as well as the energy. Owing to the orthogonality of the spherical harmonics, the decomposition of the T-matrix is unambiguous. From these equations, we can derive the equation for the T-matrix element:

$$\begin{aligned} T_m(E+i0;k,k_0) = &\frac{|g_0|^2\chi(k^2)\chi(k_0^2)}{8\pi(E-\nu_0^{(m)})} \\ &+ \frac{|g_0|^2\chi(k^2)}{2(E-\nu_0^{(m)})}\int_0^\infty \frac{k'^2dk'}{(2\pi)^3}\frac{k'^2\chi(k'^2)T_m(E+i0;k',k_0)}{E-k'^2/M+i0}. \end{aligned} \tag{2.42}$$

This is a linear integral equation for $T_m(E;k,k_0)$, but if we note that the k-dependence of the right-hand side is given by $\chi(k^2)$, $T(E;k',k)/\chi(k'^2)$ is in fact independent of k' and can be taken out of the integral. This leads to the following form of the T-matrix element,

$$T_m(E+i0;k,k_0) = \frac{1}{4\pi}\frac{\chi(k^2)\chi(k_0^2)}{\frac{2(E-\nu_0^{(m)})}{|g_0|^2} - \int_0^\infty \frac{dk'}{(2\pi)^3}\frac{k'^4\chi(k'^2)^2}{E-k'^2/M+i0}}, \tag{2.43}$$

which contains a function $\chi(k^2)$, which determines the momentum dependence. For low-energy collisions, the integral in the denominator can be evaluated as a power series in terms of E,

$$\begin{aligned} \int_0^\infty \frac{dk'}{(2\pi)^3}\frac{k'^4\chi(k'^2)^2}{E-k'^2/M+i0} = &-\frac{iM}{16\pi^2}(ME)^{3/2}\chi(ME)^2 \\ &- M\int_0^\infty \frac{dk'}{(2\pi)^3}k'^2\chi(k'^2)^2 - M^2E\int_0^\infty \frac{dk'}{(2\pi)^3}\chi(k'^2)^2 + O(E^2). \end{aligned} \tag{2.44}$$

We can substitute this into Eq. (2.43) and compare it with the low-energy expression of the on-shell T-matrix element,

$$T_m(E+i0;k,k_0)|_{k^2=k'^2=ME} = \frac{4\pi}{M}\frac{1}{v_m^{-1} - \frac{k_m}{2}ME + i(ME)^{3/2}}, \tag{2.45}$$

which yields the equations relating the bare quantities, $\nu_0^{(m)}$ and g_0, to the low-energy scattering data, the p-wave scattering volume v_m and the effective range[4] k_m,

$$\begin{aligned} v_m^{-1} &= -\frac{32\pi^2\nu_0^{(m)}}{M|g_0|^2} + \frac{2}{\pi}\int_0^\infty dk'\, k'^2\chi(k'^2)^2, \\ k_m &= -\frac{64\pi^2}{M^2|g_0|^2} - \frac{2}{\pi}\int_0^\infty dk'\, \chi(k'^2)^2 + 4v_m^{-1}\chi'(0). \end{aligned} \tag{2.46}$$

This is a p-wave analog of Eqs. (2.25) and (2.34).

[4]Note that k_m has the dimension of momentum. However, it is customary to call it the effective "range". Therefore, we follow this convention here.

Chapter 3

Universal relations in an anisotropic p-wave Fermi gas

In the vicinity of a scattering resonance, the scattering length diverges and the system becomes strongly correlated. There, controlled approximations based on perturbative expansions break down, and calculations of physical quantities become difficult. In such cases, it is of great use to have exact relations between observables that do not rely on a perturbation theory because they allow us, for example, to relate one measurement to other aspects of the system, or to test the validity of theoretical methods by imposing constraints.

For an s-wave resonance in a spin-1/2 Fermi gas in three dimensions, there are several universal relations that connect short-range and short-time correlations with thermodynamic quantities [52–60]. There, a single quantity, Tan's contact, bridges both sides of physics. On one hand, it characterizes the strength of the short-range and short-time correlations. Here, the "short" range means length scales smaller than the interparticle spacing and the thermal de Broglie length but larger than the range of interactions. For example, the momentum distribution for large momenta has a power-law tail, whose coefficient is Tan's contact:

$$n_{\boldsymbol{p}} \sim \frac{C}{p^4}. \tag{3.1}$$

Other correlation functions, such as the radio-frequency spectrum [64–67], the static [52] and dynamic [68–71] structure factors, and the viscosity spectral function [69, 72], also show characteristic power laws with coefficients solely determined by the contact, Plank's constant, the mass of atoms, and a dimensionless factor. On the other hand, Tan's contact is directly related to the thermodynamics. A prominent example is the adiabatic sweep theorem, which states that Tan's contact is the derivative of the energy

with respect to the scattering length:

$$C = 4\pi M \frac{\partial E}{\partial(-1/a)}. \tag{3.2}$$

Importantly, all these relations hold true very generally in the strongly correlated regime, regardless of the number of particles, whether the system is in the ground state or at finite temperatures. A crucial assumption is that the range of interactions is much shorter than any other length scales so that there is the window of universality where one can observe the power laws such as the one shown in Eq. (3.1). This is well satisfied in ultracold atomic gases, and the experiments have tested the universal relations and measured the contact [93–97].

Similar universal relations are also investigated for lower dimensions [58, 59, 76–78], bosonic systems [73–75], and mixtures of atomic species [73], with s-wave scattering resonances. Recently, they are also extended to p-wave [79–82] and d-wave [82, 83] resonances, and the experimental measurement of the p-wave contact was also reported [151]. The present author contributed to one of the first studies on the universal relations in the p-wave interacting Fermi gas.

The p-wave is the first partial wave that is anisotropic. This statement has twofold meanings. Firstly, the p-wave scattering amplitude has an angular dependence even when the interaction potential is isotropic. Secondly, in the case of a p-wave or higher-partial-wave Feshbach resonance, a microscopic interaction itself can be anisotropic because of an external magnetic field. Such an effect has been observed as multiplet structures of resonances [101, 102]. In the earlier studies of the universal relations in a p-wave Fermi gas, however, the latter effects are not fully taken into account.

Here, we discuss the universal relations in a spinless Fermi gas with an anisotropic p-wave resonance. In Section 3.1, we present the universal power laws in the high momentum distribution and the short-range density-density correlation function. We show that the contact in this case is not a single quantity, but a 3×3 component tensor, which we call the p-wave contact tensor. In Section 3.2, we derive the adiabatic sweep theorem, which relates the p-wave contact tensor to the derivative of the energy with respect to the p-wave scattering volume. In the derivation, we need to extend the p-wave scattering volume to anisotropic interactions. In Section 3.3, we discuss the p-wave contact tensor in the p-wave superfluid. In Section 3.4, we describe an experimental implementation to test the universal relations.

3.1 p-wave contact tensor in correlation functions

In this section, we discuss the high-momentum tail of the momentum distribution and the short-range behavior of the density-density correlation function, and introduce the notion of the p-wave contact tensor. For this purpose, we employ the following two-channel Hamiltonian:

$$\begin{aligned}\hat{H} = \sum_{\boldsymbol{p}} \left[\frac{p^2}{2M} \hat{a}^\dagger_{\boldsymbol{p}} \hat{a}_{\boldsymbol{p}} + \sum_{m=-1}^{1} \left(\frac{p^2}{4M} + \nu_0^{(m)} \right) \hat{b}^\dagger_{m\boldsymbol{p}} \hat{b}_{m\boldsymbol{p}} \right] \\ + \frac{1}{2} \sum_{\boldsymbol{p}_1, \boldsymbol{p}_2} \sum_{m=-1}^{1} \left[g_0 k Y_1^m(\hat{\boldsymbol{p}}_{12}) \chi(p_{12}^2) \hat{a}^\dagger_{\boldsymbol{p}_1} \hat{a}^\dagger_{\boldsymbol{p}_2} \hat{b}_{m\boldsymbol{p}_1+\boldsymbol{p}_2} + \text{H. c.} \right].\end{aligned} \tag{3.3}$$

Here, $\boldsymbol{p}_{12} \equiv \boldsymbol{p}_1 - \boldsymbol{p}_2$, $\hat{a}^\dagger_{\boldsymbol{p}}$ creates a fermionic atom with the momentum $\boldsymbol{p}$ in the open channel, and $\hat{b}^\dagger_{m\boldsymbol{p}}$ creates a closed-channel molecule with the projection m of the angular momentum and the momentum $\boldsymbol{p}$. This is exactly the same Hamiltonian as that given in Eq. (2.38), but in the momentum representation. The bare detuning $\nu_0^{(m)}$ and the coupling constant g_0 are determined by Eq. (2.46) so that the low-energy scattering data, the scattering volume and the effective range, are reproduced (see Sec. 2.2.2 for details of this procedure).

To discuss the correlation functions, we start from the Schrödinger equation. By noting that the Hamiltonian (3.3) conserves the total number of the atoms but not the numbers of the open-channel atoms N_o and the closed-channel molecules N_c separately, a state with the total number of atoms $N = N_\mathrm{o} + 2N_\mathrm{c}$ can be expressed as a sum of the states with different N_o and N_c:

$$\begin{aligned}|\Psi_N\rangle = \sum_{2N_\mathrm{o}+N_\mathrm{c}=N} \sum_{\{\boldsymbol{p}_k\}_k} \sum_{\{\boldsymbol{q}_k\}_k} \sum_{\{m_k\}_k} \frac{1}{N_\mathrm{o}! N_\mathrm{c}!} \Psi^{(N_\mathrm{o},N_\mathrm{c})}(\{\boldsymbol{p}_k\}_k, \{\boldsymbol{q}_k\}_k, \{m_k\}_k) \\ \times \hat{a}^\dagger_{\boldsymbol{p}_1} \dots \hat{a}^\dagger_{\boldsymbol{p}_{N_\mathrm{o}}} \hat{b}^\dagger_{m_1\boldsymbol{q}_1} \dots \hat{b}^\dagger_{m_{N_\mathrm{c}}\boldsymbol{q}_{N_\mathrm{c}}} |0\rangle .\end{aligned} \tag{3.4}$$

Here, $\{\boldsymbol{p}_k\}_k$ is the ordered set of the N_o momenta of the open-channel atoms, $\{\boldsymbol{q}_k\}_k$ and $\{m_k\}_k$ are the sets of the momenta and the projected angular momenta, respectively, of the N_c closed-channel molecules. We can then write down the time-independent Schrödinger equations in terms of the set of the wave functions:

$$(E - \hat{T})\Psi^{(N_\mathrm{o},N_\mathrm{c})} = \hat{I}_1 \left[\Psi^{(N_\mathrm{o}-2,N_\mathrm{c}+1)}\right] + \hat{I}_2 \left[\Psi^{(N_\mathrm{o}+2,N_\mathrm{c}-1)}\right], \tag{3.5}$$

where $\hat{T}$ is the kinetic energy including the detuning, and $\hat{I}_1$ and $\hat{I}_2$ denote the terms arising from $\hat{a}^\dagger\hat{a}^\dagger\hat{b}_m$ and $\hat{b}^\dagger_m\hat{a}\hat{a}$ in the Hamiltonian (3.3), respectively. The concrete forms

of $\hat{I}_1$ and $\hat{I}_2$ are as follows:

$$\begin{aligned}\hat{I}_1\left[\Psi^{(N_\mathrm{o}-2,N_\mathrm{c}+1)}\right](\{\boldsymbol{p}_k\}_k,\{\boldsymbol{q}_k\}_k,\{m_k\}_k) &= \sum_{i=1}^{N_\mathrm{o}}\sum_{j=i+1}^{N_\mathrm{o}}\sum_{m=-1}^{1}(-1)^{i+j+1}g_0 p_{ij}Y_1^m(\hat{\boldsymbol{p}}_{ij}) \\ &\times\chi(p_{ij}^2)\Psi^{(N_\mathrm{o}-2,N_\mathrm{c}+1)}\left(\{\boldsymbol{p}_k\}_k\setminus\{\boldsymbol{p}_i,\boldsymbol{p}_j\},\{\boldsymbol{q}_k\}_k+\{\boldsymbol{p}_i+\boldsymbol{p}_j\},\{m_k\}_k+\{m\}\right),\end{aligned} \tag{3.6}$$

$$\begin{aligned}\hat{I}_2\left[\Psi^{(N_\mathrm{o}+2,N_\mathrm{c}-1)}\right](\{\boldsymbol{p}_k\}_k,\{\boldsymbol{q}_k\}_k,\{m_k\}_k) &= \sum_{\boldsymbol{p}_1',\boldsymbol{p}_2'}\sum_{i=1}^{N_\mathrm{c}}\frac{g_0}{2}p_{12}'Y_1^{m_i}(\hat{\boldsymbol{p}}_{12}') \\ &\times\chi(p_{12}')\Psi^{(N_\mathrm{o}+2,N_\mathrm{c}-1)}\left(\{\boldsymbol{p}_1',\boldsymbol{p}_2'\}+\{\boldsymbol{p}_k\}_k,\{\boldsymbol{q}_k\}_k\setminus\{\boldsymbol{q}_i\},\{m_k\}_k\setminus\{m_i\}\right).\end{aligned} \tag{3.7}$$

Here, $\boldsymbol{p}_{ij}\equiv\boldsymbol{p}_i-\boldsymbol{p}_j$, $\boldsymbol{p}_{12}'\equiv\boldsymbol{p}_1'-\boldsymbol{p}_2'$, and $\setminus$ and $+$ denote the set operations of subtraction and addition, respectively.

As we are interested in the high-momentum distribution, let us analyze Eq. (3.5) for $\boldsymbol{p}_1$ that is larger than typical system's momentum scales such as the Fermi momentum p_F and the thermal momentum p_T, but smaller than the cutoff scale set by the range of the interaction. On the right-hand side, the dominant contributions come from $\hat{I}_1$, where the terms with $i=1$ in Eq. (3.6) grow linearly for a large $\boldsymbol{p}_1$ due to the factor of p_{1j}. Therefore, the Schrödinger equation (3.5) reduces asymptotically to

$$\begin{aligned}(E-\hat{T})\Psi^{(N_\mathrm{o},N_\mathrm{c})}(\{\boldsymbol{p}_k\}_k,\{\boldsymbol{q}_k\}_k,\{m_k\}_k) &\simeq \sum_{j=2}^{N_\mathrm{o}}\sum_{m=-1}^{1}(-1)^j g_0 p_{1j}Y_1^m(\hat{\boldsymbol{p}}_{1j}) \\ &\times\Psi^{(N_\mathrm{o}-2,N_\mathrm{c}+1)}\left(\{\boldsymbol{p}_k\}_k\setminus\{\boldsymbol{p}_1,\boldsymbol{p}_j\},\{\boldsymbol{q}_k\}_k+\{\boldsymbol{p}_1+\boldsymbol{p}_j\},\{m_k\}_k+\{m\}\right).\end{aligned} \tag{3.8}$$

It should be noted that the amplitude of the right-hand side concentrates around $\boldsymbol{p}_j\sim-\boldsymbol{p}_1$ with the width of the order of p_T, because it depends on the wave function with $\boldsymbol{p}_1+\boldsymbol{p}_j$ in its momentum argument of a closed-channel molecule. With this in mind, the momentum distribution in the $(N_\mathrm{o},N_\mathrm{c})$ sector can be calculated by integrating out the variables other than $\boldsymbol{p}_1$ from $\frac{1}{N_\mathrm{o}!N_\mathrm{c}!}|\Psi^{(N_\mathrm{o},N_\mathrm{c})}|^2$. Retaining only the leading terms, we find

$$n_{\boldsymbol{p}_1}^{(N_\mathrm{o},N_\mathrm{c})} \equiv \frac{N_\mathrm{o}}{N_\mathrm{o}!N_\mathrm{c}!}\sum_{\{\boldsymbol{p}_k\}_k\setminus\{\boldsymbol{p}_1\}}\sum_{\{\boldsymbol{q}_k\}_k}\sum_{\{m_k\}_k}\left|\Psi^{(N_\mathrm{o},N_\mathrm{c})}(\{\boldsymbol{p}_k\}_k,\{\boldsymbol{q}_k\}_k,\{m_k\}_k)\right|^2 \tag{3.9}$$

$$\begin{aligned}&\sim\frac{M^2|g_0|^2}{p_1^2}\frac{1}{(N_\mathrm{o}-2)!N_\mathrm{c}!}\sum_{m,m'}\sum_{\{\boldsymbol{p}_k\}_k\setminus\{\boldsymbol{p}_1\}}\sum_{\{\boldsymbol{q}_k\}_k}\sum_{\{m_k\}_k}Y_1^{m*}(\hat{\boldsymbol{p}}_1)Y_1^{m'}(\hat{\boldsymbol{p}}_1) \\ &\times\Psi^{(N_\mathrm{o}-2,N_\mathrm{c}+1)*}(\{\boldsymbol{p}_k\}_k\setminus\{\boldsymbol{p}_1,\boldsymbol{p}_2\},\{\boldsymbol{q}_k\}_k+\{\boldsymbol{p}_2\},\{m_k\}_k+\{m\}) \\ &\times\Psi^{(N_\mathrm{o}-2,N_\mathrm{c}+1)}(\{\boldsymbol{p}_k\}_k\setminus\{\boldsymbol{p}_1,\boldsymbol{p}_2\},\{\boldsymbol{q}_k\}_k+\{\boldsymbol{p}_2\},\{m_k\}_k+\{m'\}).\end{aligned} \tag{3.10}$$

The momentum distribution itself is obtained by summing up this for all the (N_o, N_c) pairs with $2N_o + N_c = N$. By inspection, we find that it has the following compact expression:

$$n_{\boldsymbol{p}_1} \sim \frac{M^2|g_0|^2}{p_1^2} \sum_{m,m'} Y_1^{m*}(\hat{\boldsymbol{p}}_1) Y_1^{m'}(\hat{\boldsymbol{p}}_1) \left\langle \Psi_N \left| \sum_{\boldsymbol{q}} \hat{b}^\dagger_{m\boldsymbol{q}} \hat{b}_{m'\boldsymbol{q}} \right| \Psi_N \right\rangle \tag{3.11}$$

$$\equiv \sum_{m,m'} C_{mm'} \frac{Y_1^{m*}(\hat{\boldsymbol{p}}_1) Y_1^{m'}(\hat{\boldsymbol{p}}_1)}{p_1^2}, \tag{3.12}$$

where we define the p-wave contact tensor $C_{mm'}$:

$$C_{mm'} \equiv M^2|g_0|^2 \left\langle \sum_{\boldsymbol{q}} \hat{b}^\dagger_{m\boldsymbol{q}} \hat{b}_{m'\boldsymbol{q}} \right\rangle. \tag{3.13}$$

This result follows from the time-independent Schrödinger equation and is applicable to pure states. The extension to thermal states is obvious; the power-law tail of Eq. (3.12) has the same power, with the definition of the p-wave contact tensor in Eq. (3.13) still applicable by regarding the average as the thermal average. Therefore, we conclude that the momentum distribution $n_{\boldsymbol{p}}$ of a spinless Fermi gas with an anisotropic p-wave resonance, whether it is in a pure state or a thermal mixture state, has a tail that is proportional to p^{-2} and has an anisotropy as shown in Eq. (3.12), and that its coefficients are given by the p-wave contact tensor, which is defined in Eq. (3.13).

By a similar argument, we can find the short-range behavior of the density-density correlation function,

$$g(\boldsymbol{r}) \equiv \langle \hat{n}(\boldsymbol{r}) \hat{n}(0) \rangle, \tag{3.14}$$

where $\hat{n}(\boldsymbol{r}) \equiv \hat{\psi}^\dagger(\boldsymbol{r}) \hat{\psi}(\boldsymbol{r})$ is the density operator of open-channel atoms. In the above discussion on the wave function in the momentum representation, one can see that the wave function diminishes with $1/p_{ij}$ when the relative momentum of the ith and jth atoms becomes large. This high-momentum behavior translates into the short-range singularity of $1/r_{ij}^2$ in the real space, where $\boldsymbol{r}_{ij}$ is the relative position of the same pair of the atoms. By collecting the leading-order terms carefully, we find the following asymptotic form of the density-density correlation function:

$$g(\boldsymbol{r}) \equiv \langle \hat{n}(\boldsymbol{r}) \hat{n}(0) \rangle = \sum_{m,m'} C_{mm'} \frac{Y_1^{m*}(\hat{\boldsymbol{r}}) Y_1^{m'}(\hat{\boldsymbol{r}})}{16\pi^2 V r^4}, \tag{3.15}$$

where V is the volume of the gas.

Some comments are in order. From its definition (3.13), we see that the p-wave contact is directly related to the closed-channel molecules. In particular, its diagonal components are the number of the closed-channel molecules with the projected angular momentum m:

$$C_{mm} = M^2 |g_0|^2 N_m. \tag{3.16}$$

Generally, $C_{mm'}$ is a 3×3 Hermitian matrix, which can be diagonalized by a unitary transformation. Once diagonalized, the diagonal components can again be interpreted as the number of the closed-channel molecules in a superposition state of $m = 0$ and ± 1. If the p-wave interaction has anisotropy, as is the case for a Feshbach resonance, however, such a superposition state does not have a well-defined energy. The projected angular momentum is thus the most natural quantum number in the case of the magnetic Feshbach resonance.

The definition of the p-wave contact tensor also implies that $C_{mm'}$ transforms under spatial rotation in the same way as the product $Y_1^m(\hat{\boldsymbol{r}}) Y_1^{m'*}(\hat{\boldsymbol{r}})$. In particular, its trace is invariant under any rotation and the diagonal components are invariant under rotation around the quantization axis, which is defined by an external magnetic field in the case of a Feshbach resonance. On the other hand, the off-diagonal components represent the breaking of axisymmetry in the short-range correlations. We will later see a concrete example where the axisymmetry breaking happens and the p-wave contact tensor acquires nonzero off-diagonal components.

The same field theory as Eq. (3.3) is also used as an effective-field theory of the halo nuclei [99]. Therefore, the results here hold true in such nuclear systems. In that case, however, the field operator $\hat{b}_{\boldsymbol{p}}$ is just an auxiliary field and no longer represents a physical entity. A physical interpretation that is also applicable to nuclear systems is obtained from Eq. (3.15). The density-density correlation function measures the number of the particles that are at a distance of $\boldsymbol{r}$ from another particle. Equation (3.15), therefore, implies that the p-wave contact tensor is a measure of the number of the pairs of atoms within a small distance.

3.2 Adiabatic sweep theorem

The p-wave contact tensor is directly related to the thermodynamics through the adiabatic sweep theorem. To derive the theorem, we need to define a generalized p-wave scattering volume $v_{mm'}$. If a p-wave scattering process from an m state into an m' state

is allowed, the scattering amplitude takes the following form:

$$f(\hat{\boldsymbol{p}}, \hat{\boldsymbol{p}}', k) = \sum_{m,m'=-1}^{1} 4\pi k^2 [\mathcal{F}(k)]_{m,m'} Y_1^m(\hat{\boldsymbol{p}}) Y_1^{m'*}(\hat{\boldsymbol{p}}'), \tag{3.17}$$

where $k\hat{\boldsymbol{p}}'$ is the incoming momentum and $k\hat{\boldsymbol{p}}$ is the outgoing momentum. The matrix $\mathcal{F}(k)$ represents the transition amplitude, whose inverse has the low-energy expansion,

$$[\mathcal{F}^{-1}(k)]_{m,m'} = -\frac{1}{v_{mm'}} + \frac{1}{2} k_{mm'} k^2 - ik^3 \delta_{m,m'} + O(k^2), \tag{3.18}$$

which defines the generalized scattering volume $v_{mm'}$ and the effective range $k_{mm'}$. When a p-wave interaction preserves axisymmetry, $\mathcal{F}(k)$ is a diagonal matrix, with the scattering volume $v_{mm'} = v_m \delta_{m,m'}$ and the effective range $k_{mm'} = k_m \delta_{m,m'}$. Similarly, we define a matrix $\mathcal{T}(E + i0; k, k_0)$ by the spherical harmonic expansion of the off-shell T-matrix:

$$T(E + i0; \boldsymbol{k}, \boldsymbol{k}_0) = \sum_{m,m'=-1}^{1} 4\pi k k_0 [\mathcal{T}(E + i0; k, k_0)]_{m,m'} Y_1^m(\hat{\boldsymbol{k}}) Y_1^{m'*}(\hat{\boldsymbol{k}}'). \tag{3.19}$$

The partial amplitude $\mathcal{F}(k)$ and the on-shell T-matrix $\mathcal{T}(k^2/M; k, k)$ are proportional to each other as in the scattering theory with spherical symmetry:

$$\mathcal{F}(k) = -\frac{M}{4\pi} \mathcal{T}(k^2/M; k, k). \tag{3.20}$$

Within the *axisymmetric* two-channel model, the scattering volume is controlled by the detuning parameters $\nu_0^{(m)}$. This can be naturally generalized by introducing the "off-diagonal" detuning[1] of the following form:

$$\sum_{m,m'=-1}^{1} \nu_0^{(m,m')} \hat{\phi}_m^\dagger \hat{\phi}_{m'} \equiv \hat{\boldsymbol{\phi}}^\dagger \tilde{\nu}_0 \hat{\boldsymbol{\phi}}, \tag{3.21}$$

where we introduce the vector of the closed-channel operators $\hat{\boldsymbol{\phi}} \equiv \left(\hat{\phi}_{-1},\ \hat{\phi}_0,\ \hat{\phi}_1\right)$ and the matrix $\tilde{\nu}_0$, whose elements are $\nu_0^{(m,m')}$. With this term, we can again solve the two-body problem. The Lippmann-Schwinger equation for the T-matrix, which is now

[1] One can also generalize the inter-channel coupling in such a way that it converts a pair of atoms with the projected relative angular momentum m into a closed-channel dimer with m'. However, such coupling constants are determined solely by $k_{mm'}$, not by $v_{mm'}$, and thus irrelevant in the current argument.

a matrix $\mathcal{T}$, reads

$$\begin{aligned}\mathcal{T}(E+i0;k,k_0) = &\frac{|g_0|^2\chi(k^2)\chi(k_0^2)}{8\pi(EI_3-\tilde{v}_0)} \\ &+\frac{|g_0|^2\chi(k^2)}{2(EI_3-\tilde{v}_0)}\int_0^\infty \frac{k'^2\,dk'}{(2\pi)^3}\frac{k'^2\chi(k'^2)}{E-k'^2/M+i0}\mathcal{T}(E+i0;k',k_0),\end{aligned} \tag{3.22}$$

where I_3 is the three-dimensional identity matrix. We can solve this in a similar manner to the argument in Section 2.2.2, yielding

$$\chi(k^2)\chi(k_0^2)\mathcal{T}^{-1}(E+i0;k,k_0) = \frac{8\pi}{|g_0|^2}(EI_3-\tilde{v}_0) - \int_0^\infty \frac{dk'}{2\pi^2}\frac{k'^4\chi(k'^2)^2}{E-k'^2/M+i0}. \tag{3.23}$$

By comparing this with the low-energy expansion of $\mathcal{F}^{-1}(k)$, we can relate the bare parameters to the scattering data, namely, the generalized scattering volume

$$v_{mm'}^{-1} = -\frac{32\pi^2\nu_0^{(m,m')}}{M|g_0|^2} + \frac{2}{\pi}\int_0^\infty dk'\,k'^2\chi(k'^2)^2, \tag{3.24}$$

and the effective range

$$k_{mm'} = -\frac{64\pi^2}{M^2|g_0|^2} - \frac{2}{\pi}\int_0^\infty dk'\,\chi(k'^2)^2 + 4v_{mm'}^{-1}\chi'(0) \tag{3.25}$$

$$\simeq -\frac{64\pi^2}{M^2|g_0|^2} - \frac{2}{\pi}\int_0^\infty dk'\,\chi(k'^2)^2, \tag{3.26}$$

where we assume the system is near resonance $v_{mm'}^{-1} \simeq 0$.

We are prepared to show the adiabatic sweep theorem for the p-wave contact tensor. By using Eqs. (3.24) and (3.26), we obtain

$$\frac{\partial\hat{H}}{\partial(-1/v_{mm'}^{-1})} = \frac{M|g_0|^2}{32\pi^2}\int d\boldsymbol{r}\,\hat{\phi}_m^\dagger(\boldsymbol{r})\hat{\phi}_{m'}(\boldsymbol{r}). \tag{3.27}$$

On the other hand, the Hellmann-Feynman theorem reads

$$\frac{\partial E}{\partial(-1/v_{mm'}^{-1})} = \left\langle\frac{\partial\hat{H}}{\partial(-1/v_{mm'}^{-1})}\right\rangle. \tag{3.28}$$

These two equations, combined with Eq. (3.13), yield the adiabatic sweep theorem:

$$C_{mm'} = 32\pi^2 M\frac{\partial E}{\partial(-1/v_{mm'})}. \tag{3.29}$$

After taking the derivative with respect to $-1/v_{mm'}$, we can set its off-diagonal elements to be zero as they should be in realistic Feshbach resonances. However, this does not necessarily make the off-diagonal components of the p-wave contact tensor vanish. As we shall see in the next section, the off-diagonal components of $C_{mm'}$ can be nonzero even in the absence of the off-diagonal components of the generalized scattering volume.

3.3 Contact tensor in p-wave superfluids

A p-wave superfluid provides an example where the multicomponent nature of the p-wave contact tensor plays a significant role. In particular, it exhibits the off-diagonal components of the p-wave contact tensor due to the spontaneous breaking of axisymmetry. To show this, we first derive the expression of the p-wave contact tensor within the mean-field approximation to the Hamiltonian (3.3) [103–105]. To this end, a convenient order parameter is the condensate wave function of the closed-channel molecules:

$$\varphi_m \equiv \langle \hat{\phi}_m(\boldsymbol{r}) \rangle \quad (m = 0, \pm 1). \tag{3.30}$$

In steady states, this is equivalent to the pair amplitude, or the gap function [152], which are the usual order parameters of fermionic superfluids; the condensate of the closed-channel molecules exists if and only if the condensate of the Cooper pairs exists. By ignoring the terms that is quadratic in terms of fluctuations of $\hat{\phi}_m(\boldsymbol{r})$ around φ_m, we find

$$\left\langle \hat{\phi}_m^\dagger(\boldsymbol{r}) \hat{\phi}_{m'}(\boldsymbol{r}) \right\rangle \simeq \varphi_m \varphi_{m'}, \tag{3.31}$$

when the system is deep in the superfluid state. Combined with Eq. (3.13), this yields

$$C_{mm'} \simeq |g_0|^2 \varphi_m \varphi_{m'}, \tag{3.32}$$

which relates the p-wave contact tensor and the order parameter of the p-wave superfluid. We would like to emphasize that this does not mean that the p-wave contact tensor vanishes in the normal phase; a normal p-wave Fermi gas is shown to have a finite p-wave contact tensor, which is, however, diagonal [80]. This is natural because the energy in the normal phase changes as the p-wave scattering volume is modulated, and with this, the adiabatic sweep theorem implies a finite p-wave contact. Therefore, Eq. (3.32) is a good approximation for lower temperatures, where the fluctuation is small. Note, however, that the off-diagonal components in a uniform Fermi gas in a normal phase are zero because the axisymmetry is preserved.

Equation (3.32) makes it clear that the p-wave contact tensor is diagonal within the mean-field approximation if and only if exactly one component of φ_m is nonzero. There are two such possibilities: the $p_x \pm ip_y$ superfluid and the p_z superfluid. The phase diagram of the spinless Fermi gas with a p-wave Feshbach resonance has been investigated by other groups [103–105]. When the interaction is spherically symmetric, the spinless Fermi gas is similar to the liquid ^{3}He in a large magnetic field, where A_1 phase is realized. Likewise, for the spinless Fermi gas, it is shown that the time-reversal symmetry broken $p_x + ip_y$ phase is realized if the Feshbach resonance is spherically symmetric. The p-wave Feshbach resonance, on the other hand, has a natural anisotropy due to the magnetic dipole-dipole interaction, in such a way that the interaction in the $m = 0$ channel is more attractive than that in the $m = \pm 1$ channels [101]. Therefore, if the splitting of the p-wave Feshbach resonances is sufficiently large, the p_z superfluid has the lowest energy. For an intermediate splitting of the resonances, the competition between the two opposite tendencies determines the phase. Indeed, it is shown that the superfluid in this regime is in the $p_z + i\beta p_y$ state, in which the order parameters satisfy

$$\varphi_0 \neq 0, \quad \varphi_{-1} = \varphi_1. \tag{3.33}$$

The time-reversal symmetry and the axisymmetry is broken in this phase. As a result, the p-wave contact tensor exhibits the off-diagonal components. Therefore, one can distinguish the different superfluid phases by measuring the p-wave contact tensor. In particular, the presence of nonzero off-diagonal components unambiguously signals the $p_z + i\beta p_y$ superfluid.

3.4 Experimental implementation

A Feshbach resonance is the most common tool of controlling interatomic interactions in ultracold atomic systems. However, since it is axisymmetric, it cannot tune $1/v_{mm'}$ for $m \neq m'$. Here, we propose an alternative path to control $1/v_{mm'}$, where we utilize a two-photon Raman process (see Figure 3.1).

Let $|e\rangle$ be a diatomic molecular state that couples to two of the closed-channel states $|m_1\rangle$ and $|m_2\rangle$ by lasers. The resonant frequencies for $|m_1\rangle$ and $|m_2\rangle$ are denoted by ω_1 and ω_2, and the Rabi frequencies by Ω_1 and Ω_2, respectively. With the rotational wave approximation, the effective Hamiltonian representing these couplings is

$$\hat{H}_{\text{Raman}} = \left(\hat{\phi}^\dagger_{m_1},\ \hat{\phi}^\dagger_{m_2},\ \hat{\phi}^\dagger_e\right) h_{\text{Raman}} \begin{pmatrix} \hat{\phi}_{m_1} \\ \hat{\phi}_{m_2} \\ \hat{\phi}_e \end{pmatrix}, \tag{3.34}$$

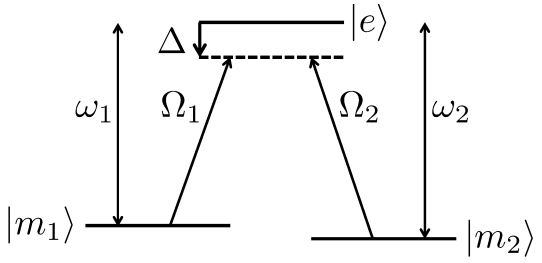

Figure 3.1: Λ-configuration to control $v_{mm'}$ and measure the p-wave contact tensor. The molecular states $|m_j\rangle$ ($j = 1, 2$) are two of the three closed-channel states, and $|e\rangle$ denotes another excited molecular state, with the energy difference ω_j. The two states $|m_j\rangle$ and $|e\rangle$ are coupled by the laser with the complex Rabi frequency Ω_j and the detuning Δ. [Figure reproduced from Yoshida and Ueda, Phys. Rev. A **94**, 033611 (2016). © 2016 American Physical Society.]

$$h_{\text{Raman}} \equiv \begin{pmatrix} 0 & 0 & \Omega_1^*/2 \\ 0 & 0 & \Omega_2^*/2 \\ \Omega_1/2 & \Omega_2/2 & \Delta \end{pmatrix} \tag{3.35}$$

where $\hat{\phi}_e^\dagger$ is the creation operator of a diatomic molecule in the state $|e\rangle$, and Δ is the detuning. For the moment, we omit the spatial argument from the bosonic operators of the diatomic molecules. By diagonalizing h_{Raman}, we find three eigenvalues,

$$0, \qquad \frac{1}{2}\left(\Delta \pm \sqrt{\Delta^2 + |\Omega_1|^2 + |\Omega_2|^2}\right) \equiv \omega_\pm, \tag{3.36}$$

with the corresponding eigenvectors,

$$|0\rangle \propto \left(\Omega_2,\ -\Omega_1,\ 0\right)^T, \tag{3.37}$$

$$|\pm\rangle \propto \left(\Omega_1^*,\ \Omega_2^*,\ 2\omega_\pm\right)^T. \tag{3.38}$$

In the weak-field limit, where $\Omega_1 \to 0$ and $\Omega_2 \to 0$, $|+\rangle$ is adiabatically connected to the excited molecular state $|e\rangle$, while the subspace spanned by $|0\rangle$ and $|-\rangle$ reduces to the subspace of the closed-channel molecules. Now, suppose that no molecules are in the excited state $|e\rangle$ at the initial time and that the intensities of the lasers are adiabatically ramped up. Then we can ignore the state $|+\rangle$ and approximate $\hat{H}_{\text{Raman}}$ to

$$\hat{H}_{\text{Raman}} \simeq \omega_- \hat{\phi}_-^\dagger \hat{\phi}_-, \tag{3.39}$$

where $\hat{\phi}_-^\dagger$ creates a molecule in the $|-\rangle$ state. For the large detuning limit $\Delta \gg |\Omega_1|$ and $\Delta \gg |\Omega_2|$, we obtain

$$\hat{H}_{\text{Raman}} \simeq \frac{1}{4\Delta}\left(|\Omega_1|^2\hat{\phi}_{m_1}^\dagger\hat{\phi}_{m_1} + |\Omega_2|^2\hat{\phi}_{m_2}^\dagger\hat{\phi}_{m_2} + \Omega_2^*\Omega_1\hat{\phi}_{m_1}^\dagger\hat{\phi}_{m_2} + \Omega_1^*\Omega_2\hat{\phi}_{m_2}^\dagger\hat{\phi}_{m_1}\right). \quad (3.40)$$

This amounts to sweeping $\nu_0^{(m_1,m_2)} = \nu_0^{(m_2,m_1)*}$ as $\Omega_2^*\Omega_1/4\Delta$, and thus to tuning $1/v_{m_1m_2}$ for $m_1 \neq m_2$.

We can use a similar configuration to measure the p-wave contact tensor. This time, the lasers are suddenly tuned on, and the frequencies are set close to the resonance so that $\Delta \ll |\Omega_1|, |\Omega_2|$. We also assume that the lifetime of the excited state $|e\rangle$ is much shorter than that of $|m_1\rangle$ and $|m_2\rangle$. In this case, immediately after one turns on the lasers, all the eigenstates of h_{Raman} are populated. After the lifetime of the excited state $|e\rangle$, on the other hand, there remain only the molecules in $|0\rangle$, so called the dark state, which does not involve $|e\rangle$. Therefore, by counting the number of the closed-channel molecules, we obtain

$$N_m = \left\langle\hat{\phi}_0^\dagger\hat{\phi}_0\right\rangle \quad (3.41)$$

$$= \frac{1}{|\Omega_1|^2 + |\Omega_2|^2}\left\langle|\Omega_2|^2\hat{\phi}_{m_1}^\dagger\hat{\phi}_{m_1} + |\Omega_1|^2\hat{\phi}_{m_2}^\dagger\hat{\phi}_{m_2} - |\Omega_1\Omega_2|e^{-i\theta}\hat{\phi}_{m_1}^\dagger\hat{\phi}_{m_2} - |\Omega_1\Omega_2|e^{i\theta}\hat{\phi}_{m_2}^\dagger\hat{\phi}_{m_1}\right\rangle, \quad (3.42)$$

where θ is the relative phase of Ω_1 and Ω_2. This means that by repeating the measurement of N_m with the different θ, we can determine $\langle\hat{\phi}_{m_1}^\dagger\hat{\phi}_{m_2}\rangle$, which in turn determines the (m_1, m_2)-component of the p-wave contact tensor with Eq. (3.13).

Chapter 4

Few-body spectrum of mass-balanced impurity-boson systems

This and the following two chapters concern universality in a single impurity immersed in a weakly interacting Bose gas, where the impurity-boson interaction is near a Feshbach resonance.

In this chapter, we consider a few bosons interacting with an impurity. This few-body problem in the impurity-boson system is interesting not only on its own, but also from the view point of the zero-density limit $n \to 0$ of the Bose gas. On one hand, if we consider an impurity in a dilute Bose gas, properties of the impurity are inevitably subject to few-body correlations. In particular, if we take the dilute limit of the background Bose gas, the energy spectrum of this many-body system reduces to that of the few-body systems. On the other hand, it exhibits the Efimov effect. When one particle interacts resonantly with two identical bosons, there is an infinite series of shallow bound states, which are related to each other by discrete scale transformation with a scaling factor of 1986.1 [6]. This property is universal; regardless of details of a resonant interaction, the scaling factor is fixed by the mass ratio of the impurity and the bosons.

Here, we explore stronger universality in the Efimov effect of the impurity-boson systems. The universal scale invariance generally applies to excited, shallow Efimov trimers, whose radii are much larger than microscopic length scales such as the range of interactions. The ground state of three identical bosons, on the other hand, is known to deviate from the universal scale invariance by 10-20% [9, 10]. Intuitively, this is because the radius of the ground state is comparable to the microscopic scales, which results in the significant probability that the particles are within the range of the interaction. However, for the impurity-boson systems, the size of the ground-state trimer greatly exceeds the range of interactions, which expectedly makes it possible that the ground and lower excited states are almost insensitive to short-range details.

To show this, we calculate the energies of the few-body bound states using the r_0- and Λ-models, whose precise definitions are given in Section 4.1. In Section 4.2, by solving the Schrödinger equations for the mass-balanced impurity-boson systems, we obtain the ground and the first-excited trimer spectra, and also two tetramer states below the ground-state Efimov trimer. The energy scale of these states depends on the microscopic details of the models. However, we show that various dimensionless ratios formed by these low-lying spectra have universal values, and that the ground and the first-excited states are already universal. As a consequence of this universality and for later use, we derive the relation between the hard-core diameter of the bosons and the three-body parameter. In Section 4.3, we argue that the scale separation between the three-body parameter and the microscopic length scales is behind the universality of the ground state of the mass-balanced impurity-boson systems. As a comparison, we calculate the energies of the ground and first-excited states in mass-imbalanced systems, and show how the universality is lost as the impurity particle is made lighter.

4.1 Models and Schrödinger equations

Consider one particle interacting with two identical bosons (the 2+1 system), where the impurity-boson interaction is of the delta-function type with the infinite s-wave scattering length and there is no interaction between bosons. It is known that the energy spectrum of the 2+1 system is not bounded from below, as noted by Thomas [153] and analyzed in more detail by Efimov [6]. To cure this situation, we need to introduce the so-called three-body parameter a_-, which is defined as the s-wave scattering length at which the lowest-energy three-body bound state appears from the three-atom continuum (see Fig. 4.1). In theoretical calculations, this can be done in various ways. One can, for example, use some finite-range potentials, or introduce repulsive interactions between the bosons. Here, we use two different approaches, based on the two-channel model discussed in Section 2.2.1, to obtain a finite three-body parameter:

- *r_0-model* — This is the two-channel model after the limit $U \to 0$ is taken. The effective range r_0 is related to the three-body parameter by $a_- = 2467 r_0$ [108].

- *Λ-model* — In this model, we impose an ultraviolet cutoff at the momentum Λ on the atoms when one atom and the impurity form a closed-channel molecule. We also take $U \to 0$ and $g \to \infty$. This is equivalent to introducing a three-body interaction in the contact-interaction model [154].

In both cases, where we take $U \to 0$, we start from the two-channel Hamiltonian of the following form:

$$\hat{H} = \sum_{\boldsymbol{p}} \left[\varepsilon_{\boldsymbol{p}} \hat{b}_{\boldsymbol{p}}^\dagger \hat{b}_{\boldsymbol{p}} + \varepsilon_{\boldsymbol{p}} \hat{c}_{\boldsymbol{p}}^\dagger \hat{c}_{\boldsymbol{p}} + (\varepsilon_{\boldsymbol{p}}^{\mathrm{d}} + \nu_0) \hat{d}_{\boldsymbol{p}}^\dagger \hat{d}_{\boldsymbol{p}} \right] + g \sum_{\boldsymbol{p},\boldsymbol{q}} \left(\hat{d}_{\boldsymbol{p}+\boldsymbol{q}}^\dagger \hat{b}_{\boldsymbol{q}} \hat{c}_{\boldsymbol{p}} + \hat{c}_{\boldsymbol{p}}^\dagger \hat{b}_{\boldsymbol{q}}^\dagger \hat{d}_{\boldsymbol{p}+\boldsymbol{q}} \right). \tag{4.1}$$

Here, $\sum_{\boldsymbol{p}} \equiv \int \frac{d\boldsymbol{p}}{(2\pi)^3}$. The operators $\hat{b}_{\boldsymbol{p}}^\dagger$ and $\hat{c}_{\boldsymbol{p}}^\dagger$ create a boson and the impurity, respectively, with the momentum $\boldsymbol{p}$ and the energy $\varepsilon_{\boldsymbol{p}} = p^2/2m$, where we assume that the impurity and the bosons have the equal mass. The operator $\hat{d}_{\boldsymbol{p}}^\dagger$ creates a closed-channel dimer formed by the impurity and a boson, which has the momentum $\boldsymbol{p}$ and the energy $\varepsilon_{\boldsymbol{p}}^{\mathrm{d}} = p^2/4m$. The bare detuning ν_0 and the inter-channel coupling[1] g are determined so as to reproduce the s-wave scattering length a and the effective range r_0 of the impurity-boson scattering. By imposing an ultraviolet cutoff k_0 and carrying out the renormalization procedure as described in Section 2.2.1, we obtain

$$a^{-1} = \frac{4\pi}{mg^2} \left(\frac{mg^2}{2\pi^2} k_0 - \nu_0 \right), \quad r_0 = -\frac{8\pi}{m^2 g^2}. \tag{4.2}$$

In the following discussion, we always take $k_0 \to \infty$ when it is possible, and therefore $\nu_0 \to \infty$ for a fixed a^{-1}, in order for k_0 to drop out of the problem.

The number of the impurities and the number of the bosons are both conserved quantities, when we count one closed-channel dimer as one impurity plus one boson. Therefore, we can write down the general wave functions for the systems with one impurity and N bosons, where the state vectors for $N = 1, 2$, and 3, are written as follows:

$$|\Psi_2\rangle = \left(\sum_{\boldsymbol{p}} \alpha_{\boldsymbol{p}} \hat{c}_{-\boldsymbol{p}}^\dagger \hat{b}_{\boldsymbol{p}}^\dagger + \gamma_0 \hat{d}_0^\dagger \right) |0\rangle , \tag{4.3}$$

$$|\Psi_3\rangle = \left(\sum_{\boldsymbol{p}_1,\boldsymbol{p}_2} \frac{1}{2} \alpha_{\boldsymbol{p}_1\boldsymbol{p}_2} \hat{c}_{-\boldsymbol{p}_1-\boldsymbol{p}_2}^\dagger \hat{b}_{\boldsymbol{p}_1}^\dagger \hat{b}_{\boldsymbol{p}_2}^\dagger + \sum_{\boldsymbol{p}} \gamma_{\boldsymbol{p}} \hat{d}_{-\boldsymbol{p}}^\dagger \hat{b}_{\boldsymbol{p}}^\dagger \right) |0\rangle , \tag{4.4}$$

$$|\Psi_4\rangle = \left(\sum_{\boldsymbol{p}_1,\boldsymbol{p}_2,\boldsymbol{p}_3} \frac{1}{6} \alpha_{\boldsymbol{p}_1\boldsymbol{p}_2\boldsymbol{p}_3} \hat{c}_{-\boldsymbol{p}_1-\boldsymbol{p}_2-\boldsymbol{p}_3}^\dagger \hat{b}_{\boldsymbol{p}_1}^\dagger \hat{b}_{\boldsymbol{p}_2}^\dagger \hat{b}_{\boldsymbol{p}_3}^\dagger + \sum_{\boldsymbol{p}_1,\boldsymbol{p}_2} \frac{1}{2} \gamma_{\boldsymbol{p}_1\boldsymbol{p}_2} \hat{d}_{-\boldsymbol{p}_1-\boldsymbol{p}_2}^\dagger \hat{b}_{\boldsymbol{p}_1}^\dagger \hat{b}_{\boldsymbol{p}_2}^\dagger \right) |0\rangle . \tag{4.5}$$

Here, $|0\rangle$ represents the zero-particle vacuum, and α and γ are the wave functions describing the states that have the impurity in the open- and closed-channels, respectively. The bosonic symmetry implies that they are invariant under exchange of their momentum arguments. In the r_0-model, the domain of α and γ is not restricted. On the other hand,

[1] As shown in Section 2.2.1, g is not renormalized when $U \to 0$. This is why we use g, instead of g_0 here.

the Λ-model is defined as the one that imposes the ultraviolet cutoff on γ, while the open-channel functions α are defined in the entire momentum space as in the r_0-model.

The Schrödinger equations $(\hat{H} - E)\,|\Psi_{N+1}\rangle = 0$ involve both α and γ. However, one can remove the open-channel wave function α to obtain the equations of the closed-channel wave function γ only. Here, we demonstrate this procedure in the four-body case. The other cases can be treated in a similar manner. The Schrödinger equation $(\hat{H} - E)\,|\Psi_4\rangle = 0$ reads

$$\left(E - \varepsilon_{\boldsymbol{p}_1+\boldsymbol{p}_2+\boldsymbol{p}_3} - \varepsilon_{\boldsymbol{p}_1} - \varepsilon_{\boldsymbol{p}_2} - \varepsilon_{\boldsymbol{p}_3}\right) \alpha_{\boldsymbol{p}_1\boldsymbol{p}_2\boldsymbol{p}_3} = g\left(\gamma_{\boldsymbol{p}_1\boldsymbol{p}_2} + \gamma_{\boldsymbol{p}_2\boldsymbol{p}_3} + \gamma_{\boldsymbol{p}_3\boldsymbol{p}_1}\right), \tag{4.6}$$

$$\left(E - \nu_0 - \varepsilon^{\mathrm{d}}_{\boldsymbol{p}_1+\boldsymbol{p}_2} - \varepsilon_{\boldsymbol{p}_1} - \varepsilon_{\boldsymbol{p}_2}\right) \gamma_{\boldsymbol{p}_1\boldsymbol{p}_2} = g \sum_{\boldsymbol{p}'} \alpha_{\boldsymbol{p}'\boldsymbol{p}_1\boldsymbol{p}_2}. \tag{4.7}$$

Here, the integral over $\boldsymbol{p}'$ is cut off at the momentum k_0 as the equations involves the bare detuning ν_0. By solving Eq. (4.6) for $\alpha_{\boldsymbol{p}_1\boldsymbol{p}_2\boldsymbol{p}_3}$ and substituting it into Eq. (4.7), one finds

$$\left(E - \nu_0 - \varepsilon^{\mathrm{d}}_{\boldsymbol{p}_1+\boldsymbol{p}_2} - \varepsilon_{\boldsymbol{p}_1} - \varepsilon_{\boldsymbol{p}_2}\right) \gamma_{\boldsymbol{p}_1\boldsymbol{p}_2} = g^2 \sum_{\boldsymbol{p}'} \frac{\gamma_{\boldsymbol{p}_1\boldsymbol{p}_2} + \gamma_{\boldsymbol{p}_2\boldsymbol{p}'} + \gamma_{\boldsymbol{p}'\boldsymbol{p}_1}}{E - \varepsilon_{\boldsymbol{p}_1+\boldsymbol{p}_2+\boldsymbol{p}'} - \varepsilon_{\boldsymbol{p}_1} - \varepsilon_{\boldsymbol{p}_2} - \varepsilon_{\boldsymbol{p}'}}. \tag{4.8}$$

Now by noting that the impurity-boson T-matrix in vacuum is given, as the special case of Eq. (2.32), by

$$T_0(E, \boldsymbol{p}) = \left[g^{-2}\left(E - \nu_0 - \varepsilon^{\mathrm{d}}_{\boldsymbol{p}}\right) - \sum_{\boldsymbol{p}'} \frac{1}{E - \varepsilon_{\boldsymbol{p}+\boldsymbol{p}'} - \varepsilon_{\boldsymbol{p}}} \right]^{-1} \tag{4.9}$$

$$\to \frac{4\pi}{m} \frac{1}{a^{-1} - r_0 m E/2 - \sqrt{-mE - i0}} \quad (k_0 \to \infty), \tag{4.10}$$

one can eliminate the bare parameters ν_0 and g and write the equation in the form explicitly independent of k_0:

$$T_0^{-1}(E - \varepsilon_{\boldsymbol{p}_1} - \varepsilon_{\boldsymbol{p}_2}, \boldsymbol{p}_1 + \boldsymbol{p}_2)\gamma_{\boldsymbol{p}_1\boldsymbol{p}_2} = \sum_{\boldsymbol{p}'} \frac{\gamma_{\boldsymbol{p}_2\boldsymbol{p}'} + \gamma_{\boldsymbol{p}'\boldsymbol{p}_1}}{E - \varepsilon_{\boldsymbol{p}_1+\boldsymbol{p}_2+\boldsymbol{p}'} - \varepsilon_{\boldsymbol{p}_1} - \varepsilon_{\boldsymbol{p}_2} - \varepsilon_{\boldsymbol{p}'}}. \tag{4.11}$$

For the three-body and two-body systems, the same procedure yields

$$T_0^{-1}(E - \varepsilon_{\boldsymbol{p}}, \boldsymbol{p})\gamma_{\boldsymbol{p}} = \sum_{\boldsymbol{p}'} \frac{\gamma_{\boldsymbol{p}'}}{E - \varepsilon_{\boldsymbol{p}+\boldsymbol{p}'} - \varepsilon_{\boldsymbol{p}} - \varepsilon_{\boldsymbol{p}'}}, \tag{4.12}$$

$$T_0^{-1}(E, 0) = 0. \tag{4.13}$$

Owing to the rotational symmetry, we can assume that the energy eigenstates are simultaneously the eigenstates of the total angular momentum. Here, we focus on the states with the zero angular momentum, which are relevant to the Efimov physics. This implies that the wave functions are of the form $\gamma_{\boldsymbol{p}_1\boldsymbol{p}_2} = \gamma(|\boldsymbol{p}_1|, |\boldsymbol{p}_2|, \cos\theta)$ for the four-body system, where θ is the angle between $\boldsymbol{p}_1$ and $\boldsymbol{p}_2$, and $\gamma_{\boldsymbol{p}} = \gamma(|\boldsymbol{p}|)$ in the three-body system. The resulting equations for these reduced wave functions are shown in Appendix A.

The few-body equations for both the r_0-model and the Λ-model are written in the form of Eqs. (4.11–4.13). However, the microscopic mechanisms that ensure the stability of this system are different in these models. In the r_0-model, the effective range r_0 is finite and negative. This two-body quantity suppresses contributions from the high-momentum particles above the momentum scale $\sim r_0^{-1}$, which saves the system from the collapse. That is, the structure of the two-body interaction leads to a finite ground-state energy in the r_0-model. By contrast, as the effective range in the Λ-model is set zero, it does not have any two-body mechanism that regulates three-body physics. Instead, the high-momentum cutoff Λ is imposed on the momentum arguments of the wave function γ. The cutoff Λ only affects the closed-channel wave function γ, while the open-channel wave function α remains cutoff-free. This implies that the integral in Eq. (4.9) is taken without the cutoff. In other words, two-body processes involving the impurity and one boson remain unaffected by Λ, and it only affects three-body processes, where two bosons interact by exchanging the impurity particle. Note that this three-body cutoff can be removed by introducing the three-body interaction whose coupling constant depends on Λ and taking $\Lambda \to \infty$ [154]. The Λ-model is in this sense equivalent to the model with the three-body interaction.

4.2 Universality of the spectrum

We solve Eqs. (4.11) and (4.12) numerically, while the solution of Eq. (4.13) is already given in Eq. (2.35). In Figure 4.1, we show the spectrum of the four-body system described by the r_0-model.

If the s-wave scattering length is positive, Eq. (4.13) has a single solution $E = -E_{\mathrm{B}}$ corresponding to a two-body bound state as shown in Eq. (2.35):

$$E_{\mathrm{B}} = \frac{\left(\sqrt{1 - 2r_0/a} - 1\right)^2}{mr_0^2}. \tag{4.14}$$

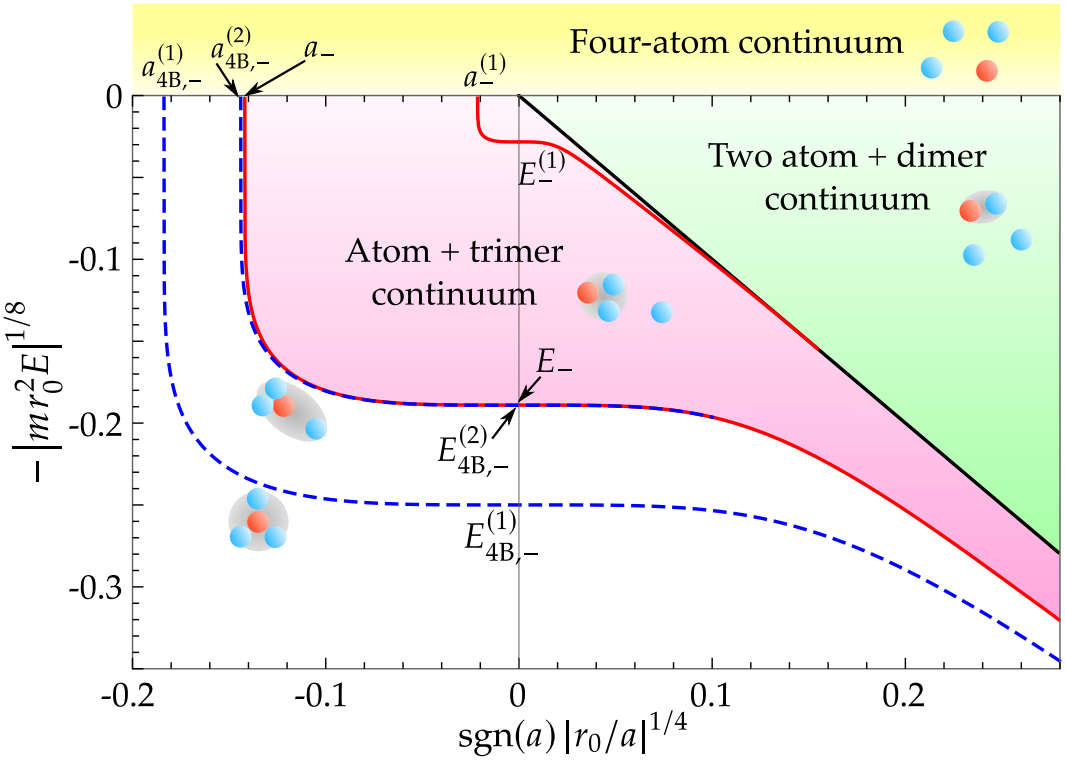

Figure 4.1: Energy spectrum of the 3+1 system within the r_0-model. We show the ground (first-excited) Efimov trimer as the red solid curve, which starts at the critical scattering length a_- ($a_-^{(1)}$), crosses $a^{-1} = 0$ at $E = E_-$ ($E_-^{(1)}$), and continues until it dissociates into the atom-dimer continuum (green region). Note that there is an infinite series of excited Efimov states including those not shown in this plot, which converge to the point $a^{-1} = 0$ and $E = 0$ following the discrete scale invariance. We also find two tetramer states below the lowest Efimov state, whose critical scattering lengths and the energies at unitarity is denoted by $a^{(i)}_{4B,-}$ and $E^{(i)}_{4B,-}$ ($i = 1, 2$), respectively. The excited tetramer exists even at unitarity $a^{-1} = 0$, and disappears at $a \simeq 9 \times 10^3 |r_0|$.

It converges to the result of the contact interaction, $1/ma^2$, in the limit of $r_0 \to -0$. This explains the fact that the dimer spectrum is an almost straight line in Fig. 4.1.

The three-body sector supports so-called Efimov trimers. Such three-body bound states can exist even when there is no dimer, i.e., when $a < 0$. Right at unitarity, where $a^{-1} = 0$, there is an infinite series of three-body bound states consisting of the impurity and two bosons. The most remarkable feature of Efimov trimers is a discrete scale symmetry. One Efimov state with the s-wave scattering length a and the energy E implies another Efimov state with $\lambda_0 a$ and $\lambda_0^{-2} E$, where the scaling factor λ_0 is determined by the mass ratio and quantum statistics of the identical particles but independent of details of interactions for sufficiently shallow trimers. In the present case, where two non-interacting bosons interact resonantly with one impurity with the same mass, the scaling factor is known $\lambda_0 = 1986.1$ [6].

Our numerical results indicate that the two lowest states already obey the predicted scaling law with high accuracy. The ratio of the s-wave scattering lengths, a_- and $a_-^{(1)}$, at which the ground and first-excited Efimov state merge with the three-atom continuum, is $a_-^{(1)}/a_- \simeq 1991$, very close to the universal scaling factor of 1986.1. Also, the ratio of the energies of the ground and the first-excited states at unitarity is $E_-/E_-^{(1)} \simeq (1986.1)^2$, which agrees to five significant digits. This is remarkable because generally the discrete scale invariance is exact only asymptotically for excited Efimov states, and the ground and the lower-excited states may not strictly follow the scaling law. For example, in three-identical Bose systems, the scaling factor between the ground and the first-excited states is known to deviate from its universal value 22.7 by 10-20% due to finite-range corrections [9, 10].

Below the deepest Efimov trimer, we find two four-body bound states. For identical bosons, it was predicted that there exist two tetramers associated with the ground-state Efimov trimer, both theoretically [17, 18, 155, 156] and experimentally [38]. Four-body bound states have also been studied in systems composed of one light particle and three heavy indentical particles [22, 23, 109]. It was found that such mass-imbalanced four-body systems also have two lower-lying bound state. However, when the mass imbalance is small, the excited tetramer state in the four-body system at unitarity $a^{-1} = 0$ has eluded previous investigations.

Now we would like to argue that these features of few-body systems, consisting of one particle interacting resonantly with a few identical bosons, are actually universal, in the sense that dimensionless ratios in the few-body spectrum are independent of specific models. To test the universality, we also calculate the energy spectrum within the Λ-mode, as shown in Fig. 4.2. The length scales of few-body physics in this model is set by Λ. For example, we find the three-body parameter $a_- \simeq 1354\Lambda^{-1}$. However, the

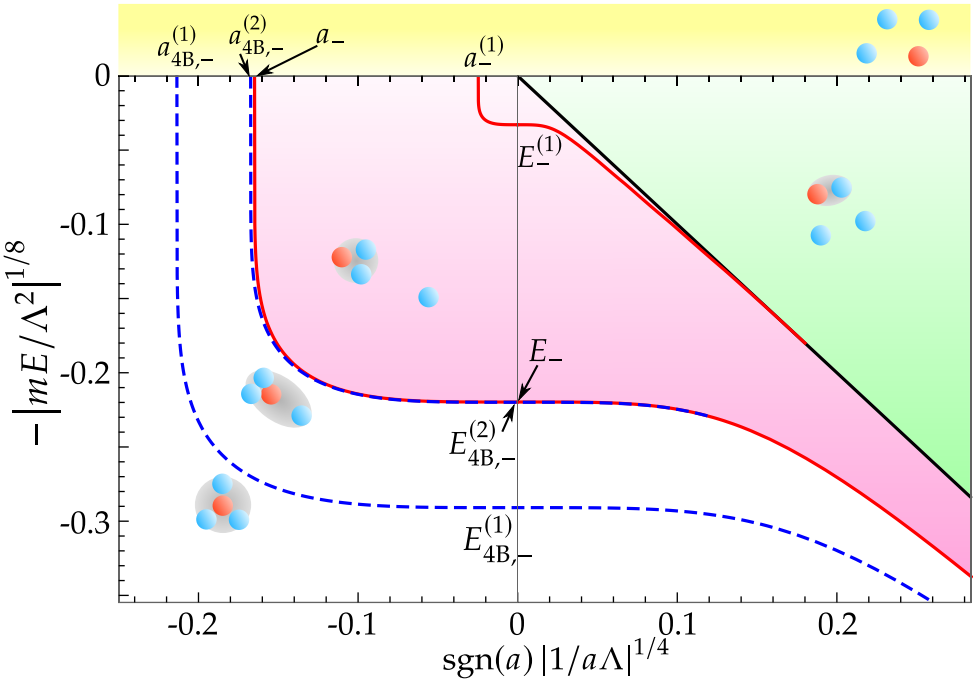

Figure 4.2: Energy spectrum of the four-body system within the Λ-model. This shares all the qualitative features with that of the r_0-model shown in Fig. 4.1, while now the quantities are scaled by Λ instead of r_0. The critical scattering length of the ground Efimov trimer a_- is related to Λ by $a_- \simeq 1354\Lambda^{-1}$. The first-excited tetramer also exists in the Λ-model at unitarity; this tetramer dissociates into the atom-trimer continuum at $a \simeq 2\times 10^3\Lambda^{-1}$.

	$\lvert a_- \rvert$	$m a_-^2 \lvert E_- \rvert$	$a_-^{(1)}/a_-$	$\sqrt{E_-/E_-^{(1)}}$
r_0-model	$2467\lvert r_0 \rvert$ [108]	9.913	1991	1986.126
Λ-model	$1354\Lambda^{-1}$	9.950	1987	1986.127
	$a_-/a_{4\mathrm{B},-}^{(1)}$	$E_{4\mathrm{B},-}^{(1)}/E_-$	$a_-/a_{4\mathrm{B},-}^{(2)}$	$E_{4\mathrm{B},-}^{(2)}/E_-$
r_0-model	2.810	9.35	1.060	1.0030(3)
Λ-model	2.814	9.43	1.061	1.0036(1)

Table 4.1: Comparison of few-body data for the r_0- and the Λ-model. While the overall length scale set by a_- depends on the details of the models, the dimensionless ratios characterizing the few-body spectra agree to an accuracy of 1% or less. These quantities include the scattering lengths at which the few-body bound states enter the continuum, as well as their energies at unitarity, as indicated in Figs. 4.1 and 4.2.

spectrum of the Λ-model shares all the qualitative features such as the number of the tetramer states with that of the r_0-model. Moreover, the spectra of the two models are almost indistinguishable if the axes are appropriately scaled.

For more quantitative comparison, we summarize the dimensionless ratios in Table 4.1. The overall length scale, which is set by a_-, depends on specific models; it is proportional to r_0 in the r_0-model and to Λ^{-1} in the Λ-model. It is natural because besides the s-wave scattering length, each model has only one parameter, r_0 or Λ, which is the only length scale that can fix the critical scattering length a_-. On the other hand, the dimensionless quantities, such as the ratios of the bound-state energies at unitarity and those of the critical scattering lengths, agree between the two models within 1%. These results suggest that the spectrum of mass-balanced four-body systems, including the ground state and the lower excited states, is highly universal, contrary to the non-universality observed for indentical bosons.

The ratio of the energies of the deepest trimer and tetramer, $E_{4\mathrm{B},-}^{(1)}/E_-$, also agrees with a recent calculation based on yet another model of the impurity-boson system [110], which further supports the universality. The model has a hard-core boson-boson interaction with the diameter a_B and an attractive square-well interaction between the impurity and bosons. They found $E_{4\mathrm{B},-}^{(1)}/E_- \simeq 9.7$ by using the diffusion Monte Carlo method, while our calculations show $E_{4\mathrm{B},-}^{(1)}/E_- \simeq 9.4$.

The observed model-independence at the four-body level indicates that we do not need such things as a four-body parameter that controls the four-body bound states. This is consistent with what have been found theoretically in identical particles [17, 18, 156] and heteronuclear systems [22, 23, 109].

As an implication of the universality and for later convenience, we derive the relation between the three-body parameter a_- and the radius of the hard-core interaction between bosons in the model used in Ref. [110]. The model has three independent parameters: the s-wave scattering length a of the impurity-boson interaction, the radius r_w of the square well, and the diameter a_B of the hard-core boson-boson interaction. Note that the depth of the square-well potential is determined in the way it reproduces the scattering length a for a given r_w. As r_w is made much smaller than a and a_B, it drops out of the problem, and the model essentially reduces to the two-parameter model. Now, the universality of the few-body spectrum implies that this model has a value of $ma_-^2\left|E_\mathrm{4B}^{(1)}\right|$ similar to that in the r_0-model, which can be extracted from our calculation. On the other hand, in Ref. [110] it is reported that $ma_\mathrm{B}{}^2\left|E_\mathrm{4B}^{(1)}\right| \simeq 4.7\times10^{-4}$. Combining these two results, we find[2]

$$a_- = 2.1(4)\times10^4 a_\mathrm{B}. \tag{4.15}$$

The uncertainty arises predominantly from the statistical one in the QMC calculation.

4.3 Scale separation behind the universality

A universality is usually accompanied by separation of scales; a physical phenomenon is insensitive to system's properties whose characteristic size is too small or too large compared with that of the phenomenon itself. Before ending this chapter, we point out the model-independence of the few-body spectrum is also backed by a large separation of scales. In the present problem, systems' characteristic length scale is r_0, Λ, or a_B. On the other hand, the few-body bound states, which are the phenomena we are investigating, are characterized by, for example, the critical scattering length, a_-, of the ground Efimov trimer. As we have already shown, a_- is related to systems' parameters by

$$|a_-| = 2.5\times10^3|r_0| \qquad (r_0\text{-model}), \tag{4.16}$$

$$= 1.4\times10^3\Lambda^{-1} \qquad (\Lambda\text{-model}), \tag{4.17}$$

$$= 2.1\times10^4 a_\mathrm{B} \qquad (\text{hard-core boson-boson interaction}). \tag{4.18}$$

This large separation between the microscopic lengths and the scale of the three-body physics is characteristic of mass-balanced impurity-boson systems. Let m_i be the mass of the impurity and m_B that of the bosons. The proportionality constants quoted in Eqs. (4.16-4.18) become smaller if $m_\mathrm{i}/m_\mathrm{B}$ is made smaller. Indeed, it is known that for a lighter impurity, the lower-lying states are sensitive to finite-range corrections. In

[2]Here, we used $E_\mathrm{4B}^{(1)}$ instead of E_- because the statistical uncertainty of the tetramer energy is smaller than that of the trimer energy [110].

	$\lvert a_- \rvert$	$a_-^{(1)}/a_-$	$a_-^{(2)}/a_-^{(1)}$	$a_-^{(3)}/a_-^{(2)}$	$a_-^{(4)}/a_-^{(3)}$	$a_-^{(5)}/a_-^{(4)}$
r_0-model	$0.6101\ \lvert r_0 \rvert$	8.706	6.040	5.463	5.308	5.267
Λ-model	$4.992\Lambda^{-1}$	6.731	5.482	5.295	5.261	5.254

Table 4.2: Critical scattering length a_- of the ground Efimov trimer and the ratios between the adjacent critical scattering lengths for $m_\mathrm{i}/m_\mathrm{B} = \frac{1}{20}$. Here, $a_-^{(i)}$ represents the s-wave scattering length at which the ith-excited Efimov trimer enters the three-atom continuum. For highly excited states, the ratios converge to their unviersal value 5.253.

Table 4.2, we show the ratios between the s-wave scattering lengths where two adjacent Efimov trimers appear from the three-atom continuum when $m_\mathrm{i}/m_\mathrm{B} = \frac{1}{20}$; this ratio of the masses is relevant to a mixture of ^{6}Li and ^{133}Cs. In this case, a_- is of the same order of magnitude as r_0 and Λ^{-1}. While the ratios of highly excited states show convergence to its universal value 5.253, $a_-/a_-^{(1)}$ deviates by 30–70% from the universal value, which depends heavily on the choice of the model. Therefore, for the study of the universal nature of resonantly interacting impurity-boson systems, the mass-balanced case offers unique possibilities that even the lower-lying states are insensitive to details of the system.

Chapter 5

Infinite-mass impurity with a few bosons

In the last section, we discuss the importance of the separation of the scales, which leads to the universal few-body spectrum in the mass-balanced impurity-boson systems. We also mention that the deviation from the universality becomes significant when the mass of the impurity becomes small. It is then natural to ask what happens in the opposite limit of the infinite-mass impurity.

One may argue that this limit is trivial if there is no boson-boson interaction, because the problem then reduces to a non-interacting Bose gas in an external field produced by the impurity. This is true, if an interaction between the impurity and bosons is described by a potential energy. The situation is not that simple, however, in the presence of a Feshbach resonance because it accompanies an effective three-body repulsion.

Mathematically, Eq. (4.12) is ill-posed for the mass-balanced case if $r_0 = 0$ and no cutoff is imposed on the integral on the right-hand side. On the other hand, when $r_0 < 0$, $T_0^{-1}(E - \varepsilon_{\boldsymbol{p}}, \boldsymbol{p})$ contains a term proportional to $r_0 p^2$, which suppresses $\gamma_{\boldsymbol{p}}$ for $p \gg r_0^{-1}$ and hinders the collapse. By noting that $\gamma_{\boldsymbol{p}}$ represents the relative motion of the closed-channel dimer and a boson, this effect can be seen as an effective three-body repulsion induced by the effective range.

This explanation is also supported by a physical intuition based on a Feshbach resonance. One boson can strongly interact with the impurity because there is a closed-channel molecular level on resonance with the open channel. When the two particles interact and form a closed-channel dimer, on the other hand, a second boson coming close to the impurity cannot undergo a Feshbach resonance because generically there is no "closed-channel trimer" that is resonant with a collision of the closed-channel dimer and a boson. This is reflected in the r_0-model as the absence of the terms like $\hat{t}^\dagger \hat{d} \hat{b}$, where $\hat{t}^\dagger$ is the creation operator of a closed-channel trimer formed by one closed-channel dimer and one boson. Therefore, the impurity can be screened by the interaction with a boson, which causes the effective three-body repulsion in the r_0-model.

To reveal physical consequences of this effective three-body force, we consider an infinitely heavy particle interacting with two identical bosons. Here again, we ignore interactions between bosons. In Section 5.1, we show that this three-body problem within the r_0-model is analytically solvable by mapping the Hamiltonian into that of a bosonic extension of Anderson's single impurity model. For a two-body system, the equivalence of the two models was pointed out in Ref. [105]. Here, we extend it to the many-body impurity-boson system, where we find that an infinite on-site repulsion is necessary. We show that a three-body bound state exists when the s-wave scattering length is positive and larger than a critical scattering length a^*. When $a = a^*$, the trimer state dissociates into the atom-dimer continuum. The binding energy of the trimer state is always smaller than twice that of the dimer state. These results are drastically different from what is expected from the single-channel picture; when an interaction between the impurity and a boson can be written as a potential energy, it just reduces to the problem of non-interacting bosons in an external field, and the ground-state energy of the N+1 system is just N times as large as that of the 1+1 system. On the other hand, our results implies that the effective three-body repulsion makes the trimer state much shallower. In the limit of $r_0 \to -0$, we recover the single-channel result, where the trimer energy is twice as large as the dimer energy. However, we show that the convergence is only logarithmic. In Section 5.2, we numerically calculate the three-body spectrum of the Λ-model in the limit of the heavy impurity. We find that the Λ-model is equipped with all the features of the three-body problem described above, including the logarithmic approach to the potential interaction. This suggests that they are universal properties of systems with the three-body forces.

5.1 Analytical results for an infinite-mass impurity

The analytical solution is obtained in three steps: First, we transform the r_0-model Hamiltonian into a bosonic version of Anderson's single impurity model with an infinite on-site repulsion. Next, we diagonalize the bilinear part of the Hamiltonian by solving the Schrödinger equation for the two-body problem. Finally, the three-body problem is solved by writing down the Schrödinger equation with the basis that diagonalizes the bilinear part and imposes the condition of no double occupancy of the closed-channel state, which derives from the on-site repulsion in the model.

5.1.1 Bosonic Anderson's single impurity model

When the impurity has an infinite mass, the r_0-model reads

$$\hat{H} = \sum_{p} \left(p^2 \hat{b}_p^\dagger \hat{b}_p + \nu_0 \hat{d}_p^\dagger \hat{d}_p \right) + g \sum_{p,q} \left(\hat{d}_{p+q}^\dagger \hat{b}_q \hat{c}_p + \hat{c}_p^\dagger \hat{b}_q^\dagger \hat{d}_{p+q} \right), \tag{5.1}$$

where $\hat{b}_p^\dagger$, $\hat{c}_p^\dagger$, and $\hat{d}_p^\dagger$ are the creation operators of the bosons, the impurity, and the closed-channel dimer, respectively, and we set the mass of the bosons as $1/2$ for simplicity. As a special case of Eq. (2.34), the bare parameters ν_0 and g are related to the lower-energy scattering data by

$$a^{-1} = \frac{4\pi}{g^2} \left(\frac{g^2}{2\pi^2} k_0 - \nu_0 \right), \quad r_0 = -\frac{8\pi}{g^2}, \tag{5.2}$$

where k_0 is the ultraviolet cutoff, which will be taken to be infinite with fixed a^{-1} and r_0. The absence of the kinetic terms of the impurity and the closed-channel dimer means that an impurity is localized and does not propagate under the time evolution generated by $\hat{H}$. Therefore, we can simply assume that the impurity is localized at the origin, and retain only the localized modes of the impurity and the closed-channel molecule:

$$\hat{H} = \sum_{p} p^2 \hat{b}_p^\dagger \hat{b}_p + \nu_0 \hat{d}^\dagger \hat{d} + g \sum_{p} \left(\hat{d}^\dagger \hat{b}_p \hat{c} + \hat{c}^\dagger \hat{b}_p^\dagger \hat{d} \right). \tag{5.3}$$

In this chapter, we refer to this expression as the r_0-model. This is bilinear in terms of $\hat{b}_p$ and $\hat{d}$, but the coupling with $\hat{c}$ makes the problem nontrivial. Here, the role of $\hat{c}$ is to conserve the number of the impurities, $N_\mathrm{i} \equiv \hat{d}^\dagger \hat{d} + \hat{c}^\dagger \hat{c}$, which is one in the present case.

To see this point, let us consider the bilinear Hamiltonian

$$\hat{H}_0 = \sum_{p} p^2 \hat{b}_p^\dagger \hat{b}_p + \nu_0 \hat{d}^\dagger \hat{d} + g \sum_{p} \left(\hat{d}^\dagger \hat{b}_p + \hat{b}_p^\dagger \hat{d} \right), \tag{5.4}$$

and compare the Schrödinger equation with that of Eq. (5.3). This Hamiltonian no longer contains the impurity degrees of freedom, and an $N+1$-body system within the r_0-model corresponds to an N-boson problem for Eq (5.4). To be specific, we take a three-body system consisting of two bosons and one impurity for example. The most general wave function for the r_0-model is

$$|\Psi\rangle = \left(\frac{1}{2} \sum_{p_1,p_2} \psi_{c p_1 p_2} \hat{c}^\dagger \hat{b}_{p_1}^\dagger \hat{b}_{p_2}^\dagger + \sum_{p} \psi_{d p} \hat{d}^\dagger \hat{b}_p^\dagger \right) |0\rangle, \tag{5.5}$$

and the Schrödinger equation $\hat{H}\,|\Psi\rangle = E\,|\Psi\rangle$ reads

$$(E - p_1^2 - p_2^2)\psi_{c\boldsymbol{p}_1\boldsymbol{p}_2} = g\left(\psi_{d\boldsymbol{p}_1} + \psi_{d\boldsymbol{p}_2}\right), \tag{5.6}$$

$$(E - p^2 - \nu_0)\psi_{d\boldsymbol{p}} = g\sum_{\boldsymbol{q}} \psi_{c\boldsymbol{p}\boldsymbol{q}}. \tag{5.7}$$

On the other hand, a two-boson state within the Hamiltonian (5.4) can be written as

$$|\Phi\rangle = \left(\frac{1}{2}\sum_{\boldsymbol{p}_1,\boldsymbol{p}_2} \phi_{\boldsymbol{p}_1\boldsymbol{p}_2}\hat{b}^\dagger_{\boldsymbol{p}_1}\hat{b}^\dagger_{\boldsymbol{p}_2} + \sum_{\boldsymbol{p}} \phi_{d\boldsymbol{p}}\hat{d}^\dagger\hat{b}^\dagger_{\boldsymbol{p}} + \frac{1}{2}\phi_{dd}\hat{d}^\dagger\hat{d}^\dagger\right)|0\rangle\,, \tag{5.8}$$

whose Schrödinger equation reads

$$(E - p_1^2 - p_2^2)\phi_{\boldsymbol{p}_1\boldsymbol{p}_2} = g\left(\phi_{d\boldsymbol{p}_1} + \phi_{d\boldsymbol{p}_2}\right), \tag{5.9}$$

$$(E - p^2 - \nu_0)\phi_{d\boldsymbol{p}} = g\sum_{\boldsymbol{q}} \phi_{\boldsymbol{p}\boldsymbol{q}} + g\phi_{dd}, \tag{5.10}$$

$$(E - 2\nu_0)\phi_{dd} = 2g\sum_{\boldsymbol{q}} \phi_{d\boldsymbol{q}}. \tag{5.11}$$

The first two equations are equivalent to those for $\psi_{c\boldsymbol{p}_1\boldsymbol{p}_2}$ and $\psi_{d\boldsymbol{p}}$ if we set $\phi_{\boldsymbol{p}_1\boldsymbol{p}_2} = \psi_{c\boldsymbol{p}_1\boldsymbol{p}_2}$, $\phi_{d\boldsymbol{p}} = \psi_{d\boldsymbol{p}}$, and $\phi_{dd} = 0$. In the r_0-model, the impurity-number conservation implies that $1 - \hat{d}^\dagger\hat{d} = \hat{c}^\dagger\hat{c} \geq 0$, or $\hat{d}^\dagger\hat{d} \leq 1$, which prohibits the double occupancy of the closed-channel state. A similar correspondence applies to systems with multiple bosons with one impurity, where the Schrödinger equation for Eq. (5.4) reduces to that of the r_0-model when the amplitude for multi-dimer states is suppressed.

This observation implies that for systems with a single, infinite-mass impurity, the Hamiltonian (5.4), with some additional mechanism to avoid the multiple occupancy of the dimer state, leads to the same results as the r_0-model. Here, we adopt the "on-site" repulsive interaction,

$$\hat{H} = \hat{H}_0 + \frac{U}{2}\hat{d}^\dagger\hat{d}^\dagger\hat{d}\hat{d}, \tag{5.12}$$

which will be taken to be infinite at the end of calculations. This additional term penalizes the states in which the $\hat{d}$-state is multiply occupied, leading to $\phi_{dd} \to 0$ in the above example. This results in exactly the same form of the Schrödinger equations as those for the pair of $\psi_{c\boldsymbol{p}_1\boldsymbol{p}_2}$ and $\psi_{d\boldsymbol{p}}$. Therefore, the two Hamiltonians give the same results for the problem of two bosons (plus one impurity, in the case of the r_0-model).

We can also extend the derivation to three or more bosons. It should be noted, however, that the derivation of Eq. (5.12) relies on the fact that the number of the

impurity is one. Therefore, the equivalence of the Hamiltonians (5.3) and (5.12) is restricted to the single-impurity sector.

The mapping from the r_0-model to Eq. (5.12) has transformed the $N+1$-body problem with the conserved impurity number into the unconstrained N-body problem with the on-site interaction. This interaction has an important property called separability. A two-body potential is called separable if it can be written as a finite-dimensional projector. Separability often simplifies analyses of few-body problems [157] and many-body problems [158]. Here, the on-site repulsion term is the two-boson interaction, which is proportional to the projection operator onto the two-dimer state. Its separability can be exploited to derive the analytic solution as discussed below.

Note that the Hamiltonian (5.12), combined with Eq. (5.4), has exactly the same structure as Anderson's single impurity model [159], except that in the present case, the particles are spinless bosons. This bosonic model has not attracted as much attention as the fermionic one, but was recently studied by using the numerical renormalization group method [160, 161]. We also note that the model can be mapped to a spin-boson model as well [162, 163], where the open and closed channels are represented as the spin up and down. Our study sheds light on the few-body aspects in the presence of resonant interactions in these models. In particular, the mapping between the two-channel model and the Anderson model has revealed that such physics is naturally realized in mass-imbalanced mixtures of atomic gases with a Feshbach resonance.

5.1.2 Diagonalization of the bilinear part

In the following discussion, we assume that the s-wave scattering length is positive, where we have one two-body bound state.

We can diagonalize the bilinear part $\hat{H}_0$ by solving the two-body problem. This is a special case of Section 2.2.1. As the mass of the impurity is infinite, the reduced mass m_r is equal to the mass of the bosons, which is $1/2$ in the present unit. The solutions of this two-body problem include the scattering states $|B_{\boldsymbol{k}}\rangle$ with the incoming momentum $\boldsymbol{k}$ and the bound state $|D\rangle$. They can be expanded in terms of $\hat{b}^\dagger_{\boldsymbol{p}}$ and $\hat{d}^\dagger$ as

$$|B_{\boldsymbol{k}}\rangle = \left(\sum_{\boldsymbol{p}} \hat{b}^\dagger_{\boldsymbol{p}} U_{\boldsymbol{p}\boldsymbol{k}} + \hat{d}^\dagger V_{\boldsymbol{k}}\right)|0\rangle \equiv \hat{B}^\dagger_{\boldsymbol{k}}|0\rangle\,, \tag{5.13}$$

$$|D\rangle = \left(\sum_{\boldsymbol{p}} \hat{b}^\dagger_{\boldsymbol{p}} \phi_{\boldsymbol{p}} + \hat{d}^\dagger Z^{1/2}\right)|0\rangle \equiv \hat{D}^\dagger|0\rangle\,, \tag{5.14}$$

where the operators $\hat{B}_{\boldsymbol{k}}^\dagger$ and $\hat{D}^\dagger$ create the scattering state and the bound state, respectively. By using these operators, the bilinear part can be written as

$$\hat{H}_0 = \sum_{\boldsymbol{k}} k^2 \hat{B}_{\boldsymbol{k}}^\dagger \hat{B}_{\boldsymbol{k}} - E_{\mathrm{B}} \hat{D}^\dagger \hat{D}, \tag{5.15}$$

where E_{B} is the binding energy of the dimer. The explicit expressions of the expansion coefficients can be derived by solving the Schrödinger equation (see Section 2.2.1),

$$U_{\boldsymbol{pk}} = (2\pi)^3 \delta(\boldsymbol{p} - \boldsymbol{k}) + \frac{T(k^2)}{k^2 - p^2 + i0}, \quad V_{\boldsymbol{k}} = g^{-1} T(k^2), \tag{5.16}$$

$$\phi_{\boldsymbol{p}} = -\frac{g Z^{1/2}}{E_{\mathrm{B}} + p^2}, \quad Z = \left(1 + \frac{1}{|r_0| E_{\mathrm{B}}^{1/2}}\right)^{-1}, \tag{5.17}$$

where $T(E)$ is again the T-matrix element given by

$$T(E) = \frac{4\pi}{a^{-1} - \frac{1}{2} r_0 E - \sqrt{-E - i0}}. \tag{5.18}$$

It is independent of the center-of-mass momentum because the pair of the impurity and one boson has the infinite total mass and therefore the zero kinetic energy. The completeness and the orthonormality of the transformed basis can be checked by direct calculations, and $\hat{B}_{\boldsymbol{k}}$ and $\hat{D}$ satisfy the canonical commutation relations:

$$[\hat{B}_{\boldsymbol{k}_1}, \hat{B}_{\boldsymbol{k}_2}^\dagger] = (2\pi)^3 \delta(\boldsymbol{k}_1 - \boldsymbol{k}_2), \quad [\hat{D}, \hat{D}^\dagger] = 1, \ldots. \tag{5.19}$$

The dimer binding energy is determined by solving the equation $T(-E_{\mathrm{B}})^{-1} = 0$. For later convenience[1], we adopt the unit where $E_{\mathrm{B}} = 1$, and remove a^{-1} from Eq. (5.18) by using $T(-1)^{-1} = 0$:

$$T(E) = \frac{4\pi}{\frac{1}{2}|r_0|(E+1) + 1 - \sqrt{-E - i0}}. \tag{5.20}$$

With $\hbar = 2m_{\mathrm{B}} = E_{\mathrm{B}} = 1$, we completely fix the scales of time, mass, and length. Therefore, all the variables are now dimensionless.

[1]We use the residue theorem later to integrate certain functions. There, the operations will be slightly simpler by using E_{B} as the unit of energy. Also, we are interested in E/E_{B}, and this is a natual choice of the unit for this purpose.

5.1.3 Three-body problem

Now we solve the 2+1 problem. This time, the "on-site repulsion" plays a role. Importantly, this interaction term is separable, which has the form of the projector onto the states where the closed-channel state is doubly occupied. This structure allows us to obtain an analytical solution for the three-body problem.

The basis diagonalizing $\hat{H}_0$ is the most convenient for our purpose. Therefore, we write down the wave function in the following form:

$$|\Psi_{2+1}\rangle = \left(\sum_{\boldsymbol{k}_1,\boldsymbol{k}_2} \frac{1}{2} \alpha_{\boldsymbol{k}_1\boldsymbol{k}_2} \hat{B}^\dagger_{\boldsymbol{k}_1} \hat{B}^\dagger_{\boldsymbol{k}_2} + \sum_{\boldsymbol{k}} \beta_{\boldsymbol{k}} \hat{B}^\dagger_{\boldsymbol{k}} \hat{D}^\dagger + \frac{1}{2} \gamma \hat{D}^\dagger \hat{D}^\dagger \right) |0\rangle \,. \tag{5.21}$$

If we recall that we take the two-body binding energy E_B as the unit of energy, the Schrödinger equation $(E - \hat{H}) |\Psi_{2+1}\rangle = 0$ reads

$$(E - k_1^2 - k_2^2)\alpha_{\boldsymbol{k}_1\boldsymbol{k}_2} = V^*_{\boldsymbol{k}_1} V^*_{\boldsymbol{k}_2} \tau, \tag{5.22}$$

$$(E - k^2 + 1)\beta_{\boldsymbol{k}} = V^*_{\boldsymbol{k}} Z^{1/2} \tau, \tag{5.23}$$

$$(E + 2)\gamma = Z\tau, \tag{5.24}$$

where $\tau \equiv U \left\langle 0 \middle| \hat{d}\hat{d} \middle| \Psi_{2+1} \right\rangle$. The amplitude τ can be zero or non-zero. If $\tau = 0$, the above equations immediately give

$$E = k_1^1 + k_2^2, k^2 - 1, \text{or } -2. \tag{5.25}$$

We can always construct the wave functions corresponding to the first two solutions. For $E = k_1^2 + k_2^2$, the doubly occupied closed-channel state interferes destructively in the superposition state

$$\left(\hat{B}^\dagger_{\boldsymbol{k}_1} \hat{B}^\dagger_{\boldsymbol{k}_2} - \hat{B}^\dagger_{\boldsymbol{k}'_1} \hat{B}^\dagger_{\boldsymbol{k}'_2} \right) |0\rangle \,, \tag{5.26}$$

if $|\boldsymbol{k}_1| = |\boldsymbol{k}'_1| = k_1$ and $|\boldsymbol{k}_2| = |\boldsymbol{k}'_2| = k_2$. This is therefore one solution with that energy. A wave function for $E = k^2 - 1$ can also be constructed as a superposition state of $\hat{B}^\dagger_{\boldsymbol{k}} \hat{D}^\dagger |0\rangle$ and $\hat{B}^\dagger_{\boldsymbol{k}'} \hat{D}^\dagger |0\rangle$ for $|\boldsymbol{k}| = |\boldsymbol{k}'| = k$. On the other hand, the solution with $E = -2$ does not necessarily exist because at that energy, there is only one unperturbed solution $\hat{D}^\dagger \hat{D}^\dagger |0\rangle$. This solution is consistent with $\left\langle 0 \middle| \hat{d}\hat{d} \middle| \Psi_{2+1} \right\rangle = \tau/U \to 0$ if and only if $Z = 0$, which is also equivalent to $r_0^2 E_\mathrm{B} = 0$, or equivalently $r_0/a = 0$, owing to Eq. (5.17). Therefore, a three-body bound state having $E < -1$, if any, necessarily has $\tau \neq 0$ for a generic set of the parameters.

To find a possible three-body bound state, we invert Eqs. (5.22–5.24),

$$\alpha_{\boldsymbol{k}_1\boldsymbol{k}_2} = \frac{V^*_{\boldsymbol{k}_1} V^*_{\boldsymbol{k}_2} \tau}{E - k_1^2 - k_2^2}, \quad \beta_{\boldsymbol{k}} = \frac{V^*_{\boldsymbol{k}} Z^{1/2} \tau}{E - k^2 + 1}, \quad \gamma = \frac{Z\tau}{E+2}. \tag{5.27}$$

A condition for the bound-state energy is then given by the condition of no double occupancy of the closed-channel state in the limit of $U \to \infty$. By using the solution (5.27), this condition reads

$$\left\langle 0 \middle| \hat{d}\hat{d} \middle| \Psi_{2+1} \right\rangle \equiv \sum_{\boldsymbol{k}_1,\boldsymbol{k}_2} \frac{|V_{\boldsymbol{k}_1} V_{\boldsymbol{k}_2}|^2 \tau}{E - k_1^2 - k_2^2} + \sum_{\boldsymbol{k}} \frac{2|V_{\boldsymbol{k}}|^2 Z\tau}{E - k^2 + 1} + \frac{Z^2\tau}{E+2} = 0. \tag{5.28}$$

Since $\tau \neq 0$, we can just remove it from the above equation. The resulting equation determines one unknown quantity, the energy E, from the known quantities $V_{\boldsymbol{k}}$ and Z, which depend on the single parameter r_0. This nonlinear equation is more amenable to analytic investigations than the integral equations as the one that we solved in the previous chapter.

Note that the numerator of each term in Eq. (5.28) is positive, while for the presumed three-body bound state with $E < -1$, the denominators of the first two terms are negative. Therefore, Eq. (5.28) can be satisfied only if $E > -2$, which makes the third term positive.

With this restriction of the energy in mind, we can actually perform all the integration in Eq. (5.28). By using Eqs. (5.16), (5.17) and (5.20), we can rewrite Eq. (5.28) as

$$\begin{aligned} \frac{1}{E+2} = &\sum_{\boldsymbol{k}_1,\boldsymbol{k}_2} \frac{1}{k_1^2 + k_2^2 - E} \frac{2\pi(1+|r_0|)}{[\frac{|r_0|}{2}(k_1^2+1)+1]^2 + k_1^2} \frac{2\pi(1+|r_0|)}{[\frac{|r_0|}{2}(k_2^2+1)+1]^2 + k_2^2} \\ &+ \sum_{\boldsymbol{k}} \frac{2}{k^2 - 1 - E} \frac{2\pi(1+|r_0|)}{[\frac{|r_0|}{2}(k^2+1)+1]^2 + k^2}. \end{aligned} \tag{5.29}$$

As the integrands are the rational functions of the momentum variables, the integration over $\boldsymbol{k}_1$ and $\boldsymbol{k}$ can be done with the help of the residue theorem, leading to

$$\begin{aligned} \frac{1}{E+2} = &\sum_{\boldsymbol{k}} \frac{1}{(1+\sqrt{k^2+|E|})(2+|r_0|+\sqrt{k^2+|E|}|r_0|)} \frac{2\pi(1+|r_0|)}{[\frac{|r_0|}{2}(k^2+1)+1]^2 + k^2} \\ &+ \frac{2}{(1+\sqrt{-1+|E|})(2+|r_0|+\sqrt{-1+|E|}|r_0|)}. \end{aligned} \tag{5.30}$$

By setting $k = \frac{\sqrt{|E|}}{2}(x - x^{-1})$, the square root $\sqrt{k^2+|E|}$, and therefore the entire integrand, can be made a rational function of x. Remarkably, finding the poles of the resulting integrand reduces to solving quadratic equations, which means that we can obtain the expressions of all the poles. This allows us to perform the remaining integration by

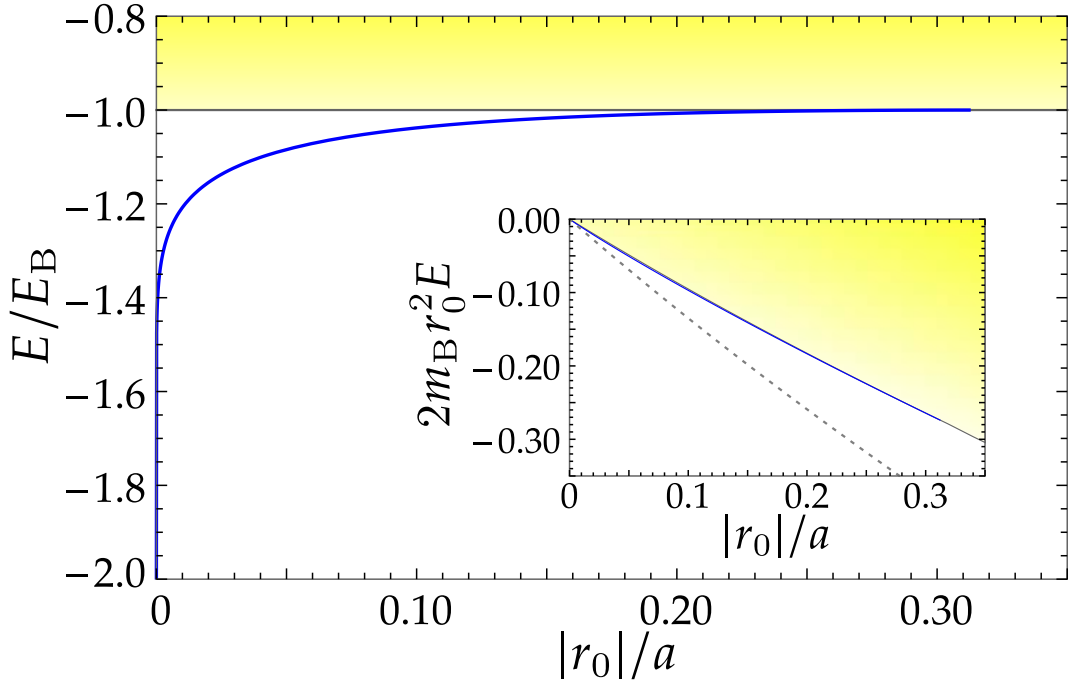

Figure 5.1: Spectrum of the three-body problem with the infinite-mass impurity as a function of $|r_0|$. The three-body bound state (blue curve) exists in the interval $0 < |r_0|/a < 0.31821$. At $|r_0|/a = 0.31821$, the trimer state crosses the atom-dimer threshold energy (gray line). In the inset, we show the spectrum as a function of a^{-1}, taking $|r_0|$ as the unit of length. The gray-dotted line corresponds to $E = -2E_B$. In this plot, the trimer state is almost degenerate with the dimer state, and these two states merge at the tricritical point $|r_0|/a = 0$.

using the residue theorem again and obtain a closed-form result. In this way, we obtain the equation determining the trimer energy in the form

$$\begin{aligned} 0 = {} & \pi(1+|r_0|)\left[r_0^2E^2 - 4|E|(1+|r_0|)^2 + 4(2+|r_0|)^2\right] \\ & + 4\sqrt{|E|-1}\left[2(2+|r_0|)^2 - |E|r_0^2\right]\left(\pi - \arctan\sqrt{|E|-1}\right) \\ & - 4(2-|E|)(2+|r_0|)\sqrt{(2+|r_0|)^2 - |E|r_0^2}\,\operatorname{arctanh}\sqrt{1 - \frac{r_0^2|E|}{(2+|r_0|)^2}}, \end{aligned} \tag{5.31}$$

which can be now solved numerically or analyzed by hand.

In Figure 5.1, we show the numerical solution of Eq. (5.31). We find that there is one trimer state when $0 < \sqrt{2mE_B}|r_0| < 0.279226$, or equivalently $0 < a^{-1} < 0.31821|r_0|^{-1} \equiv (a^*)^{-1}$. At the critical scattering length $a = a^*$, the trimer state crosses the atom-dimer threshold, dissolving into the continuum. As shown in the inset of Fig. 5.1, the opposite limit of $|r_0|/a \to +0$ is the "tricritical point", at which both the trimer and the dimer merge into the unbound continuum. This is consistent with Efimov's prediction that $|a_-/r_0| \to \infty$ in the limit of $m_i/m_B \to \infty$. The energy approaches $-2E_B$, which is

expected because the limit $r_0 \to -0$ makes the two-channel model behave more like the single-channel model, as discussed in Section 2.2.1. Also, this observation agrees with the earlier one that $E = -2E_B$ is achieved if and only if $Z = 0$, because it vanishes as $Z \propto |r_0|^{1/2}$. However, the approach to $E = -2E_B$ is very slow. We find that the trimer is almost degenerate with the dimer except in the very close vicinity of $|r_0|/a = 0$.

We can discuss this limiting behavior more quantitatively. First, note that $\operatorname{arctanh} x \sim -\frac{1}{2}\log(1-x)$ as $x \to 1$. This implies that the limit $r_0 \to 0$ accompanies a logarithmic divergence of arctanh in the third line of Eq. (5.31). As the first and the second terms of Eq. (5.31) remain finite in the limits of $E \to -2$ and $r_0 \to -0$, the divergence needs to be compensated by the vanishing factor of $(2 - |E|)$ in order for Eq. (5.31) to hold. We thus find that

$$\frac{E}{E_B} \sim -2 + \frac{2\pi}{\log(a/|r_0|)} \quad (r_0 \to -0), \tag{5.32}$$

up to the leading-logarithmic correction, where we have used $E_B \to 1/ma^2$ for $r_0 \to 0$. This explains the slow convergence of E/E_B to the single-channel value of 2. At the level of the two-body physics, the finite-r_0 corrections to the quantities such as the bound-state energy and the scattering amplitude is given by powers of r_0/a. Therefore in many cases, it does not change the qualitative behavior of the system. On the other hand, our results reveal that once we consider three-body systems, a finite effective range drastically changes the spectrum, and that the correction from the zero-effective-range limit vanishes only logarithmically.

5.2 Universality of the logarithmic correction

In this section, we argue that the logarithmic correction found in the previous section is not peculiar to the r_0-model, but is a universal feature associated with the three-body repulsion. We also find that the four-body system exhibits a similar logarithmic correction with a different coefficient.

For this purpose, we first solve the integral equation for the three-body problem within the Λ-model. In the limit of the infinite-mass impurity, the equation reads

$$T^{-1}(E - \varepsilon_{\boldsymbol{p}})\gamma_{\boldsymbol{p}} = \sum_{|\boldsymbol{p}'|<\Lambda} \frac{\gamma_{\boldsymbol{p}'}}{E - \varepsilon_{\boldsymbol{p}} - \varepsilon_{\boldsymbol{p}'}}, \tag{5.33}$$

where $T(E) \equiv \frac{4\pi}{a^{-1} - \sqrt{-E - i0}}$. Compared with Eq. (4.12), the T-matrix in Eq. (5.33) is independent of the momentum, and the denominator of the integrand does not have

the term corresponding to the kinetic energy of the impurity, both of which are the consequences of the infinite mass of the impurity.

In Figure 5.2(a), we show the plot of $E_B/(E + 2E_B)$ calculated within the r_0-model and the Λ-model, where E is the ground-state energy of the three-body system. The result for the Λ-model has the same asymptotic slope for $a \to +\infty$ as the r_0-model. This suggests the following universal expression of the energy of the three-body bound state:

$$\frac{E}{E_B} \sim -2 + \frac{2\pi}{\log a} \quad (a \to +\infty). \tag{5.34}$$

A similar logarithmic correction is found in the four-body problem. The bound-state energy is found by solving the integral equation,

$$T^{-1}(E - \varepsilon_{\boldsymbol{p}_1} - \varepsilon_{\boldsymbol{p}_2})\gamma_{\boldsymbol{p}_1\boldsymbol{p}_2} = \sum_{\boldsymbol{p}'} \frac{\gamma_{\boldsymbol{p}_1\boldsymbol{p}'} + \gamma_{\boldsymbol{p}_2\boldsymbol{p}'}}{E - \varepsilon_{\boldsymbol{p}_1} - \varepsilon_{\boldsymbol{p}_2} - \varepsilon_{\boldsymbol{p}'}}, \tag{5.35}$$

where the cutoff Λ is imposed on the integral for the Λ-model, and the T-matrix has a finite effective range for the r_0-model. In Figure 5.2(b), we show the plots of $E_B/(E + 3E_B)$ for the two models, where $3E_B$ is the energy expected for the four-body system without the three-body repulsion. They approach straight lines with the same slope, indicating the following asymptotic expression:

$$\frac{E}{E_B} \sim -3 + \frac{2\pi c}{\log a}, \tag{5.36}$$

where $c \simeq 3$ is a universal constant.

Equations (5.34) and (5.36) involve only the s-wave scattering length. This suggests that it is the only relevant parameter around the unitarity limit, and that the unitarity limit, in particular, is scale-invariant, at least up to the four-body sector. Since there is no logarithmic correction in interactions described by two-body potentials, we conclude that the logarithmic correction is a universal feature of the effective three-body interaction.

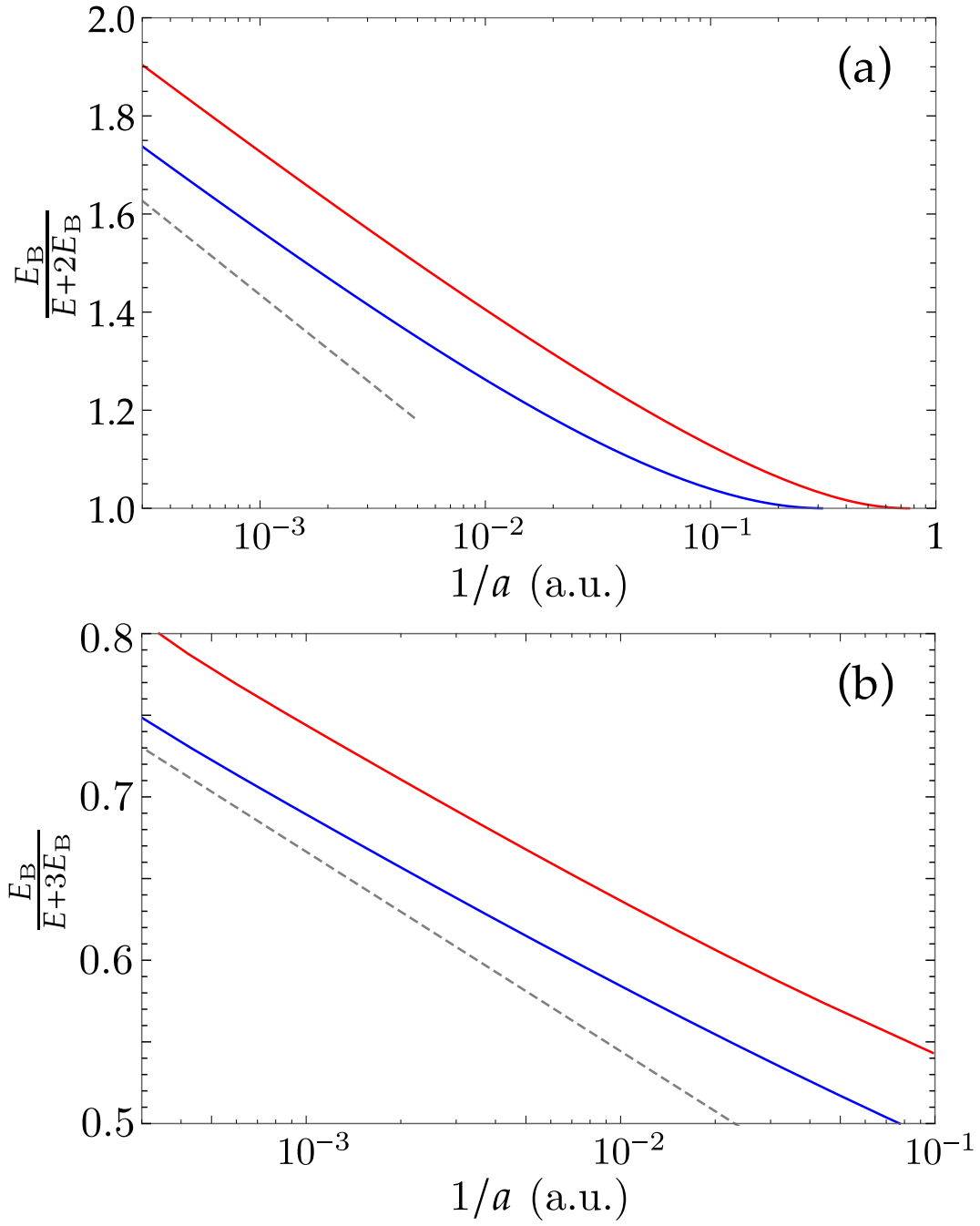

Figure 5.2: Universal logarithmic correction for (a) the three-body bound state and (b) the four-body bound state. Both the r_0-model (blue) and the Λ-model (red) show the logarithmic correction $2\pi/\log a$ to the limiting energy $E = -2E_B$. The unit of the length is r_0 in the r_0-model and Λ^{-1} in the Λ-model. The gray-dashed lines are eyeguides, which are parallel to (a) $\frac{\log a}{2\pi}$ and (b) $\frac{\log a}{6\pi}$.

Chapter 6

Ground-state properties of a Bose polaron

Now we turn to a many-body system, where a single impurity is immersed in a scalar Bose gas. This system is called a Bose polaron [108, 110–125]. The concept of the polaron was originally introduced to describe properties of an electron in polar crystals [164–166]. Coupling with phonons modifies electronic properties; for example, an electron acquires an effective mass and the self-energy, which can be measured from the electronic and magnetic response [167]. An impurity particle immersed in a Bose-Einstein condensate was also pointed out to be polaronic, and its weak-coupling limit is described by a model similar to the Fröhlich model [112, 115, 117], which is the paradigmatic theoretical model of the polaron [168, 169].

Our focus here is on the strong-coupling regime, where the s-wave scattering length a characterizing the impurity-boson interaction is larger than any other length scales of the system such as the average inter-particle spacing. In particular, we seek for universal properties in the ground state of the strongly coupled Bose polaron. A prime example of such universality in strongly coupled many-body systems is the unitary Fermi gas; at zero temperature, the only length scale in the unitary Fermi gas is the inter-particle spacing l, and thus physical quantities are completely determined by l, Planck's constant $\hbar$, the mass of the particles, and some universal dimensionless numbers [49, 50]. Motivated by this fact, we examine whether a similar universality emerges in a strongly coupled Bose system. Specifically, we investigate the ground-state properties of the Bose polaron and identify the characteristic parameters that are necessary to describe the Bose polaron.

In the case of the Bose systems, there are additional complications, which are irrelevant in the Fermi gas. First of all, scalar bosons can interact with each other, while fermions in the same spin state are almost non-interacting at ultra-low temperatures due to Pauli's exclusion principle. This introduces additional length scale, a_{B}, which is the s-wave scattering length between bosons. We assume that a_{B} is positive and much smaller than l, and what is more, we take $a_{\mathrm{B}} \to 0$ whenever possible. One issue

here is the stability of the Bose polaron when $a_B \to 0$; we will address this point in this chapter. Another, more fundamental issue is the presence of the Efimov effect in this system [5–7]. This gives rise to the three-body parameter a_-, which controls the three-body Efimov spectrum. Having these parameters in hand, we investigate in this chapter which quantities are sensitive to which length scales in the ground-state Bose polaron.

The outline of this chapter is as follows. In Section 6.1, we describe the model Hamiltonian and our theoretical approach. Here, we employ a variational method, which takes three Bogoliubov excitations into account. Variational wave functions with one [114] and two [108] Bogoliubov excitations have been used to describe the Bose polaron. We argue, however, that taking three excitations into account is minimal to examine the universality. In Section 6.2, we discuss the ground-state energy. In particular, we argue that the ground-state energy is a universal, model-independent function of the three-body parameter when the density is not too large. The high-density limit is weakly coupled, though highly model-dependent, and admits controlled analysis. We therefore derive analytical expressions of the energies for this regime and compare with the numerical results. In Section 6.3, we examine universality of other observables: the quasi-particle residue, the effective mass, and Tan's contact. We find that the residue approaches zero by adding a Bogoliubov excitation and is significantly sensitive to a_B. A perturbation theory reveals that the orthogonality of the ground-state wavefunction to the decoupled state for $a_B \to 0$ is caused by the infrared divergence, which is suppressed in the presence of a finite a_B.

6.1 Model and variational approach

6.1.1 Model Hamiltonian

A description of an impurity immersed in a weakly interacting Bose-Einstein condensate involves several length scales. The Bose medium is characterized by its density n and the s-wave scattering length between the bosons a_B. Since we focus on the weakly interacting regime, we assume that $n{a_B}^3 \ll 1$ and treat the condensate and excitations within the Bogoliubov theory. We also need the length scales describing the interactions between the impurity and bosons. For a short-range, resonant interaction, the foremost one is the s-wave scattering length a of the impurity-boson interaction. Here, we focus on the unitary regime near a Feshbach resonance, where $|a|$ is much larger than any other length scales, and therefore we fix $a^{-1} = 0$. Another important length scale associated

with the impurity-boson interaction is the three-body parameter a_-, which fixes the three-body spectrum of this system.

We model the interaction between the impurity and bosons by the r_0-model and the Λ-model, as defined in Chapter 4. We can also incorpolate a repulsive interaction between bosons by adding an interaction term, which leads to the following Hamiltonian:

$$\begin{aligned}
\hat{H} &= \hat{H}_{\mathrm{B}} + \hat{H}_{\mathrm{i}} + \hat{H}_{\mathrm{FR}}, \\
\hat{H}_{\mathrm{B}} &= \int d\boldsymbol{r} \left[\frac{1}{2m} \nabla\hat{\psi}_{\mathrm{B}}^\dagger \cdot \nabla\hat{\psi}_{\mathrm{B}} + \frac{U}{2} \hat{\psi}_{\mathrm{B}}^\dagger \hat{\psi}_{\mathrm{B}}^\dagger \hat{\psi}_{\mathrm{B}} \hat{\psi}_{\mathrm{B}} \right], \quad \hat{H}_{\mathrm{i}} = \int d\boldsymbol{r}\, \frac{1}{2m} \nabla\hat{\psi}_{\mathrm{i}}^\dagger \cdot \nabla\hat{\psi}_{\mathrm{i}}, \\
\hat{H}_{\mathrm{FR}} &= \int d\boldsymbol{r} \left[\frac{1}{4m} \nabla\hat{\phi}^\dagger \cdot \nabla\hat{\phi} + \nu_0 \hat{\phi}^\dagger \hat{\phi} + g_0 \left(\hat{\phi}^\dagger \hat{\psi}_{\mathrm{B}} \hat{\psi}_{\mathrm{i}} + \hat{\psi}_{\mathrm{i}}^\dagger \hat{\psi}_{\mathrm{B}}^\dagger \hat{\phi} \right) \right].
\end{aligned} \tag{6.1}$$

Here, $\hat{\psi}_{\mathrm{B}}^\dagger$, $\hat{\psi}_{\mathrm{i}}^\dagger$, and $\hat{\phi}^\dagger$ are the creation operators of a boson, the impurity, and a closed-channel molecule, respectively. The two-channel interaction is controlled by the detuning ν_0 and the inter-channel coupling g_0. The inter-boson interaction is also introduced, which is assumed to be a contact interaction with the strength $U = 4\pi a_{\mathrm{B}}/m$. As we concentrate on the single-impurity properties, the quantum statistics of the impurity and the closed-channel molecule is irrelevant, but for the sake of definiteness, we assume that they are bosons[1].

In the weakly interacting regime of the Bose gas, where $n{a_{\mathrm{B}}}^3 \ll 1$, we can apply the Bogoliubov approximation to the BEC [145], and consider interactions between the impurity and the Bogoliubov excitations on the condensate. This allows us to replace $\hat{\psi}_{\mathrm{B}}$ by $\sqrt{n_0} + \sum_{\boldsymbol{p}\neq 0} e^{i\boldsymbol{p}\cdot\boldsymbol{r}} \hat{\beta}_{\boldsymbol{p}}$, where $\hat{\beta}_{\boldsymbol{p}}$ is the annihilation operator of the Bogoliubov excitation with momentum $\boldsymbol{p}$, and to approximate $\hat{H}_{\mathrm{B}}$ as

$$\hat{H}_{\mathrm{B}} = \sum_{\boldsymbol{p}} E_{\boldsymbol{p}} \hat{\beta}_{\boldsymbol{p}}^\dagger \hat{\beta}_{\boldsymbol{p}}, \tag{6.2}$$

where we have omitted a constant energy arising from the inter-boson interaction as it is irrelevant for later discussions. Here, $E_{\boldsymbol{p}}$ is the Bogoliubov dispersion relation defined as

$$E_{\boldsymbol{p}} \equiv \sqrt{\varepsilon_{\boldsymbol{p}}(\varepsilon_{\boldsymbol{p}} + 8\pi n_0 a_{\mathrm{B}}/m)} = \sqrt{\varepsilon_{\boldsymbol{p}}(\varepsilon_{\boldsymbol{p}} + 1/m\xi^2)}, \tag{6.3}$$

where $\varepsilon_{\boldsymbol{p}} \equiv p^2/2m$ is the single-particle dispersion in vacuum, and $\xi \equiv 1/\sqrt{8\pi n_0 a_{\mathrm{B}}}$ is the coherence length of the condensate. The Bogoliubov operator $\hat{\beta}_{\boldsymbol{p}}$ is related to the

[1]This is a natural assumption in this mass-balanced case because an impurity particle with the same mass as the bosons is created by transferring atoms in the Bose gas to another hyperfine state [107]. More generally, however, impurity-boson systems with small mass imbalance can be realized by using fermions as impurity particles (e.g. a mixture of ^{41}K (boson) and ^{40}K (fermion)); we expect that the small mass imbalance does not affect our conclusion.

bosonic field operator $\hat{b}_{\boldsymbol{p}}$, which is the Fourier transform of $\hat{\psi}_{\mathrm{B}}(\boldsymbol{r})$, by the Bogoliubov transformation

$$\hat{b}_{\boldsymbol{p}} = u_p \hat{\beta}_{\boldsymbol{p}} - v_p \hat{\beta}^{\dagger}_{-\boldsymbol{p}}, \tag{6.4}$$

where

$$u_p^2 = [(\varepsilon_p + \mu)/E_p + 1]/2, \quad v_p^2 = [(\varepsilon_p + \mu)/E_p - 1]/2, \tag{6.5}$$

with the chemical potential of the bosons given by $\mu = 1/2m\xi^2$.

We also apply the Bogoliubov approximation to the coupling term $\hat{H}_{\mathrm{FR}}$. This leads to the following model Hamiltonian of an impurity in the weakly interacting BEC [108]:

$$\begin{aligned} \hat{H} = &\sum_{\boldsymbol{p}} \left[E_p \hat{\beta}^{\dagger}_{\boldsymbol{p}} \hat{\beta}_{\boldsymbol{p}} + \varepsilon_p \hat{c}^{\dagger}_{\boldsymbol{p}} \hat{c}_{\boldsymbol{p}} + (\varepsilon^{\mathrm{d}}_{\boldsymbol{p}} + \nu_0) \hat{d}^{\dagger}_{\boldsymbol{p}} \hat{d}_{\boldsymbol{p}} \right] \\ &+ g_0 \sqrt{n_0} \sum_{\boldsymbol{p}} \left(\hat{d}^{\dagger}_{\boldsymbol{p}} \hat{c}_{\boldsymbol{p}} + \hat{c}^{\dagger}_{\boldsymbol{p}} \hat{d}_{\boldsymbol{p}} \right) + g_0 \sum_{\boldsymbol{p},\boldsymbol{q}} \left(\hat{d}^{\dagger}_{\boldsymbol{p}+\boldsymbol{q}} \hat{b}_{\boldsymbol{q}} \hat{c}_{\boldsymbol{p}} + \hat{c}^{\dagger}_{\boldsymbol{p}} \hat{b}^{\dagger}_{\boldsymbol{q}} \hat{d}_{\boldsymbol{p}+\boldsymbol{q}} \right), \end{aligned} \tag{6.6}$$

where $\varepsilon^{\mathrm{d}}_{\boldsymbol{p}} = p^2/4m$, and $\hat{c}_{\boldsymbol{p}}$ and $\hat{d}_{\boldsymbol{p}}$ are the Fourier transforms of the impurity field $\hat{\psi}_{\mathrm{i}}(\boldsymbol{r})$ and the closed-channel field $\hat{\phi}(\boldsymbol{r})$, respectively. Note that the bosonic operator in the second line is the bare one $\hat{b}_{\boldsymbol{p}}$, not the Bogoliubov operator $\hat{\beta}_{\boldsymbol{p}}$. This is because the resonance occurs between the impurity and a bare boson, not between the impurity and a Bogoliubov excitation. We can of course write $\hat{b}_{\boldsymbol{p}}$ in terms of $\hat{\beta}_{\boldsymbol{p}}$, but we choose this form just for notational simplicity.

The Hamiltonian (6.6) depends on the inter-boson scattering length a_{B} through the Bogoliubov dispersion and the Bogoliubov transformation, where it appears only in the combination $n_0 a_{\mathrm{B}}$, or equivalently the coherence length $\xi = 1/\sqrt{8\pi n_0 a_{\mathrm{B}}}$. Consequently, the bosons are non-interacting in the dilute limit $n_0 \to 0$ within the present approximation, while the interaction between the impurity and bosons survives in the same limit. This implies that the three-body parameter a_- associated with the three-body Efimov state is independent of a_{B}; instead, it is determined by r_0 or Λ^{-1}, depending on the model chosen, in exactly the same way as discussed in Chapter 4. This is a consequence of the Bogoliubov approximation, which ignores higher-order contributions from the boson-boson interaction. This approximation is reasonable when a_{B} is much smaller than $|r_0|$ or Λ^{-1}, in which case the latter lengths predominantly determine a_-. One may also consider the opposite situation, where a_- is determined by a_{B}. Such a setting was investigated in Refs. [110, 119], where they considered an impurity interacting via a single-channel contact interaction with a hard-core Bose gas with the diameter a_{B}, as we have pointed out in Chapter 4.

6.1.2 Variational wavefunction

The interaction between the impurity and bosons, as modeled by the Hamiltonian (6.6), excites bosons out of the condensate. This means that the ground state is a superposition of states containing an arbitrary number of Bogoliubov excitations. Here, to evaluate the ground-state energy of the Bose polaron, we truncate the highly excited states and retain the states with at most three Bogoliubov excitations:

$$|\Psi\rangle = |\psi_1\rangle + |\psi_2\rangle + |\psi_3\rangle + |\psi_4\rangle\,, \tag{6.7}$$

$$|\psi_1\rangle = \alpha_0 \hat{c}_0^\dagger |0\rangle\,, \tag{6.8}$$

$$|\psi_2\rangle = \left(\sum_{\boldsymbol{p}} \alpha_{\boldsymbol{p}} \hat{c}_{-\boldsymbol{p}}^\dagger \hat{\beta}_{\boldsymbol{p}}^\dagger + \gamma_0 \hat{d}_0^\dagger\right)|0\rangle\,, \tag{6.9}$$

$$|\psi_3\rangle = \left(\frac{1}{2}\sum_{\boldsymbol{p}_1,\boldsymbol{p}_2} \alpha_{\boldsymbol{p}_1,\boldsymbol{p}_2} \hat{c}_{-\boldsymbol{p}_1-\boldsymbol{p}_2}^\dagger \hat{\beta}_{\boldsymbol{p}_1}^\dagger \hat{\beta}_{\boldsymbol{p}_2}^\dagger + \sum_{\boldsymbol{p}} \gamma_{\boldsymbol{p}} \hat{d}_{-\boldsymbol{p}}^\dagger \hat{\beta}_{\boldsymbol{p}}^\dagger\right)|0\rangle\,, \tag{6.10}$$

$$|\psi_4\rangle = \left(\frac{1}{6}\sum_{\boldsymbol{p}_1,\boldsymbol{p}_2,\boldsymbol{p}_3} \alpha_{\boldsymbol{p}_1\boldsymbol{p}_2\boldsymbol{p}_3} \hat{c}_{-\boldsymbol{p}_1-\boldsymbol{p}_2-\boldsymbol{p}_3}^\dagger \hat{\beta}_{\boldsymbol{p}_1}^\dagger \hat{\beta}_{\boldsymbol{p}_2}^\dagger \hat{\beta}_{\boldsymbol{p}_3}^\dagger + \frac{1}{2}\sum_{\boldsymbol{p}_1,\boldsymbol{p}_2} \gamma_{\boldsymbol{p}_1\boldsymbol{p}_2} \hat{d}_{-\boldsymbol{p}_1-\boldsymbol{p}_2}^\dagger \hat{\beta}_{\boldsymbol{p}_1}^\dagger \hat{\beta}_{\boldsymbol{p}_2}^\dagger\right)|0\rangle\,. \tag{6.11}$$

Here, $|0\rangle$ is the ground state of the condensate without the impurity, which satisfies $\hat{\beta}_{\boldsymbol{p}}^\dagger |0\rangle = 0$ for any $\boldsymbol{p}$. Each component $|\psi_i\rangle$ has $i-1$ bosons that are excited out of the condensate.

The c-number coefficients, denoted by α and γ, are determined variationally by the stationary condition, $\partial(\langle\Psi|(\hat{H}-E)|\Psi\rangle)/\partial(\alpha^*,\gamma^*) = 0$, where the Lagrange multiplier, E, is introduced to ensure the normalization condition $\langle\Psi|\Psi\rangle = 1$. This represents the energy measured with respect to the ground state without the impurity. This leads to a set of seven coupled equations, from which we can remove α and obtain the coupled integral equations,

$$\left[T_{\mathrm{BEC}}^{-1}(E,0) - \frac{n_0}{E}\right]\gamma_0 = \sqrt{n_0}\sum_{\boldsymbol{p}}\left(\frac{u_{\boldsymbol{p}}\gamma_{\boldsymbol{p}}}{E-\varepsilon_{\boldsymbol{p}}-E_{\boldsymbol{p}}} - \frac{v_{\boldsymbol{p}}\gamma_{\boldsymbol{p}}}{E}\right) - \sum_{\boldsymbol{p},\boldsymbol{q}}\frac{u_{\boldsymbol{p}}v_{\boldsymbol{q}}\gamma_{\boldsymbol{p}\boldsymbol{q}}}{E-\varepsilon_{\boldsymbol{p}}-E_{\boldsymbol{p}}}, \tag{6.12}$$

$$\begin{aligned}\left[T_{\mathrm{BEC}}^{-1}(E-E_{\boldsymbol{p}},\boldsymbol{p}) - \frac{n_0}{E-\varepsilon_{\boldsymbol{p}}-E_{\boldsymbol{p}}}\right]\gamma_{\boldsymbol{p}} &= \sqrt{n_0}\left(\frac{u_{\boldsymbol{p}}\gamma_0}{E-\varepsilon_{\boldsymbol{p}}-E_{\boldsymbol{p}}} - \frac{v_{\boldsymbol{p}}\gamma_0}{E}\right)\\ &+ \sum_{\boldsymbol{q}}\left(\frac{u_{\boldsymbol{p}}u_{\boldsymbol{q}}\gamma_{\boldsymbol{q}}}{E-E_{\boldsymbol{p}\boldsymbol{q}}} + \frac{v_{\boldsymbol{p}}v_{\boldsymbol{q}}\gamma_{\boldsymbol{q}}}{E}\right) + \sqrt{n_0}\sum_{\boldsymbol{q}}\left(\frac{u_{\boldsymbol{q}}\gamma_{\boldsymbol{p}\boldsymbol{q}}}{E-E_{\boldsymbol{p}\boldsymbol{q}}} - \frac{v_{\boldsymbol{q}}\gamma_{\boldsymbol{p}\boldsymbol{q}}}{E-\varepsilon_{\boldsymbol{p}}-E_{\boldsymbol{p}}}\right),\end{aligned} \tag{6.13}$$

$$\begin{aligned}\left[T_{\mathrm{BEC}}^{-1}(E-E_{\boldsymbol{p}_1}-E_{\boldsymbol{p}_2},\boldsymbol{p}_1+\boldsymbol{p}_2) - \frac{n_0}{E-E_{\boldsymbol{p}_1\boldsymbol{p}_2}}\right]\gamma_{\boldsymbol{p}_1\boldsymbol{p}_2} &= -\frac{u_{\boldsymbol{p}_1}v_{\boldsymbol{p}_2}\gamma_0}{E-\varepsilon_{\boldsymbol{p}_1}-E_{\boldsymbol{p}_1}}\\ &+ \sqrt{n_0}\left(\frac{u_{\boldsymbol{p}_1}\gamma_{\boldsymbol{p}_2}}{E-E_{\boldsymbol{p}_1\boldsymbol{p}_2}} - \frac{v_{\boldsymbol{p}_1}\gamma_{\boldsymbol{p}_2}}{E-\varepsilon_{\boldsymbol{p}_2}-E_{\boldsymbol{p}_2}}\right) + \sum_{\boldsymbol{q}}\left(\frac{u_{\boldsymbol{p}_1}u_{\boldsymbol{q}}\gamma_{\boldsymbol{p}_2\boldsymbol{q}}}{E-E_{\boldsymbol{p}_1\boldsymbol{p}_2\boldsymbol{q}}} + \frac{v_{\boldsymbol{p}_1}v_{\boldsymbol{q}}\gamma_{\boldsymbol{p}_2\boldsymbol{q}}}{E-\varepsilon_{\boldsymbol{p}_2}-E_{\boldsymbol{p}_2}}\right) + (\boldsymbol{p}_1 \leftrightarrow \boldsymbol{p}_2).\end{aligned} \tag{6.14}$$

Here, $(\boldsymbol{p}_1 \leftrightarrow \boldsymbol{p}_2)$ denotes the terms that symmetrize the right-hand side of Eq. (6.14), $E_{pq} \equiv E_{p+q} + \varepsilon_p + \varepsilon_q$ and $E_{kpq} \equiv E_{k+p+q} + \varepsilon_k + \varepsilon_p + \varepsilon_q$. The medium T-matrix, $T_{\mathrm{BEC}}(E, \boldsymbol{p})$, is defined as

$$T_{\mathrm{BEC}}^{-1}(E, \boldsymbol{p}) = T_0^{-1}(E, \boldsymbol{p}) + \sum_{\boldsymbol{q}} \left[\frac{1}{E - \varepsilon_{\boldsymbol{q}} - \varepsilon_{\boldsymbol{p}+\boldsymbol{q}}} - \frac{u_{\boldsymbol{q}}^2}{E - E_{\boldsymbol{q}} - \varepsilon_{\boldsymbol{p}+\boldsymbol{q}}} \right], \tag{6.15}$$

where $T_0(E, \boldsymbol{p}) = \frac{4\pi}{m} \left[a^{-1} - \frac{r_0}{2} m(E - \varepsilon_{\boldsymbol{p}}^{\mathrm{d}}) - \sqrt{-m(E - \varepsilon_{\boldsymbol{p}}^{\mathrm{d}})} \right]^{-1}$ is the two-body T-matrix in vacuum. The procedure that yields these equations is similar to that used in Chapter 4 and is detailed in Appendix A. In the r_0-model, we have a finite effective range r_0 in the vacuum T-matrix and take the integration in Eqs. (6.12–6.14) without an ultraviolet cutoff. On the other hand, in the Λ-model, we set $r_0 = 0$ and truncate the integration at $|\boldsymbol{q}| = \Lambda$. Note, however, that the integration in Eq. (6.15) is kept without the UV-cutoff so that Λ leaves two-body physics unaffected. We solve the integral equations (6.12–6.14) numerically to evaluate the energy and other properties of the Bose polaron in the ground state.

It is essential for our purpose to keep the full three-excitation component $|\psi_4\rangle$ in the truncated ansatz. First of all, to see the effects of beyond-two-body physics, especially the Efimov physics, we need at least two excitations that are correlated in a way that supports the Efimov states involving the impurity and two bosons. Here, we take the most general form of $\alpha_{p_1 p_2}$, $\alpha_{p_1 p_2 p_3}$, and so on, within the zero-angular-momentum sector, and therefore have enough room to observe the Efimov physics in the Bose polaron. Furthermore, to examine whether polaron properties are fully determined by parameters characterizing two- and three-body physics such as a and a_-, or controlled by an additional "more-body" parameter, the three-excitation ansatz offers the minimal starting point, which fully takes four-body correlations into account.

6.2 Ground-state energy

We now present the ground-state energy of the Bose polaron at unitarity. The discussions here mainly deal with the non-interacting limit of the Bose gas, $a_{\mathrm{B}} \to 0$ and $\xi \to \infty$. In this case, the Bogoliubov excitation is identical with the bare bosonic excitation, and the Bogoliubov spectrum reduces to the single-particle kinetic energy $p^2/2m$ in free space. In Fig 6.1(a), we compare the ground-state energy of the r_0-model with that of the Λ-model. In order to compare the results of two different models and reveal the role of the Efimov physics in the Bose polaron, we convert the short-range parameter, r_0 or Λ^{-1}, into the dimensionless three-body parameter $n^{1/3}|a_-|$. We also calculate

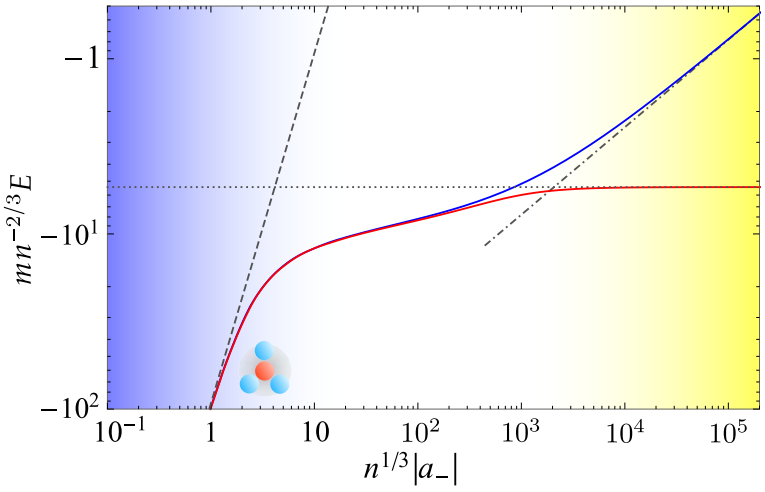

(a)

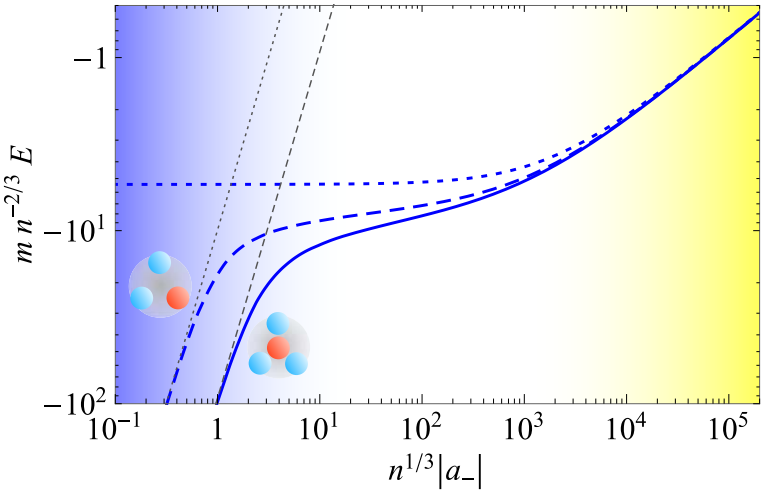

(b)

Figure 6.1: Ground-state energy of the Bose polaron at unitarity as a function of $n_0^{1/3}|a_-|$ for $a_B \to 0$. (a) We show the results for the r_0-model (blue) and the Λ-model (red). When the Bose gas is dilute ($n_0^{1/3}|a_-| \ll 1$), the energies approach the energy of the ground-state tetramer (gray dashed). The high-density regime displays highly model-dependent behavior. The ground-state energy in the r_0-model is consistent with the perturbation theory up to $O(g_0^2)$ (gray dot-dashed). On the other hand, the ground-state energy of the Λ-model saturates at $-\frac{2^{4/3}\pi^{2/3}n^{2/3}}{m} \simeq -\frac{5.405n^{2/3}}{m}$, which corresponds to the solution of the one-excitation ansatz within the Λ-model. (b) We show the results for the r_0-model, within the variational ansatz with one (dotted), two (dashed), and three (solid) Bogoliubov excitations. The gray dotted and dashed lines denote the energy of the ground-state Efimov trimer and that of the ground-state tetramer, respectively.

the ground-state energy within the variational ansatz with one and two Bogoliubov excitations, whose results for the r_0-model are shown in Fig. 6.1(b). In the following subsections, we discuss three different regimes of the density in detail.

6.2.1 Low-density limit

As we have already shown in Chapter 4, impurity-boson systems at unitarity have three- and four-body bound states, whose energies are universal. Therefore, as the low-density limit is taken, the Boes polaron at zero temerature should transform into the deepest bound cluster, whether or not there is a phase transition along the way.

Equations (6.12–6.14) can capture the crossover to at least four-body cluster. There is no obvious singularity in the equations, implying no phase transition within the approximation. The low-density limit $n_0 \to 0$ leads to $u_{\boldsymbol{p}} \to 1$, $v_{\boldsymbol{p}} \to 0$, and $T_{\mathrm{BEC}}(E, \boldsymbol{p}) \to T_0(E, \boldsymbol{p})$. As a result, Eqs. (6.12–6.14) reduce to Eqs. (4.11-4.13), which describe the few-body systems in vacuum. This implies that the approximate ground-state energy converges to that of the deepest 3+1–body cluster, which indeed happens without a phase transition within the present variational approach using the r_0-model and the Λ-model. The ground-state energy is independent of the density in this limit and can be written as $E = -\eta_4/ma_-^2$, where $\eta_4 \simeq 93$ is the universal, model-independent constant, as discussed in Chapter 4.

Within the current variational ansatz, larger bound states with more bosons cannot appear. However, theoretically, such states are not ruled out. In the case of identical bosons, it has been theoretically predicted that there exist five- and more-body clusters [19–21], and a five-body resonance in an ultracold Bose gas has been reported [40]. Similarly, a five-body bound state is predicted by a diffusion Monte Carlo calculation in the mass-balanced impurity-boson system at unitarity, while the same calculation suggests that there is no six- or more-body clusters [110].

Remarkably, the energy of the five-body cluster is estimated in Ref. [119] to be $E = -\eta_5/ma_-^2$ with $\eta_5 \simeq 300$, indicating that the size of the cluster is $O(|a_-|/20)$. This is still much larger than the microscopic length scale, which is a_{B} in the QMC calculation and r_0 and Λ^{-1} in our study. We would like to emphasize that it is natural that there is the largest cluster state having the maximal number of bosons. In the impurity-boson system, the pairwise attraction acts between the impurity and bosons and scales only linearly with the number of bosons. This is in contrast to identical boson systems, where the pairwise interaction scales quadratically with the number of the particles. Moreover, as argued in the previous chapters, the presence of r_0 or Λ implies the presence of an effective three-body repulsion. It is thus reasonable that the costs of kinetic energy

and three-body repulsion exceed the gain from the attractive interaction at some point, prohibiting formation of a larger bound cluster.

These considerations lead us to conclude that the dimensionless value η_5 and the absence of larger bound states than the five-body cluster are the universal features of the impurity-boson system. In other words, the ground-state energy of the Bose polaron is universal in the low-density limit of the background Bose gas even if we take the arbitrary number of the Bogoliubov excitations into account. An important consequence of this is that the Bose polaron can have a finite ground-state energy, even without repulsive interactions between the bosons. It is indeed the three-body repulsion, not necessarily the two-body repulsion between bosons, that saves this many-body system from collapsing.

6.2.2 Many-body universal regime

As the density of the Bose gas is made higher such that $n_0^{1/3} a_- \gtrsim 1$, the ground-state energy deviates from that of the few-body systems. This is because the size of the few-body cluster becomes comparable to or larger than the interparticle spacing of the Bose gas, and the few-body picture that is useful in the low-density limit is no longer applicable. Notably, the ground-state energy significantly depends on the three-body parameter in this regime of both models. This is in stark contrast to the unitary Fermi gas, which does not depend on any interaction length scales and whose physical quantities are determined by $\hbar$, the mass of the particles, the density, and the universal dimensionless numbers such as the Bertsch parameter.

Although the Bose polaron at unitarity does not have a universal value of the ground-state energy, we argue that it is a model-independent, universal function of $n_0^{1/3}|a_-|$ when the density is not too large. We have already discussed the universality in the dilute regime. Figure 6.1 further shows that even for $n_0^{1/3} a_- \gtrsim 1$, the curves of the two models collapse when they are plotted as a function of $n_0^{1/3}|a_-|$.

Since our calculation is based on the variational method, it can be subject to a criticism that the results are biased. In particular, one may argue that the observed universality is a consequence of the bias. It should be pointed out, however, that the ansatz that we adopt takes full four-body correlations, and that a bias, if any, would result from five- or more-body correlations. If such an effect causes nonuniversality, there should be a significant probability that four or more bosons gather around the impurity within the microscopic length scales such as r_0 and Λ^{-1}. This is not likely to happen unless particles form tight clusters, which, however, is not consistent with the discussion in the previous section.

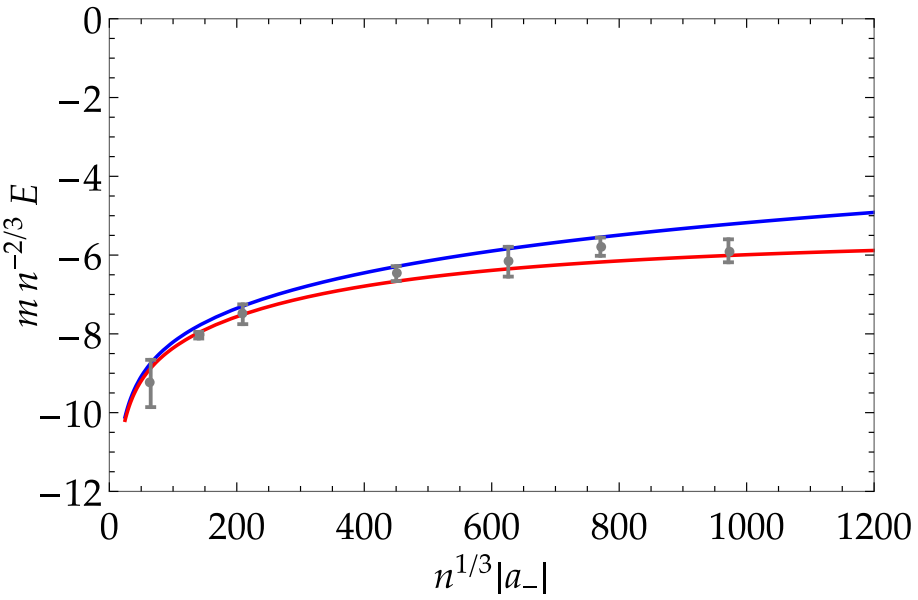

Figure 6.2: Comparison with the quantum Monte Carlo calculation [119] based on the hard-core model of the Bose polaron. The blue and red curves correspond to the results of the variational calculations within the r_0-model and the Λ-model, respectively, and the gray dots show the results of the QMC calculation. The error bars attached to the QMC results display the statistical uncertainty.

This argument is intuitive but not conclusive. A further evidence of the universality is offered by the comparison of our results with the diffusion Monte Carlo calculation based on the hard-core model of the Bose polaron [119]. This model incorporates the hard-core interaction between bosons with the diameter a_B and the contact interaction between the impurity and bosons. In Figure 6.2, we show the ground-state energy of the three different models of the Bose polaron. Here, we use Eq. (4.15) to convert the boson-boson scattering length a_B to the three-body parameter a_-. Although the results scatter within the range of 10-20% when $n_0|a_-| \sim 10^3$, they converge to a single curve as $n_0|a_-|$ is lowered. This demonstrates that the ground-state energy of the Bose polaron is universally determined by $n_0^{1/3}|a_-|$, independent of the microscopic details.

Note that the effects of a finite a_B are twofold in the hard-core model; it controls the three-body Efimov physics and also the properties of the Bose gas such as the coherence length of the condensate. On the other hand, in the r_0-model and the Λ-model, the three-body parameter and the coherence length are two independent parameter. The agreement between the three models when a_B is set zero in the latter two models reveals that the ground-state energy is predominantly determined by the three-body parameter, rather than the coherence length. We can also take a finite coherence length into account in the variational calculation. In Figure 6.3, we show the ground-state energy within the r_0-model with a_B set to be zero (solid) and finite (dashed). In the latter calculation,

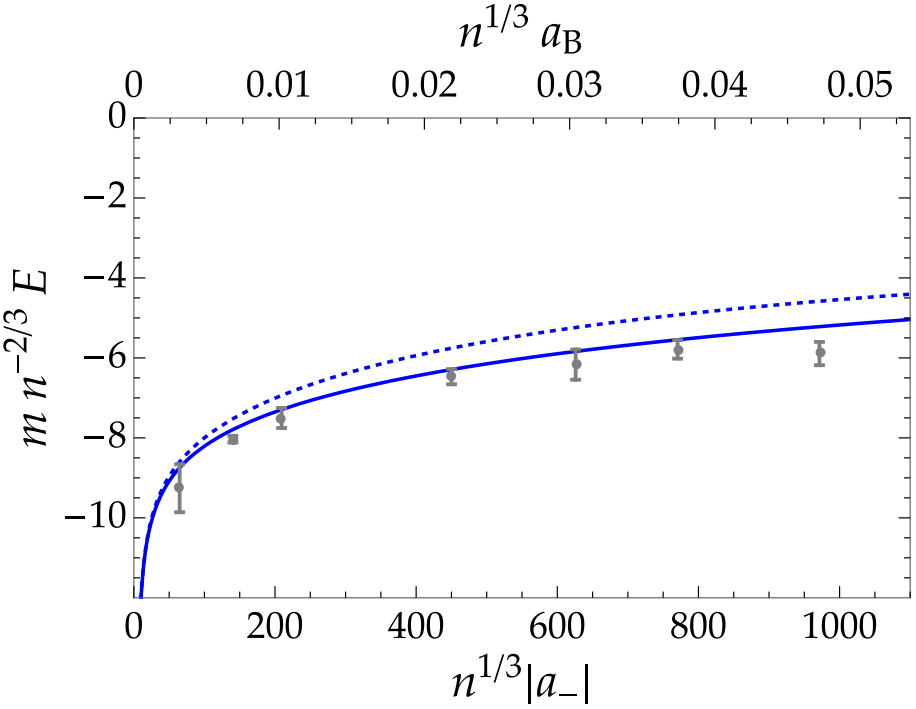

Figure 6.3: Ground-state energy of the Bose polaron within the r_0-model for $a_B \to 0$ (solid) and $a_B = |a_-|/(2.1 \times 10^4)$ (dashed). The gray dots are the results of the QMC calculation in Ref. [119]. The top horizontal axis shows $n^{1/3}a_B$ corresponding to the dashed curve and the gray dots.

we fix a_B by $a_B = a_-/(2.1 \times 10^4)$, to be consistent with the hard-core interaction. We again emphasize that a_B in the current calculation does not affect a_- while it controls the cohence length ξ. The energy is almost insensitive to ξ in the low-density regime where the few-body physics dominates. On the other hand, as we increase the density, there is a visible shift in the ground-state energy. The change of this shift with ξ is, however, much smaller than the variation caused by the three-body parameter alone. We also show the data points of the hard-core model, which clarify that the shift caused by ξ is too small to account for the energy variation in the hard-core model. Thus, we conclude that the ground-state energy of the Bose polaron is a universal function of a_-, and that it is insensitive to other details including the coherence length of the condensate.

6.2.3 High-density limit

The properties of the Bose polaron are highly model-dependent in this regime. It is a natural consequence of the fact that the interparticle spacing $n^{-1/3}$ is comparable to or smaller than the microscopic lengths such as the effective range. At the same time, the Bose polaron in the r_0-model and the Λ-model is weakly correlated in this

limit, as discussed below[2]. We can exploit this property to calculate the ground-state energy and compare the results with the variational calculation. Here, we present the many-body perturbation theory in the r_0-model and show that they are consistent with the variational calculation in the high-density regime. Next, we calculate the limiting energy within the Λ-model in the case of $a_B = 0$ by using the truncated ansatz with the arbitrary (but finite) number of excitations, and show that it is given as the solution of $T_0^{-1}(E, 0) = n_0/E$, which is

$$E = -\frac{2^{4/3}\pi^{2/3}n^{2/3}}{m} \simeq -\frac{5.405n^{2/3}}{m}. \tag{6.16}$$

This is also consistent with the variational calculation. Note that this is same as the variational equation based on the trial wave function truncated at one Bogoliubov excitation, instead of three.

Note that Fig. 6.1(b) clearly shows that the variational approach for the r_0-model converges fast with the number of the Bogoliubov excitations in this regime. This is also true for the Λ-model. The consistency of the analytical expressions and the variational results is, therefore, indicative of the finite ground-state energies of this many-body system even without the boson-boson repulsion for high densities. Combining this and the discussion in the low-density limit, we conclude that the Bose polaron at unitarity is stabilized by the three-body repulsion at any density.

The r_0-model

In the r_0-model, the dimensionless coupling constant of a Feshbach resonance is $n^{-1/3}g_0^2$ in finite-density systems [105][3]. This indicates that the high density is equivalent to the small coupling constant, and that the perturbation theory in terms of this coupling constant is applicable in this regime. Physically, a small g_0 is of interest because it corresponds to a narrow Feshbach resonance, whose weak-coupling nature has been exploited mostly in a Fermi gas [105] and an impurity immersed in a Fermi sea (a Fermi polaron) [170]. Here, we present the perturbation theory to the next-to-the-leading order.

Figures 6.4(a, b) show the impurity self-energy up to $O(g_0^4)$, which reads

$$\Sigma(\omega, \boldsymbol{p}) = \Sigma^{(2)}(\omega, \boldsymbol{p}) + \Sigma^{(4)}(\omega, \boldsymbol{p}), \tag{6.17}$$

[2]This statement itself is model-dependent. It should be clear if we consider the hard-core interaction between bosons, which restricts the density of the Bose gas and does not have the high-density limit.

[3]Here we square the coupling constant g_0. This is because in scattering processes the formation of a closed-channel molecule always accompanies its dissociation, which is overall a second-order process in terms of g_0.

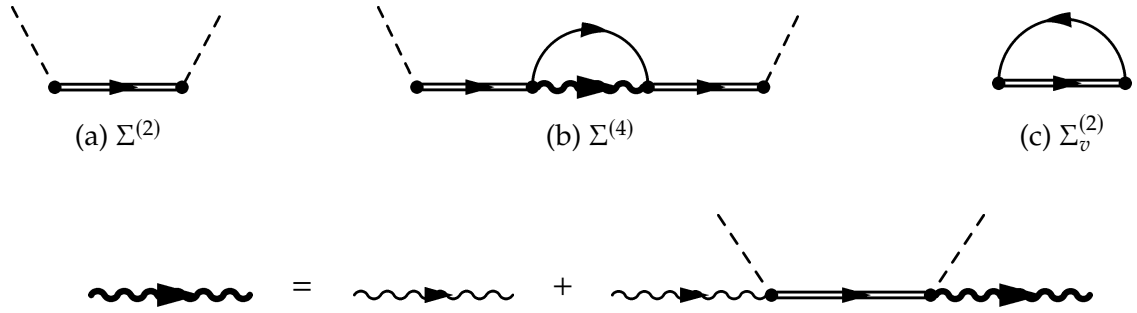

(a) $\Sigma^{(2)}$ (b) $\Sigma^{(4)}$ (c) $\Sigma_v^{(2)}$

(d) Dressed impurity propagator

Figure 6.4: Self-energy diagrams that contribute to the ground-state energy up to the next-to-the-leading order. When the boson-boson scattering length a_B is zero, there are only two diagrams (a, b) up to this order. Here, the dashed lines and the solid line denote the condensate and excited bosons, respectively, while the double line represents the closed-channel molecules and the wavy line shows the impurity propagator. The impurity propagator in the next-to-the-leading order diagram (b) is dressed by the leading-order self-energy and its definition is given in the Dyson equation (d). If there is a finite boson-boson scattering length, the other $O(g_0^2)$ diagram (c) also gives rise to the next-to-the-leading order correction.

$$\Sigma^{(2)}(\omega, \boldsymbol{p}) = \frac{g_0^2 n_0}{\omega - \varepsilon_{\boldsymbol{p}}^\mathrm{d}}, \tag{6.18}$$

$$\Sigma^{(4)}(\omega, \boldsymbol{p}) = \frac{g_0^4 n_0}{(\omega - \varepsilon_{\boldsymbol{p}}^\mathrm{d})^2} \sum_{\boldsymbol{q}} \left[\frac{1}{\omega - \varepsilon_{\boldsymbol{q}} - \varepsilon_{\boldsymbol{p}+\boldsymbol{q}} - \frac{g_0^2 n_0}{\omega - \varepsilon_{\boldsymbol{q}} - \varepsilon_{\boldsymbol{p}+\boldsymbol{q}}^\mathrm{d}}} + \frac{1}{2\varepsilon_{\boldsymbol{q}}} \right]. \tag{6.19}$$

Here, we have used the assumption that $a_\mathrm{B} = 0$, which implies that $u_{\boldsymbol{q}} = 1, v_{\boldsymbol{q}} = 0$, and that the Bogoliubov dispersion $E_{\boldsymbol{q}}$ reduces to the single-particle dispersion $\varepsilon_{\boldsymbol{q}}$ in vacuum. In the momentum integral, the subtraction of $1/2\varepsilon_{\boldsymbol{q}}$ is necessary to compensate the ultraviolet divergence, which comes from the impurity-boson scattering in vacuum. This is equivalent to the renormalization procedure described in Section 2.2.1.

The polaron energy is found from the equation $E = \Sigma(E, 0)$. At the order of $O(g_0^2)$, this reads $E = g_0^2 n_0 / E$, leading to $E = E^{(2)} \equiv -\sqrt{8\pi n_0 / |r_0|}/m$. Here, we used $g_0^2 = 8\pi / m^2 |r_0|$. This is consistent with the asymptotic behavior of the variational calculation with the r_0-model as shown in Fig. 6.1. Now, suppose that $E = E^{(2)} + \delta E$. The energy equation can be rewritten within the current approximation as follows:

$$E = \Sigma(E, 0), \tag{6.20}$$

$$\Leftrightarrow \quad E^{(2)} + \delta E \simeq \Sigma^{(2)}(E, 0) + \Sigma^{(4)}(E, 0) \simeq E^{(2)} - \delta E + \Sigma^{(4)}(E^{(2)}, 0), \tag{6.21}$$

$$\Leftrightarrow \quad \delta E \simeq \frac{1}{2} \Sigma^{(4)}(E^{(2)}, 0). \tag{6.22}$$

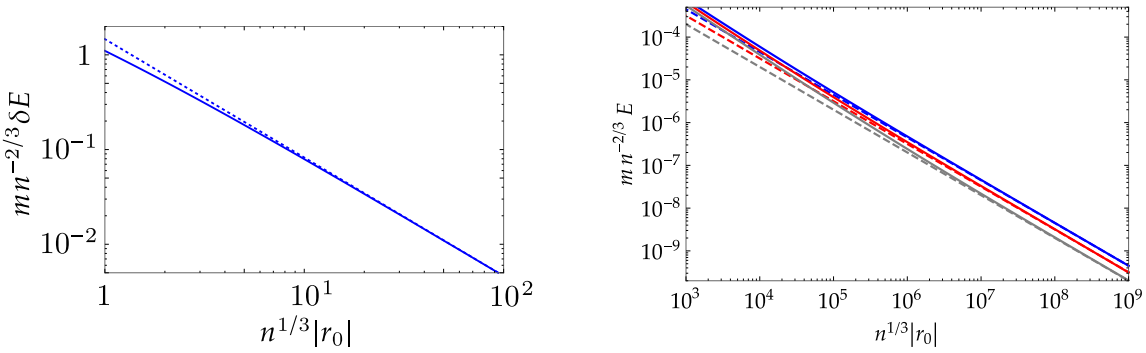

(a) $a_B = 0$ (b) $a_B = 0.02$ (gray), 0.05 (red), and 0.1 (blue)

Figure 6.5: Next-to-the-leading order correction of the ground-state energy within the r_0-model. We show $\delta E = E - E^{(2)}$ of the variational calculations (solid) and the perturbation theory (dashed), where $E^{(2)} \equiv -\sqrt{8\pi n_0/|r_0|}/m$ is the energy determined from the self-energy of $O(g_0^2)$. (a) When the background Bose gas is non-interacting, the $O(g_0^4)$ correction to the self-energy gives $\delta E = \frac{1}{m}\sqrt{\frac{3}{7}}\left(\frac{8\pi n_0}{|r_0|^5}\right)^{1/4}$, which is correctly captured by the variational calculation. (b) If a_B is small and positive, $\delta E \propto \frac{\sqrt{n_0 a_B}}{|r_0|}$ as $r_0 \to \infty$ with a fixed a_B. This scaling and the coefficient is also reproduced by the variational calculation.

By noting that $(E^{(2)})^2 = g_0^2 n_0$, $\Sigma^{(4)}(E^{(2)}, 0)$ is readily calculated:

$$\Sigma^{(4)}(E^{(2)}, 0) = g_0^2 \sum_q \left[\frac{1}{E^{(2)} - q^2/m - \frac{(E^{(2)})^2}{E^{(2)} - 3q^2/4m}} + \frac{m}{q^2} \right] \tag{6.23}$$

$$= \frac{2}{m}\sqrt{\frac{3}{7}}\left(\frac{8\pi n_0}{|r_0|^5}\right)^{1/4}. \tag{6.24}$$

Figure 6.5(a) shows that this correction is also captured by the variational calculation. The range of validity of this calculation, especially the validity of $a_B \to 0$, becomes clear when we consider a finite $a_B > 0$. In this case, the additional diagram in Fig. 6.4(c) contributes to the same order[4]. The $O(g_0^4)$-correction $\Sigma^{(4)}$ is also modified, while $\Sigma^{(2)}$ is unchanged. These finite-a_B corrections read

$$\Sigma_v^{(2)}(\omega, \boldsymbol{p}) = g_0^2 \sum_{\boldsymbol{q}} \frac{v_{\boldsymbol{q}}^2}{\omega - E_{\boldsymbol{q}} - \varepsilon^{\mathrm{d}}_{\boldsymbol{p}+\boldsymbol{q}}}, \tag{6.25}$$

[4]Although there are five other diagrams of the self-energy up to $O(g_0^4)$, they only give higher-order corrections in the limit of $|r_0| \to \infty$ with a fixed a_B. The detailed diagrammatic analysis on this is given in Appendix B.

$$\Sigma^{(4)}(\omega, \boldsymbol{p}) = \frac{g_0^4 n_0}{(\omega - \varepsilon_{\boldsymbol{p}}^{\mathrm{d}})^2} \sum_{\boldsymbol{q}} \left[\frac{u_{\boldsymbol{q}}^2}{\omega - E_{\boldsymbol{q}} - \varepsilon_{\boldsymbol{p}+\boldsymbol{q}} - \frac{g_0^2 n_0}{\omega - E_{\boldsymbol{q}} - \varepsilon_{\boldsymbol{p}+\boldsymbol{q}}^{\mathrm{d}}}} + \frac{1}{2\varepsilon_{\boldsymbol{q}}} \right]. \tag{6.26}$$

In these integrals, the comparison between ω and $1/(2m\xi^2)$ defines two different regimes. Let us focus on $\omega = E^{(2)}$ and $\boldsymbol{p} = 0$. When $\omega \gg 1/(2m\xi^2)$, or equivalently $n_0 {a_{\mathrm{B}}}^3 \ll a_{\mathrm{B}}/|r_0|$ ($\ll 1$)[5], the momentum-dependence of the integrand becomes significant only when $|\boldsymbol{q}| \gg \sqrt{2m|\omega|} \gg \xi^{-1}$, and thus we can take $u_{\boldsymbol{q}} \to 1$, $v_{\boldsymbol{q}} \to 0$, and $E_{\boldsymbol{q}} \to \varepsilon_{\boldsymbol{q}}$. In this limit, the resulting expressions reduce to those of $a_{\mathrm{B}} = 0$ as given in Eq. (6.24). On the other hand, when $\omega \ll 1/(2m\xi^2)$ ($\Leftrightarrow a_{\mathrm{B}}/|r_0| \ll n_0 {a_{\mathrm{B}}}^3 \ll 1$), we can ignore ω from the integrand except in a small fraction of the integration range. Also, the contribution to the final results from such a small region only gives higher-order corrections. We thus obtain

$$\Sigma_v^{(2)}(E^{(2)}, 0) + \Sigma^{(4)}(E^{(2)}, 0) \simeq g_0^2 \sum_{\boldsymbol{q}} \left[\frac{u_{\boldsymbol{q}}^2}{-E_{\boldsymbol{q}} - \varepsilon_{\boldsymbol{q}}} + \frac{v_{\boldsymbol{q}}^2}{-E_{\boldsymbol{q}} - \varepsilon_{\boldsymbol{q}}^{\mathrm{d}}} + \frac{1}{2\varepsilon_{\boldsymbol{q}}} \right] \tag{6.27}$$

$$= \frac{16\sqrt{3}\pi - 72}{3\sqrt{\pi}m} \frac{\sqrt{n_0 a_{\mathrm{B}}}}{|r_0|} \simeq \frac{2.83268}{m} \frac{\sqrt{n_0 a_{\mathrm{B}}}}{|r_0|}, \tag{6.28}$$

which results in $\delta E = \frac{8\sqrt{3}\pi - 36}{3\sqrt{\pi}m} \frac{\sqrt{n_0 a_{\mathrm{B}}}}{|r_0|}$. Therefore, if $a_{\mathrm{B}}/|r_0| \ll n_0 {a_{\mathrm{B}}}^3$, the next-to-the-leading correction to the ground-state energy scales as $\sqrt{a_{\mathrm{B}}}/|r_0|$, instead of $|r_0|^{-5/4}$ as found in Eq. (6.24) for $a_{\mathrm{B}} \to 0$. This is also consistent with the variational calculation with a finite a_{B}, as shown in Fig. 6.5(b).

Importantly, the next-to-the-leading order correction is positive, which implies that the ground-state energy is bounded by $E^{(2)}$ from below. This reveals that the ground-state energy has a well-defined limit even if we take $a_{\mathrm{B}} \to 0$. This is possible because of the effective three-body repulsion, as discussed in the previous chapter. Although the coupling in the r_0-model is zero-ranged, it still has a non-zero effective range r_0, which stabilizes this many-body system.

The Λ-model

Here, the dimensionless cutoff is $n^{-1/3}\Lambda$, which vanishes in the high-density limit, and consequently, three-body processes are prohibited at any momentum. This leads to the observed convergence of the energy to the value corresponding to the one-excitation ansatz. We can show this when $a_{\mathrm{B}} = 0$ within the variational ansatz by taking into

[5]The latter inequality is implied when we use the Bogoliubov approximation. See the discussion on the model Hamiltonian in the previous section.

account an arbitrary (but finite) number of Bogoliubov excitations. For convenience, we set $n_0 = 1$ in this discussion.

Let N be the maximum number of excitations that we take into account. The variational equations in this case constitute a set of the equations of the form

$$\left[T_{\mathrm{BEC}}^{-1}(E - E_k, \boldsymbol{P}_k) - \frac{1}{E - E_{\boldsymbol{p}_1 \ldots \boldsymbol{p}_k}}\right] \gamma_{\boldsymbol{p}_1 \ldots \boldsymbol{p}_k} = \frac{\gamma_{\boldsymbol{p}_2 \boldsymbol{p}_3 \ldots \boldsymbol{p}_k} + \cdots + \gamma_{\boldsymbol{p}_1 \boldsymbol{p}_2 \ldots \boldsymbol{p}_{k-1}}}{E - E_{\boldsymbol{p}_1 \ldots \boldsymbol{p}_k}} + \sum_{\boldsymbol{q}, |\boldsymbol{q}| < \Lambda} \left(\frac{\gamma_{\boldsymbol{q} \boldsymbol{p}_2 \boldsymbol{p}_3 \ldots \boldsymbol{p}_k} + \cdots + \gamma_{\boldsymbol{q} \boldsymbol{p}_1 \boldsymbol{p}_2 \ldots \boldsymbol{p}_{k-1}}}{E - E_{\boldsymbol{q} \boldsymbol{p}_1 \ldots \boldsymbol{p}_k}} + \frac{\gamma_{\boldsymbol{q} \boldsymbol{p}_1 \boldsymbol{p}_2 \ldots \boldsymbol{p}_k}}{E - E_{\boldsymbol{q} \boldsymbol{p}_1 \ldots \boldsymbol{p}_k}} \right), \tag{6.29}$$

for $k = 1, 2, \ldots, N-2$, and

$$\left[T_{\mathrm{BEC}}^{-1}(E, 0) - \frac{1}{E}\right] \gamma_0 = \sum_{\boldsymbol{q}, |\boldsymbol{q}| < \Lambda} \frac{\gamma_{\boldsymbol{q}}}{E - E_{\boldsymbol{q}} - \varepsilon_{\boldsymbol{q}}}, \tag{6.30}$$

$$\left[T_{\mathrm{BEC}}^{-1}(E - E_{N-1}, \boldsymbol{P}_{N-1}) - \frac{1}{E - E_{\boldsymbol{p}_1 \ldots \boldsymbol{p}_{N-1}}}\right] \gamma_{\boldsymbol{p}_1 \ldots \boldsymbol{p}_{N-1}} = \frac{\gamma_{\boldsymbol{p}_2 \boldsymbol{p}_3 \ldots \boldsymbol{p}_{N-1}} + \cdots + \gamma_{\boldsymbol{p}_1 \boldsymbol{p}_2 \ldots \boldsymbol{p}_{N-2}}}{E - E_{\boldsymbol{p}_1 \ldots \boldsymbol{p}_{N-1}}} + \sum_{\boldsymbol{q}, |\boldsymbol{q}| < \Lambda} \left(\frac{\gamma_{\boldsymbol{q} \boldsymbol{p}_2 \boldsymbol{p}_3 \ldots \boldsymbol{p}_{N-1}} + \cdots + \gamma_{\boldsymbol{q} \boldsymbol{p}_1 \boldsymbol{p}_2 \ldots \boldsymbol{p}_{N-2}}}{E - E_{\boldsymbol{q} \boldsymbol{p}_1 \ldots \boldsymbol{p}_{N-1}}} \right). \tag{6.31}$$

Here, $E_k \equiv \sum_{i=1}^{k} E_{\boldsymbol{p}_i}$, $\boldsymbol{P}_k \equiv \sum_{i=1}^{k} \boldsymbol{p}_i$, and $E_{\boldsymbol{p}_1 \boldsymbol{p}_2 \ldots \boldsymbol{p}_k} \equiv E_{\sum_{i=1}^{k} \boldsymbol{p}_i} + \sum_{i=1}^{k} \varepsilon_{\boldsymbol{p}_i}$. The T-matrix is given by $T_{\mathrm{BEC}}^{-1}(E, \boldsymbol{p}) = -\frac{m}{4\pi}\sqrt{-m(E - p^2/4m)}$ in the Λ-model with $a_{\mathrm{B}} = 0$.

When the limit $\Lambda \to 0$ is taken, the functions denoted by γ are defined only in the close vicinity of the point at which all the momentum variables are zero. Around this point, unless the energy exactly satisfies $T_{\mathrm{BEC}}^{-1}(E, 0) - \frac{1}{E} = 0$, the equations above are smooth. Therefore we can approximate $\gamma_{\boldsymbol{p}_1 \boldsymbol{p}_2 \ldots \boldsymbol{p}_k}$ by $\gamma_{00\ldots0} \equiv \gamma_k$ ($k = 1, 2, \ldots, N-1$), and set all the $\boldsymbol{p}_i$ to 0. This enables us to derive the linear equations for the set of γ_k:

$$f(E)\boldsymbol{\Gamma} = \mathcal{M}\boldsymbol{\Gamma}, \tag{6.32}$$

where $f(E) \equiv E T_{\mathrm{BEC}}^{-1}(E, 0) - 1$, $\boldsymbol{\Gamma} \equiv (\gamma_0, \gamma_1, \ldots, \gamma_{N-1})^T$, and

$$\mathcal{M} \equiv \begin{pmatrix} 0 & \Omega & 0 & 0 & \ldots & 0 & 0 \\ 1 & \Omega & \Omega & 0 & \ldots & 0 & 0 \\ 0 & 2 & 2\Omega & \Omega & \ldots & 0 & 0 \\ 0 & 0 & 3 & 3\Omega & \ldots & 0 & 0 \\ \vdots & \vdots & \vdots & \vdots & \ddots & \vdots & \vdots \\ 0 & 0 & 0 & 0 & \ldots & N-1 & (N-1)\Omega \end{pmatrix} \quad \left(\Omega \equiv \frac{\Lambda^3}{6\pi^2}\right). \tag{6.33}$$

For negative, real energies E, $f(E)$ is real and $df(E)/dE < 0$. This implies that the largest eigenvalue of the matrix $\mathcal{M}$, which is positive, corresponds to the ground state. We cannot set $\Omega = 0$ in the above equation because the diagonalizability of $\mathcal{M}$ is lost at this point and the limit $\Omega \to 0$ is not continuous. To take this limit, we make $\mathcal{M}$ Hermitian and thus explicitly diagonalizable as follows:

$$\mathcal{P}\mathcal{M}\mathcal{P}^{-1} = \begin{pmatrix} 0 & \Omega^{1/2} & 0 & 0 & \dots \\ \Omega^{1/2} & \Omega & \sqrt{2}\Omega^{1/2} & 0 & \dots \\ 0 & \sqrt{2}\Omega^{1/2} & 2\Omega & \sqrt{3}\Omega^{1/2} & \dots \\ 0 & 0 & \sqrt{3}\Omega^{1/2} & 3\Omega & \dots \\ \vdots & \vdots & \vdots & \vdots & \ddots \end{pmatrix} \tag{6.34}$$

$$= \Omega^{1/2} \begin{pmatrix} 0 & 1 & 0 & 0 & \dots \\ 1 & \Omega^{1/2} & \sqrt{2} & 0 & \dots \\ 0 & \sqrt{2} & 2\Omega^{1/2} & \sqrt{3} & \dots \\ 0 & 0 & \sqrt{3} & 3\Omega^{1/2} & \dots \\ \vdots & \vdots & \vdots & \vdots & \ddots \end{pmatrix}, \tag{6.35}$$

where

$$\mathcal{P} \equiv \mathrm{diag}\left(1, \Omega^{1/2}, \dots, \frac{\Omega^{k/2}}{\sqrt{k!}}, \dots, \frac{\Omega^{(N-1)/2}}{\sqrt{(N-1)!}}\right). \tag{6.36}$$

This makes it clear that the largest eigenvalue scales as $\Omega^{1/2} \propto \Lambda^{3/2}$ in the limit of $\Lambda \to 0$. In particular, this implies that the limiting energy is determined by $f(E) = 0$, which gives $E = E_0 \equiv -\frac{2^{4/3}\pi^{2/3}n_0^{2/3}}{m}$. Note that this is exactly the same equation as the one that derives from the one-excitation ansatz. Therefore, we conclude that the Bose polaron with $a_B = 0$ has a finite ground-state energy within the Λ-model in the high-density limit of the background Bose gas.

The above equation also indicates that the leading correction to the ground-state energy vanishes as $\Lambda^{3/2}$ in the limit of $\Lambda \to 0$. More precisely, suppose that the largest eigenvalue of $\mathcal{M}$ is α. Then the energy is determined by

$$\alpha = f(E) \simeq \delta E \cdot f'(E_0) = -\frac{3}{2^{7/3}\pi^{2/3}}\delta E, \tag{6.37}$$

where $\delta E \equiv E - E_0$ and E_0 is the solution of $f(E) = 0$. For example, when the maximum number of excitations is $N = 3$, we obtain $\alpha \simeq \sqrt{3}\Omega^{1/2} = \Lambda^{3/2}/\sqrt{2}\pi$. We thus obtain $\delta E \simeq -2^{11/6}\Lambda^{3/2}/3\pi^{1/2}$. This is consistent with the numerical solution of the variational equation, as shown in Fig. 6.6.

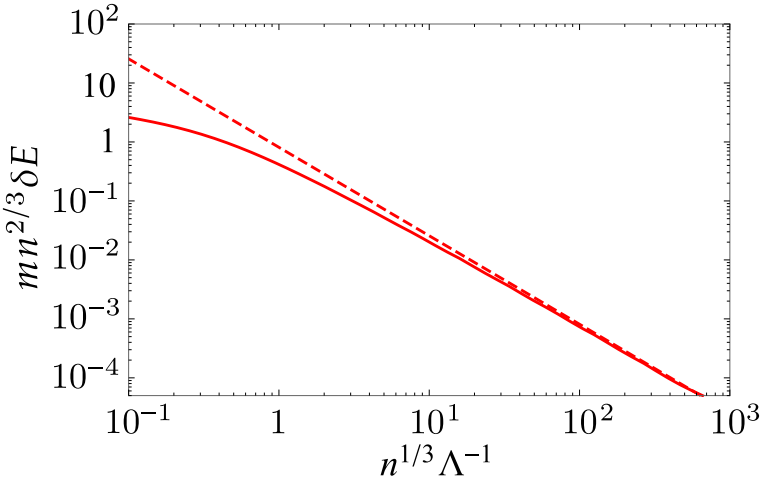

Figure 6.6: Correction to the dense limit in the Λ-model. We calculate $\delta E \equiv E - E_0$ within the trial wavefunction with three excitations, by directly solving the variational equations (solid) and from the largest eigenvalue of $\mathcal{M}$ (dashed). Here, $E_0 \equiv -\frac{2^{4/3}\pi^{2/3}n^{2/3}}{m}$ is the ground-state energy in the high-density limit.

6.2.4 Measurement of the ground-state energy

Before ending the discussion on the ground-state energy, we would like to point out that it is experimentally accessible in ultracold atomic systems as demonstrated in the recent experiments [106, 107]. Here, we summarize an experimental scheme to determine the ground-state energy of the Bose polaron relative to the non-interacting system. We focus on the homonuclear setting, where we use the same atomic species for the impurity and the background Bose gas and they are distinguished by hyperfine states [107].

Let $|\uparrow\rangle$ be the hyperfine state corresponding to the Bose gas and $|\downarrow\rangle$ to the impurity. Since they are two internal states of the same atomic species, there is a well-defined energy difference $\Delta \equiv E_\downarrow - E_\uparrow$, which is a single-atom property. This can be used as an absolute energy reference to measure the ground-state energy of the Bose polaron. Suppose that we prepare a gas of atoms in the $|\uparrow\rangle$ state and shine on it a radio-frequency pulse of ω to transfer atoms from $|\uparrow\rangle$ to $|\downarrow\rangle$. The transition rate then has a peak at $\omega = \omega_{\rm peak}$, which is generally different from Δ due to the initial- and final-state interactions, the latter of which leads to the polaron ground-state energy $E_{\rm pol}$. Therefore, one can find

$$E_{\rm pol} = \omega_{\rm peak} - \Delta, \tag{6.38}$$

where we have retained the leading order in $n_0 {a_{\rm B}}^3$, assuming that the atoms in the $|\uparrow\rangle$ state interact weakly with each other.

The linear response theory allows us to make more quantitative discussion [107, 171]. The coupling of the two states is described by the Hamiltonian,

$$\hat{H}_{\mathrm{rf}} = \sum_{p} \begin{pmatrix} \hat{b}_p^\dagger & \hat{c}_p^\dagger \end{pmatrix} \begin{pmatrix} 0 & \Omega^* e^{i\omega t} \\ \Omega e^{-i\omega t} & \Delta \end{pmatrix} \begin{pmatrix} \hat{b}_p \\ \hat{c}_p \end{pmatrix} \tag{6.39}$$

where Ω is the Rabi frequency, and ω is the frequency of the pulse. Here, $\hat{b}_p$ and $\hat{c}_p$ represent atoms of the same species in the different hyperfine states $|\uparrow\rangle$ and $|\downarrow\rangle$, respectively. From the Kubo formula, the rate of transfer is

$$\dot{N}_\downarrow = -2\Omega^2 \,\mathrm{Im}\tilde{D}(\omega), \tag{6.40}$$

where $\tilde{D}(\omega)$ is the Fourier transform of

$$D(t-t') = -i\theta(t-t') \left\langle 0 \middle| \left[\sum_{p} \hat{b}_p^\dagger(t)\hat{c}_p(t), \sum_{q} \hat{c}_q^\dagger(t')\hat{b}_q(t') \right] \middle| 0 \right\rangle, \tag{6.41}$$

and $|0\rangle$ is the ground state of a gas composed of $|\uparrow\rangle$ atoms. By noting that up to the leading order in ${n_0 a_{\mathrm{B}}}^3$,

$$\hat{b}_{\boldsymbol{p}} |0\rangle = \sqrt{n_0}\delta_{\boldsymbol{p},0} |0\rangle , \quad \hat{c}_{\boldsymbol{p}} |0\rangle = 0, \tag{6.42}$$

we can rewrite $D(t-t')$ as

$$D(t-t') = -in_0 \left\langle 0 \middle| \mathrm{T}\hat{c}_{\boldsymbol{p}=0}(t)\hat{c}^\dagger_{\boldsymbol{q}=0}(t') \middle| 0 \right\rangle \equiv n_0 G_{\mathrm{imp}}(\boldsymbol{p}=0, t-t'), \tag{6.43}$$

where T is the time-ordering operator, and G_{imp} represents the impurity Green function. This means that the measurement of the transfer rate gives the information on impurity's spectral function $A(\boldsymbol{p},\omega) \equiv -2\mathrm{Im}\tilde{G}_{\mathrm{imp}}(\boldsymbol{p},\omega)$:

$$\dot{N}_\downarrow = \Omega^2 A(\boldsymbol{p}=0,\omega). \tag{6.44}$$

Here, $\omega = 0$ is not the interacting ground-state energy, but the ground-state energy of the Bose gas without the impurity. If the $|\downarrow\rangle$ state does not interact with the $|\uparrow\rangle$ state, it has a peak at $\omega = \Delta$ because of the energy difference between $|\uparrow\rangle$ and $|\downarrow\rangle$. The ground-state energy of the interacting Bose polaron with respect to the non-interacting system can be found from the shift of the peak frequency from Δ.

A similar method has also been used for a heteronuclear setting, where the impurity and bosons are different atomic species [106]. One needs two internal states of the impurity atom, one of which resonantly interacts with bosons and the other does not or

only weakly interact. If this is the case, one can extract the ground-state energy of the Bose polaron from a shift of the peak frequency from its known value for a single atom. Therefore, by using these methods, we can measure the ground-state energy of the Bose polaron and test its universality experimentally.

6.3 Other observables

We now discuss the ground-state properties of the Bose polaron other than the energy. Here, we calculate the quasi-particle residue, the effective mass, and the Tan's contact. We focus especially on how sensitive they are to the three-body parameter a_- and the boson-boson scattering length a_B.

6.3.1 Quasi-particle residue

The quasi-particle residue Z is defined as the squared overlap between the true ground-state wave function of the Bose polaron and that of the decoupled system. In terms of the variational wave function, it is written as

$$Z = |\alpha_0|^2 \tag{6.45}$$

$$= \frac{g_0^2}{E^2}\left(\sqrt{n_0}\gamma_0 - \sum_{\boldsymbol{q}} v_{\boldsymbol{q}}\gamma_{\boldsymbol{q}}\right)^2, \tag{6.46}$$

where we have assumed that the wave function $|\Psi\rangle$ is normalized.

In Figure 6.7(a), we show the results for the quasi-particle residue at unitarity for $a_B = 0$. Over the entire range of $n_0^{1/3}|a_-|$, Z is significantly smaller than unity. It is natural to have $Z \to 0$ in the dilute limit because the few-body cluster is orthogonal to the decoupled impurity state. On the other hand, we find that Z does not show the convergence to finite values with the increasing number of Bogoliubov excitations, even in the intermediate-density regime. This suggests that the residue vanishes at unitarity when $a_B = 0$, and that the impurity loses the quasi-particle nature. We note that the vanishing residue in the limit of $a_B \to 0$ is not unique to the Bose polaron in the unitary regime; it is known within a perturbation theory for weak impurity-boson interactions that the residue approaches zero when $a_B \to 0$.

Remarkably, the quasi-particle residue is highly sensitive to the scattering length a_B between bosons. In Figure 6.7(b), we plot the residue within the r_0-model with $a_B = |a_-|/(2.1 \times 10^4)$, which is compatible with the hard-core model. It demonstrates that a finite a_B significantly enhances Z. In addition, it makes the residue converge fast; the trial wave functions with two and three Bogoliubov excitations give close results.

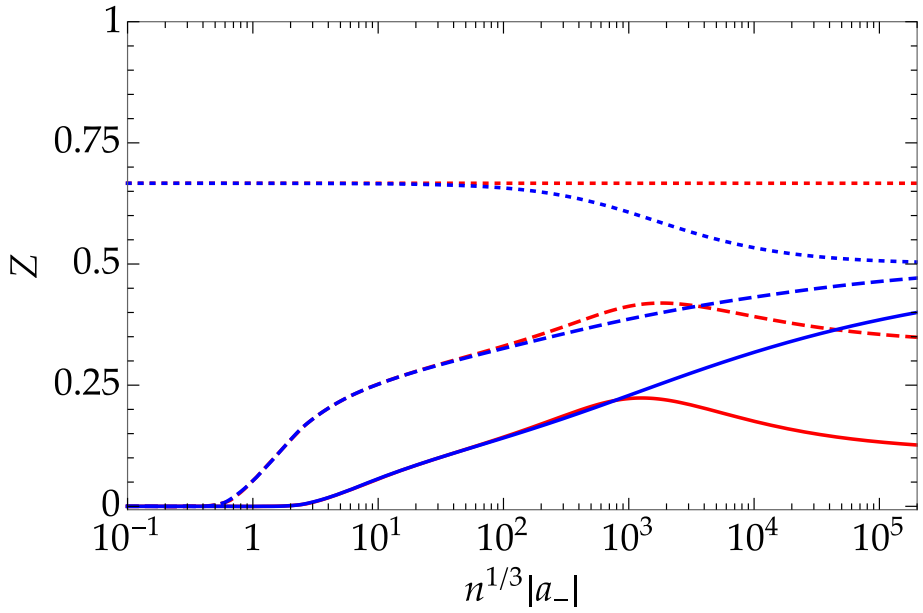

(a) $a_B = 0$

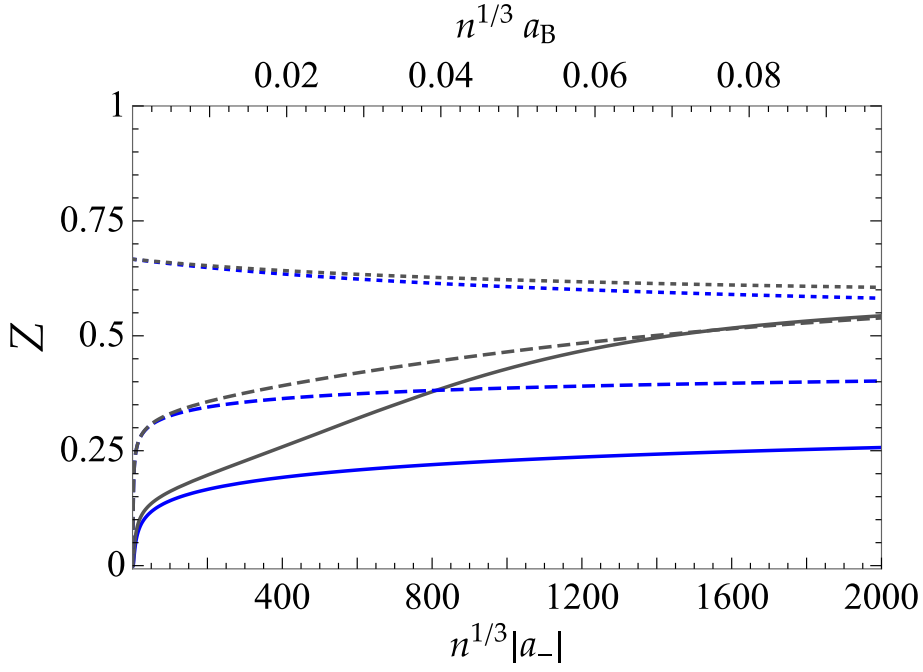

(b) $a_B = |a_-|/(2.1 \times 10^4)$

Figure 6.7: Quasi-particle residue of the Bose polaron at unitarity. (a) We show the results for the r_0-model (blue) and the Λ-model (red) for $a_B \to 0$. The different curves (dotted, dashed, and solid) represent the number of Bogoliubov excitations in the trial wave function (from one to three). (b) We calculate the residue with $a_B = |a_-|/(2.1 \times 10^4)$, in a way compatible with the hard-core model in Refs. [110, 119]. Here, we show the results of the r_0-model with zero (blue) and finite (gray) a_B.

These qualitative results, that the residue is zero for $a_B = 0$ while it is nonzero for $a_B \neq 0$, are also reproduced by the next-to-the-leading order perturbation theory within the r_0-model, which is valid in the high-density regime. From Eq. (6.19), we find

$$\partial_\omega \Sigma^{(4)}(\omega, 0)\big|_{\omega=E^{(2)}} = -\frac{1}{E^{(1)}}\Sigma^{(4)}(E^{(2)}, 0) + g_0^2 \sum_{\boldsymbol{q}} \frac{(E^{(2)} - 3q^2/4m)^2 + (E^{(2)})^2}{(-7E^{(2)}q^2/4m + 3q^4/4m)^2}, \tag{6.47}$$

$$\sim 2\sqrt{\frac{3}{7}}\left(\frac{1}{8\pi n_0 |r_0|^3}\right)^{1/4} + \frac{L}{|r_0|}, \tag{6.48}$$

where L denotes a diverging length scale, indicating that the integral has a linear infrared divergence. This implies that the wave function of the polaron is orthogonal to that of the impurity decoupled from the Bose gas due to the large amplitude of the low-energy excitations. Such excitations are, however, suppressed when the Bose gas has a finite coherence length. A detailed diagrammatic analysis is given in Appendix B. In short, the linear Bogoliubov dispersion and the cancellation of the particle and hole propagation lead to a infrared-finite result. In particular, we find

$$Z - \frac{1}{2} \propto \sqrt{\frac{a_B}{|r_0|}} \tag{6.49}$$

when $a_B/|r_0| \ll n_0 {a_B}^3 \ll 1$.

Therefore, we conclude that the residue is suppressed when $a_B \to 0$ and is sensitive to a_B. Although the three-body repulsion can stabilize the Bose polaron even when $a_B \to 0$, it is not enough to prevent unbounded excitations of the low-energy modes.

6.3.2 Effective mass

The impurity acquires an effective mass m^* due to the interaction with the bosonic bath. To define the effective mass, suppose that $E(p)$ is the energy of a Bose polaron with a given momentum $\boldsymbol{p}$, where the rotational symmetry is assumed. The effective mass m^* is then given as the second derivative of $E(p)$:

$$(m^*)^{-1} = \left.\frac{\partial^2 E(p)}{\partial p^2}\right|_{p=0}. \tag{6.50}$$

We can calculate it within the variational ansatz; however, due to the complexity of the calculation, we here truncate the variational wave function at two Bogoliubov excitations. We describe in Appendix C how to calculate m^* within the variational approach.

In Figure 6.8(a), we plot the inverse effective mass of the Bose polaron at unitarity for $a_B \to 0$. For the densities $n_0|a_-| \lesssim 100$, the two models give almost the same

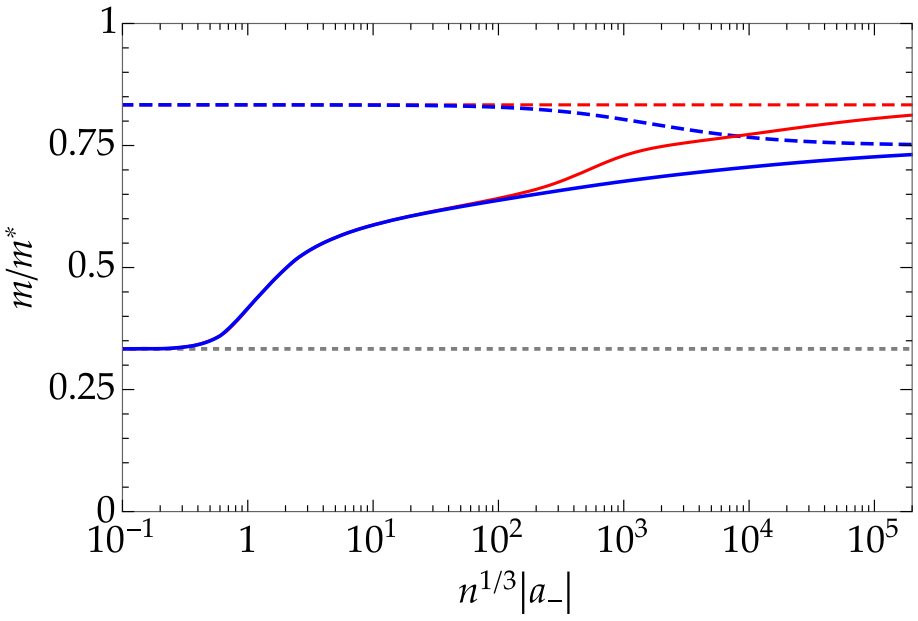

(a) $a_B = 0$

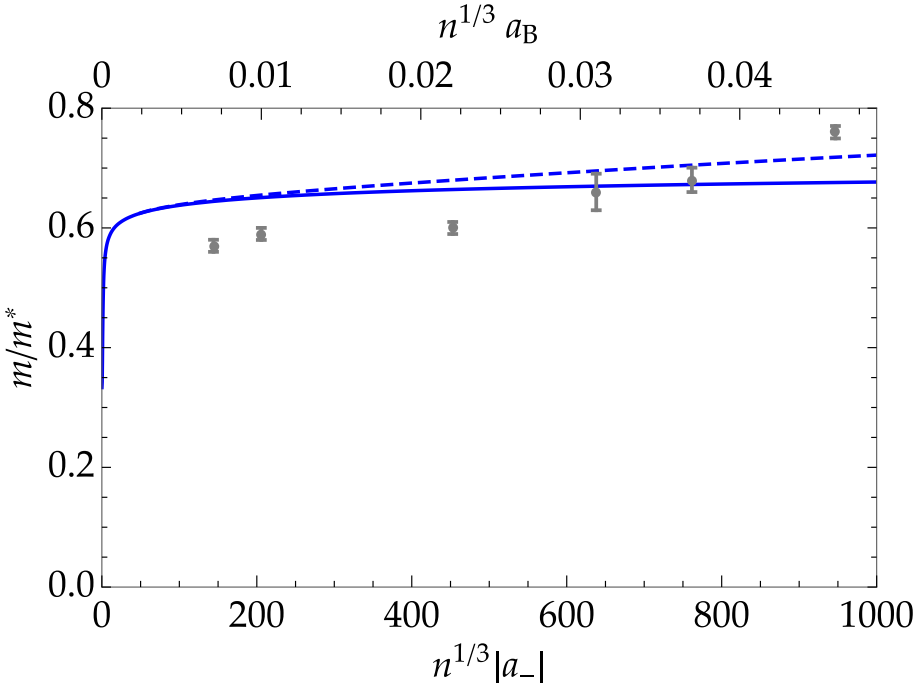

(b) $a_B = |a_-|/(2.1 \times 10^4)$

Figure 6.8: The inverse effective mass of the Bose polaron as a function of the dimensionless three-body parameter. (a) Results for the r_0-model (blue) and the Λ-model (red) for $a_B \to 0$. The solid line denotes the results obtained for the two-excitation ansatz, and the dashed line for the one-excitation ansatz. (b) Comparison of the results for the r_0-model with the QMC calculation for the hard-core model (gray dots). For the r_0-model, we show the results for $a_B \to 0$ (solid) and $a_B = |a_-|/(2.1 \times 10^4)$ (dashed).

effective masses. In particular, they converge to $1/3m$ as $n_0 \to 0$. This is because we truncate the wave function with two Bogoliubov excitations and the ground state for $n_0 \to 0$ within the approximation is the lowest Efimov trimer, whose mass is $3m$. If N bosons can be bound to the impurity to form a cluster state, the effective mass should converge to $(N+1)m$ in the dilute limit. In the high-density regime, the results become model-dependent.

In Figure 6.8(b), we also compare our results with the QMC calculation based on the hard-core model of the Bose polaron [119]. Here, we show the results within the r_0-model for $a_B = 0$ and $a_B \neq 0$; in the latter case we fix $a_B = a_-/(2.1 \times 10^4)$ again. The variation of the effective mass within the plotted region is similar between the two models when a finite a_B is taken into account in the r_0-model. However, we also find a significant discrepancy between them. It is possible that we would have better agreement by taking more excitations into account, but at this point, it is difficult to reach any conclusion on the universality of the effective mass and the effect of a finite a_B.

6.3.3 Tan's contact

Tan's contact C is defined from the energy as

$$C \equiv 4\pi m \frac{\partial E}{\partial(-1/a)}, \tag{6.51}$$

where a is the s-wave scattering length of the impurity-boson interaction [53]. Experimentally, the contact can be measured by using a Feshbach resonance to tune the scattering length and applying the above definition [93]. It is also accessible from the high momentum tail of the momentum distribution, the short-range singularity of the density-density correlation function [52], and the high-frequency tail of the radio-frequency spectroscopy [64–67]. Physically, it gives a measure of the number of pairs at short distances [52].

For the two-channel Hamiltonian (6.1), it is shown that the contact can be written in terms of the closed-channel dimers [172]. In particular, within the variational wave function, it is given as

$$C = m^2 g_0^2 \sum_{\boldsymbol{q}} \left\langle \Psi \middle| \hat{d}_{\boldsymbol{q}}^\dagger \hat{d}_{\boldsymbol{q}} \middle| \Psi \right\rangle \tag{6.52}$$

$$= m^2 g_0^2 \left(|\gamma_0|^2 + \sum_{\boldsymbol{q}} |\gamma_{\boldsymbol{q}}|^2 + \frac{1}{2} \sum_{\boldsymbol{q}_1, \boldsymbol{q}_2} |\gamma_{\boldsymbol{q}_1 \boldsymbol{q}_2}|^2 \right). \tag{6.53}$$

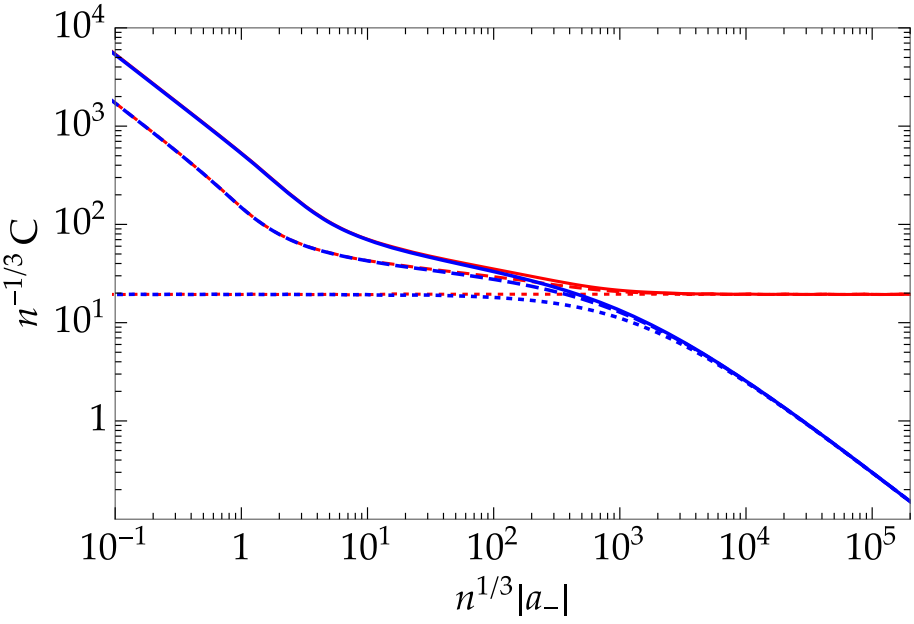

(a) $a_B = 0$

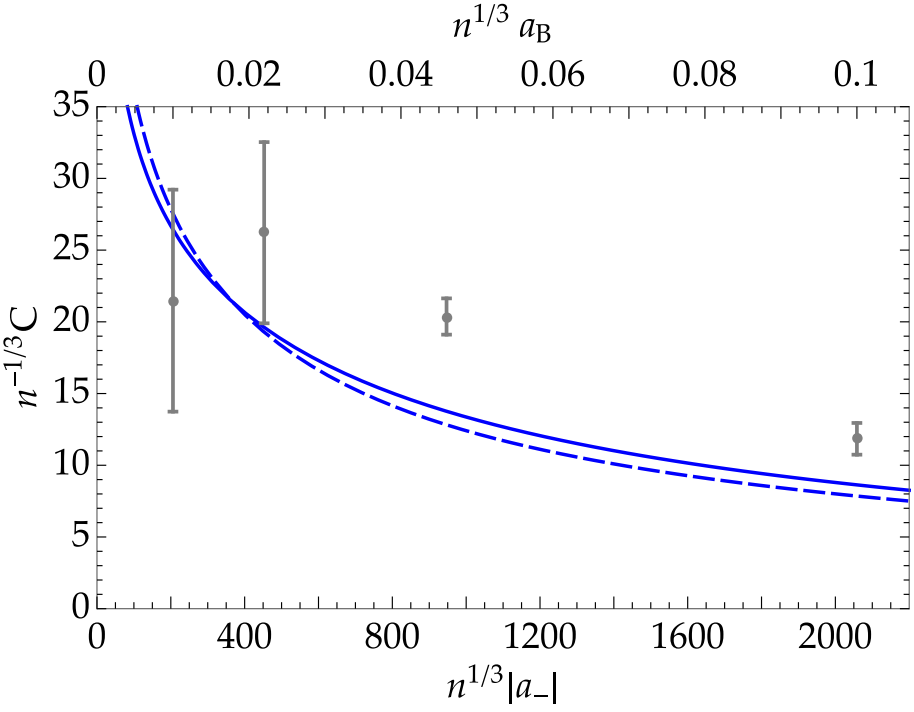

(b) $a_B = |a_-|/(2.1 \times 10^4)$

Figure 6.9: Tan's contact for the Bose polaron at unitarity as a function of the dimensionless three-body parameter. (a) Results for the r_0-model (blue) and the Λ-model (red) with one (dotted), two (dashed), and three (solid) Bogoliubov excitations for $a_B \to 0$. (b) Comparison of the results for the r_0-model with those for the hard-core model (gray dots). We show the results for the r_0-model for $a_B \to 0$ (solid) and $a_B = |a_-|/(2.1 \times 10^4)$ (dashed).

Note that this is well-defined in the limit of $g_0 \to \infty$ because the closed-channel amplitude γ scales as $O(g_0^{-1})$ (see the discussion in Section 2.2.1). Therefore, this expression is also applicable to the Λ-model, where $g_0 \to \infty$ is implied.

We show the results for the contact in Fig. 6.9(a). In the dilute limit, $n^{-1/3}C$ is proportional to $(n^{1/3}|a_-|)^{-1}$, indicating that the contact is constant in this limit and proportional to $|a_-|^{-1}$. It is a natural consequence of the fact that the only length scale at unitarity is a_- when $n_0 \to 0$ and $a_B \to 0$. The numerical results demonstrate that Tan's contact is a model-independent function of $n_0^{1/3}|a_-|$. We also compare our results with the QMC calculation of the hard-core model in Fig. 6.9(b). Note that some of the data points of the QMC are given for relatively high densities, where $n_0^{1/3}|r_0|$, $n_0^{1/3}\Lambda^{-1} \sim 1$ and the model dependence is significant. For the points in the many-body universal regime, they are consistent with our results, although the statistical uncertainty is large. In the same plot, we also show the variational results with a finite a_B, which indicates that the contact has a relatively weak dependence on a_B. Therefore, we conclude that the contact in the ground-state Bose polaron is also a universal function of $n_0^{1/3}|a_-|$.

Chapter 7

Conclusions

In this thesis, we have investigated universal few-body phenomena and their consequences in many-body systems in an anisotropic p-wave Fermi gas and an impurity-boson system.

Chapter 2 is devoted to reviewing the physics of a Feshbach resonance and the construction of the effective-field theory, which is called the two-channel model. Such an effective-field theory is particularly suited for discussing without referring to microscopic details the universal properties that emerge in resonantly interacting systems. Indeed, although we have constructed the two-channel model to faithfully reproduce a Feshbach resonance, the two-channel model is the same field theory as the ones that have been used to describe low-energy nuclear systems. Thus, the results that follow are relevant not only to ultracold atomic gases but also to nuclei and other systems with resonant interactions.

In Chapter 3, we have discussed the universal relations in an anisotropic p-wave Fermi gas. Firstly, we have shown the short-range singularity in correlation functions. Specifically, we have found that the momentum distribution at large momenta $\boldsymbol{p}$ has a characteristic p^{-2}-decay, whose coefficients define the p-wave contact tensor $C_{mm'}$. We have also found that the density-density correlation function has a short-range r^{-4}-divergence, whose coefficients are the p-wave contact tensor. Secondly, we have proved the adiabatic sweep theorem, which states that the p-wave contact tensor is the derivative of the energy with respect to the generalized p-wave scattering volume. This gives the direct connection of the p-wave contact tensor and the thermodynamic quantity. In the p-wave superfluids, where axisymmetry can be spontaneously broken, we have derived the expression of the p-wave contact tensor within the mean-field theory. The result indicates that the different superfluid phase can be distinguished by measuring the p-wave contact tensor. One concern about these findings is that the generalized p-wave scattering volume cannot be controlled by magnetic Feshbach

resonances. Instead, we propose using the Λ-configuration of the Raman lasers to control the generalized scattering volume and test our results.

In Chapter 4 and 5, we have addressed the universality of the few-body spectra in the impurity-boson systems at unitarity. In Chapter 4, we have investigated the mass-balanced case, where the mass of the impurity is equal to that of a boson. We have calculated the three-body and four-body spectra within the r_0-model and the Λ-model, and shown that dimensionless ratios constructed from the energies at unitarity and the critical values of the s-wave scattering length are independent of the models with high accuracy. This universality is more than the one expected in the identical-boson Efimov states, because in that case, the universality holds for excited states but not for the ground state. We have argued that the separation of the scales of the two-body physics and the Efimov effect is at the core of our results. We have demonstrated it by the results for a lighter impurity, for which the two scales are of the same order of magnitude and the lower Efimov states deviate from the discrete scaling relation. The opposite limit of a heavy impurity has been studied in Chapter 5. In this limit, we have shown that the r_0-model can be mapped to a Hamiltonian similar to Anderson's single impurity model. By using this mapping, we have solved the three-body problem analytically, and found the logarithmic correction to the binding energy for finite s-wave scattering lengths. We have compared this result with the numerical solution of the Λ-model, and argued that this logarithmic correction is, in fact, a universal consequence of the effective three-body repulsion.

In Chapter 6, we have addressed the many-body problem of the Bose polaron. In particular, we have discussed the ground-state properties of the Bose polaron. We have employed the variational wave function that incorporates three Bogoliubov excitations on top of the Bose-Einstein condensate formed by the background Bose gas. This enables us to examine effects of four-body correlations. By comparing the ground-state energies that we calculate within the r_0-model and the Λ-model with the result for the hard-core model [119], we have found that for sufficiently low densities, the ground-state energy is a universal function of $n^{1/3}a_-$ and is relatively insensitive to the boson-boson interaction a_B. The high-density regime is model-dependent but analytically tractable. By comparing the numerical data with analytical results, we have argued that the ground-state energy is indeed finite even in the absence of the repulsive interaction between bosons. We have also discussed the quasi-particle residue, the effective mass, and Tan's contact of the Bose polaron at zero temperature. While Tan's contact as well as the ground-state energy is relatively insensitive to a_B and thus universal, the a_B-dependence of the quasi-particle residue and the effective mass is comparable to or greater than their a_--dependence. In particular, the quasi-particle residue is strongly

suppressed in the limit of $a_{\mathrm{B}} \to 0$. This is consistent with the results of the perturbation theory for a large $n^{1/3}|r_0|$, which suggests that the infrared divergence leads to the vanishing quasi-particle residue. However, the residue converges to a finite value when we take a finite a_{B} into account; this is also consistent with the perturbation theory.

Our study raises several questions for future research. Regarding the universal relations in an anisotropic p-wave Fermi gas, theoretical calculations of the p-wave contact tensor are only done in the mean-field regime of the superfluid phase and the high-temperature regime. The finite-temperature behavior of the p-wave contact tensor, especially near the phase transition, is yet to be explored. The connection to the lower dimensions is also an issue that should be investigated. Universal relations in a p-wave Fermi gas in one [173] and two dimensions [174, 175] have already been discussed. In ultracold atomic gases, a resonance in lower dimensions can be realized by the confinement-induced resonance, where an external confinement introduces additional anisotropy to the system. In this regard, what is a p-wave contact tensor in such a confined gas, and how it is related to the contacts defined in lower dimensions, are interesting questions.

There are also open issues related to the impurity-boson systems. Firstly, there is a renormalization-group study on a Bose polaron near a Feshbach resonance [121], but, so far, the three-body interaction has been omitted in their action and thus the three-body parameter cannot be fixed. It is therefore desirable to have a renormalization group that incorporates the Efimov effect correctly to characterize the universality that we have found in this thesis. Such a study may be useful to gain an insight into the universality of quantities other than the ground-state energy. Secondly, a finite density of impurities may bring non-trivial many-body effects because two impurities and one boson can form an Efimov trimer, depending on quantum statistics and the mass of an impurity. So far, there is a study on two bosonic impurities in a Bose-Einstein condensate [176], but otherwise, such many-body systems remain largely to be investigated. Another issue concerns the case with the infinite-mass impurity. Since there is no Efimov effect in this limit, the unitarity limit becomes scale-invariant. This may lead to a universal equation of state of an infinite-mass Bose polaron that is parameter-free and resembles the one in the unitary Fermi gas.

Appendix A

Integral equations for states with rotational symmetry

In this appendix, we present a detailed derivation of the integral equations for the Bose polaron with rotational symmetry. We can also derive the equations for the rotationally symmetric bound states in the vacuum in a similar way, and the resulting equations are obtained as the zero-density limit of those for the Bose polaron.

From the Hamiltonian (6.6) and the variational ansatz (6.7–6.11), the stationary condition $\partial(\langle\Psi|(\hat{H}-E)|\Psi\rangle)/\partial(\alpha^*,\gamma^*)=0$ gives the seven coupled equations,

$$E\alpha_0 = g_0\sqrt{n_0}\gamma_0 - g_0\sum_q v_q\gamma_q, \tag{A.1}$$

$$(E-E_p-\varepsilon_p)\alpha_p = g_0u_p\gamma_0 + g_0\sqrt{n_0}\gamma_p - g_0\sum_q v_q\gamma_{qp}, \tag{A.2}$$

$$(E-E_{p_1p_2})\alpha_{p_1p_2} = g_0(u_{p_1}\gamma_{p_2}+u_{p_2}\gamma_{p_1}) + g_0\sqrt{n_0}\gamma_{p_1p_2}, \tag{A.3}$$

$$(E-E_{p_1p_2p_3})\alpha_{p_1p_2p_3} = g_0(u_{p_1}\gamma_{p_2p_3}+u_{p_2}\gamma_{p_3p_1}+u_{p_3}\gamma_{p_1p_2}), \tag{A.4}$$

$$(E-\nu_0)\gamma_0 = g_0\sqrt{n_0}\alpha_0 + g_0\sum_q u_q\alpha_q, \tag{A.5}$$

$$(E-\nu_0-E_p-\varepsilon_p^{\mathrm{d}})\gamma_p = -g_0v_p\alpha_0 + g_0\sqrt{n_0}\alpha_p + \sum_q u_q\alpha_{qp}, \tag{A.6}$$

$$\begin{aligned}(E-\nu_0-E^{\mathrm{d}}_{p_1p_2})\gamma_{p_1p_2} = {}& -g_0(v_{p_1}\alpha_{p_2}+v_{p_2}\alpha_{p_1}) \\ & + g_0\sqrt{n_0}\alpha_{p_1p_2} + g_0\sum_q u_q\alpha_{qp_1p_2},\end{aligned} \tag{A.7}$$

where we have introduced the following notations:

$$E_{p_1p_2} \equiv E_{p_1}+E_{p_2}+\varepsilon_{p_1+p_2}, \tag{A.8}$$

$$E_{p_1p_2p_3} \equiv E_{p_1}+E_{p_2}+E_{p_3}+\varepsilon_{p_1+p_2+p_3}, \tag{A.9}$$

$$E^{\mathrm{d}}_{p_1p_2} \equiv E_{p_1} + E_{p_2} + \varepsilon^{\mathrm{d}}_{p_1+p_2}. \tag{A.10}$$

Note that for the Λ-model, the domains of the α functions are the entire momentum space while those of the γ functions are restricted by Λ. For $n_0 \to 0$, the equations for α_0, the pairs $(\alpha_{\boldsymbol{p}}, \gamma_0)$, $(\alpha_{\boldsymbol{p}_1\boldsymbol{p}_2}, \gamma_0)$, and $(\alpha_{\boldsymbol{p}_1\boldsymbol{p}_2\boldsymbol{p}_3}, \gamma_{\boldsymbol{p}_1\boldsymbol{p}_2})$ are decoupled from each other, yielding the Schrödinger equations for the few-body systems in the vacuum, such as Eqs. (4.6) and (4.7) for the four-body system. Substituting the first four equations into the latter three to eliminate the α functions, we obtain

$$\begin{aligned}
&\left[g_0^{-2}(E-\nu_0) - \sum_{\boldsymbol{q}} \frac{u_{\boldsymbol{q}}^2}{E - E_{\boldsymbol{q}} - \varepsilon_{\boldsymbol{q}}}\right]\gamma_0 \\
&\quad = \frac{n_0\gamma_0}{E} + \sum_{\boldsymbol{q}}\left(\frac{u_{\boldsymbol{q}}\gamma_{\boldsymbol{q}}}{E - E_{\boldsymbol{q}} - \varepsilon_{\boldsymbol{q}}} - \frac{v_{\boldsymbol{q}}\gamma_{\boldsymbol{q}}}{E}\right) - \sum_{\boldsymbol{k},\boldsymbol{q}} \frac{u_{\boldsymbol{k}} v_{\boldsymbol{q}} \gamma_{\boldsymbol{k}\boldsymbol{q}}}{E - E_{\boldsymbol{k}} - \varepsilon_{\boldsymbol{k}}},
\end{aligned} \tag{A.11}$$

$$\begin{aligned}
&\left[g_0^{-2}(E - \varepsilon^{\mathrm{d}}_{\boldsymbol{p}} - \nu_0 - E_{\boldsymbol{p}}) - \sum_{\boldsymbol{q}} \frac{u_{\boldsymbol{q}}^2}{E - E_{\boldsymbol{p}\boldsymbol{q}}}\right]\gamma_{\boldsymbol{p}} = \sqrt{n_0}\left(\frac{u_{\boldsymbol{p}}\gamma_0}{E - E_{\boldsymbol{p}} - \varepsilon_{\boldsymbol{p}}} - \frac{v_{\boldsymbol{p}}\gamma_0}{E}\right) \\
&\quad + \frac{n_0\gamma_{\boldsymbol{p}}}{E - E_{\boldsymbol{p}} - \varepsilon_{\boldsymbol{p}}} + \sum_{\boldsymbol{q}}\left(\frac{u_{\boldsymbol{p}}u_{\boldsymbol{q}}\gamma_{\boldsymbol{q}}}{E - E_{\boldsymbol{p}\boldsymbol{q}}} - \frac{v_{\boldsymbol{p}}v_{\boldsymbol{q}}\gamma_{\boldsymbol{q}}}{E}\right) + \sqrt{n_0}\sum_{\boldsymbol{q}}\left(\frac{u_{\boldsymbol{q}}\gamma_{\boldsymbol{p}\boldsymbol{q}}}{E - E_{\boldsymbol{p}\boldsymbol{q}}} - \frac{v_{\boldsymbol{q}}\gamma_{\boldsymbol{p}\boldsymbol{q}}}{E - \varepsilon_{\boldsymbol{p}} - E_{\boldsymbol{p}}}\right),
\end{aligned} \tag{A.12}$$

$$\begin{aligned}
&\left[g_0^{-2}(E - \nu_0 - E^{\mathrm{d}}_{\boldsymbol{p}_1\boldsymbol{p}_2}) - \sum_{\boldsymbol{q}} \frac{u_{\boldsymbol{q}}^2}{E - E_{\boldsymbol{p}_1\boldsymbol{p}_2\boldsymbol{q}}}\right]\gamma_{\boldsymbol{p}_1\boldsymbol{p}_2} = \frac{n_0\gamma_{\boldsymbol{p}_1\boldsymbol{p}_2}}{E - E_{\boldsymbol{p}_1\boldsymbol{p}_2}} \\
&\quad + \left\{\left[-\frac{u_{\boldsymbol{p}_1}v_{\boldsymbol{p}_2}\gamma_{\boldsymbol{p}_1\boldsymbol{p}_2}}{E - E_{\boldsymbol{p}_1} - \varepsilon_{\boldsymbol{p}_1}} + \sqrt{n_0}\sum_{\boldsymbol{q}}\left(\frac{u_{\boldsymbol{p}_1}\gamma_{\boldsymbol{p}_2}}{E - E_{\boldsymbol{p}_1\boldsymbol{p}_2}} - \frac{v_{\boldsymbol{p}_1}\gamma_{\boldsymbol{p}_2}}{E - E_{\boldsymbol{p}_2} - \varepsilon_{\boldsymbol{p}_2}}\right)\right.\right. \\
&\qquad \left.\left. + \sum_{\boldsymbol{q}}\left(\frac{u_{\boldsymbol{p}_1}u_{\boldsymbol{q}}\gamma_{\boldsymbol{q}\boldsymbol{p}_2}}{E - E_{\boldsymbol{q}\boldsymbol{p}_1\boldsymbol{p}_2}} + \frac{v_{\boldsymbol{p}_1}v_{\boldsymbol{q}}\gamma_{\boldsymbol{q}\boldsymbol{p}_2}}{E - E_{\boldsymbol{p}_2} - \varepsilon_{\boldsymbol{p}_2}}\right)\right] + (\boldsymbol{p}_1 \leftrightarrow \boldsymbol{p}_2)\right\},
\end{aligned} \tag{A.13}$$

where $(\boldsymbol{p}_1 \leftrightarrow \boldsymbol{p}_2)$ represents the terms that symmetrize the expression within $\{\}$ with respect to the exchange of $\boldsymbol{p}_1$ and $\boldsymbol{p}_2$. It is clear by inspection that the coefficients of the γ functions on the left-hand side can be written in terms of the medium T-matrix defined as

$$T^{-1}_{\mathrm{BEC}}(E, \boldsymbol{p}) \equiv g_0^{-2}\left(E - \varepsilon^{\mathrm{d}}_{\boldsymbol{p}} - \nu_0\right) - \sum_{\boldsymbol{q}} \frac{u_{\boldsymbol{q}}^2}{E - E_{\boldsymbol{q}} - \varepsilon_{\boldsymbol{q}+\boldsymbol{p}}}. \tag{A.14}$$

The momentum integral in this definition is apparently ultraviolet divergent. This is also the case for the Λ-model because the restriction on the domain of the γ functions does not affect the range of the integration in the definition of T_{BEC}. However, the restriction can be removed by recalling the definition of the T-matrix of the vacuum two-body

scattering,

$$T_0^{-1}(E,\boldsymbol{p}) = g_0^{-2}\left(E-\varepsilon_p^{\mathrm{d}}-\nu_0\right) - \sum_q \frac{1}{E-\varepsilon_q-\varepsilon_{q+p}} \tag{A.15}$$

$$\equiv \frac{m}{4\pi}\left[a^{-1} - \frac{r_0}{2}m(E-\varepsilon_p^{\mathrm{d}}) - \sqrt{-m(E-\varepsilon_p^{\mathrm{d}})}\right], \tag{A.16}$$

and subtracting this from T_{BEC}^{-1}:

$$T_{\mathrm{BEC}}^{-1}(E,\boldsymbol{p}) = T_0^{-1}(E,\boldsymbol{p}) + \sum_q \left[\frac{1}{E-\varepsilon_q-\varepsilon_{q+p}} - \frac{u_q^2}{E-E_q-\varepsilon_{q+p}}\right]. \tag{A.17}$$

This is explicitly UV-finite because for a large $\boldsymbol{q}$, the integrand is of $O(q^{-4})$. By using $T_{\mathrm{BEC}}(E,\boldsymbol{p})$, we obtain the coupled integral equations:

$$\left[T_{\mathrm{BEC}}^{-1}(E,0) - \frac{n_0}{E}\right]\gamma_0 = \sqrt{n_0}\sum_p\left(\frac{u_p\gamma_p}{E-\varepsilon_p-E_p} - \frac{v_p\gamma_p}{E}\right) - \sum_{p,q}\frac{u_p v_q\gamma_{pq}}{E-\varepsilon_p-E_p}, \tag{A.18}$$

$$\begin{aligned}\left[T_{\mathrm{BEC}}^{-1}(E-E_p,\boldsymbol{p}) - \frac{n_0}{E-\varepsilon_p-E_p}\right]\gamma_p &= \sqrt{n_0}\left(\frac{u_p\gamma_0}{E-\varepsilon_p-E_p} - \frac{v_p\gamma_0}{E}\right)\\ &+ \sum_q\left(\frac{u_p u_q\gamma_q}{E-E_{pq}} + \frac{v_p v_q\gamma_q}{E}\right) + \sqrt{n_0}\sum_q\left(\frac{u_q\gamma_{pq}}{E-E_{pq}} - \frac{v_q\gamma_{pq}}{E-\varepsilon_p-E_p}\right),\end{aligned} \tag{A.19}$$

$$\begin{aligned}\left[T_{\mathrm{BEC}}^{-1}(E-E_{p_1}-E_{p_2},\boldsymbol{p}_1+\boldsymbol{p}_2) - \frac{n_0}{E-E_{p_1p_2}}\right]\gamma_{p_1p_2} &= -\frac{u_{p_1}v_{p_2}\gamma_0}{E-\varepsilon_{p_1}-E_{p_1}}\\ &+ \sqrt{n_0}\left(\frac{u_{p_1}\gamma_{p_2}}{E-E_{p_1p_2}} - \frac{v_{p_1}\gamma_{p_2}}{E-\varepsilon_{p_2}-E_{p_2}}\right) + \sum_q\left(\frac{u_{p_1}u_q\gamma_{p_2q}}{E-E_{p_1p_2q}} + \frac{v_{p_1}v_q\gamma_{p_2q}}{E-\varepsilon_{p_2}-E_{p_2}}\right)\\ &+ (\boldsymbol{p}_1\leftrightarrow\boldsymbol{p}_2).\end{aligned} \tag{A.20}$$

For the Λ-model, all the integrations in Eqs. (A.18–A.20) are cut off at Λ.

For states with rotational symmetry, we can restrict our consideration to the γ functions of the following form:

$$\gamma_p = \gamma_1(|\boldsymbol{p}|), \qquad \gamma_{p_1p_2} = \gamma_2\left(|\boldsymbol{p}_1|,|\boldsymbol{p}_2|,\frac{\boldsymbol{p}_1\cdot\boldsymbol{p}_2}{|\boldsymbol{p}_1||\boldsymbol{p}_2|}\right), \tag{A.21}$$

together with a single number γ_0. This reduces the dimensions of the domain of $\gamma_{p_1p_2}$ from six to three, in particular, and makes it viable to solve them directly by discretization. Moreover, we can perform the integration over all the angular variables except for the ones that are the arguments of the unknown functions. For Eqs. (A.18) and (A.19), we

immediately obtain the following form:

$$\begin{aligned}
&\left[T_{\mathrm{BEC}}^{-1}(E,0)-\frac{n_0}{E}\right]\gamma_0=\sqrt{n_0}\int\frac{q^2\,dq}{2\pi^2}\left[\frac{u_q\gamma_1(q)}{E-E_q-\varepsilon_p}-\frac{v_q\gamma_1(q)}{E}\right]\\
&\quad-\int\frac{p^2q^2\,dp\,dq\,dz}{8\pi^4}\frac{u_pv_q\gamma_2(p,q,z)}{E-\varepsilon_p-E_p},
\end{aligned}\tag{A.22}$$

$$\begin{aligned}
&\left[T_{\mathrm{BEC}}^{-1}(E-E_p,p)-\frac{n_0}{E-\varepsilon_{\boldsymbol{p}}-E_{\boldsymbol{p}}}\right]\gamma_1(p)=\sqrt{n_0}\left(\frac{u_p\gamma_0}{E-E_p-\varepsilon_p}-\frac{v_p\gamma_0}{E}\right)\\
&\quad+\int\frac{q^2\,dq}{2\pi^2}\left\{\frac{mu_pu_q}{2pq}\ln\left[\frac{\frac{1}{2m}(p-q)^2+E_p+E_q-E}{\frac{1}{2m}(p+q)^2+E_p+E_q-E}\right]+\frac{v_pv_q}{E}\right\}\gamma_1(q)\\
&\quad+\sqrt{n_0}\int\frac{q^2\,dq\,dz}{4\pi^2}\left[\frac{u_q\gamma_2(p,q,z)}{E-E_p-E_q-\frac{1}{2m}(p^2+q^2+2pqz)}-\frac{v_q\gamma_2(p,q,z)}{E-E_p-\varepsilon_p}\right].
\end{aligned}\tag{A.23}$$

For Eq. (A.20), care is necessary to perform the angular integral in

$$\sum_{\boldsymbol{q}}\frac{u_{\boldsymbol{p}_1}u_{\boldsymbol{q}}\gamma_{\boldsymbol{p}_2\boldsymbol{q}}}{E-E_{\boldsymbol{p}_1\boldsymbol{p}_2\boldsymbol{q}}}=\sum_{\boldsymbol{q}}\frac{u_{\boldsymbol{p}_1}u_{\boldsymbol{q}}\gamma_2(p_2,q,z_{\boldsymbol{p}_2\boldsymbol{q}})}{E-E_{\boldsymbol{p}_1}-E_{\boldsymbol{p}_2}-E_{\boldsymbol{q}}-\varepsilon_{\boldsymbol{p}_1+\boldsymbol{p}_2+\boldsymbol{q}}}.\tag{A.24}$$

Here, we introduce the notations

$$z_{\boldsymbol{p}_1\boldsymbol{p}_2}\equiv\cos\theta_{\boldsymbol{p}_1\boldsymbol{p}_2}\equiv\frac{\boldsymbol{p}_1\cdot\boldsymbol{p}_2}{|\boldsymbol{p}_1||\boldsymbol{p}_2|}.\tag{A.25}$$

In the integrand, we can simultaneously take $\boldsymbol{p}_2$ as the zenith direction and the polar angle $\theta_{\boldsymbol{p}_2\boldsymbol{q}}$ and the azimuth angle as the independent variables. Since $z_{\boldsymbol{p}_2\boldsymbol{q}}$ is one of the arguments of γ_2 in the integrand, we cannot integrate over $z_{\boldsymbol{p}_2\boldsymbol{q}}$ in advance. On the other hand, in principle, the azimuthal integration can be done. To show the results explicitly, first we note that $z_{\boldsymbol{p}_1\boldsymbol{q}}$ appears in $\varepsilon_{\boldsymbol{p}_1\boldsymbol{p}_2\boldsymbol{q}}$ as

$$\varepsilon_{\boldsymbol{p}_1\boldsymbol{p}_2\boldsymbol{q}}=\frac{1}{2m}\left(p_1^2+p_2^2+q^2+2p_1p_2z_{\boldsymbol{p}_1\boldsymbol{p}_2}+2p_1qz_{\boldsymbol{p}_1\boldsymbol{q}}+2p_2qz_{\boldsymbol{p}_2\boldsymbol{q}}\right).\tag{A.26}$$

It can be written in terms of the independent angles as

$$z_{\boldsymbol{p}_1\boldsymbol{q}}=z_{\boldsymbol{p}_1\boldsymbol{p}_2}z_{\boldsymbol{p}_2\boldsymbol{q}}+\sqrt{1-(z_{\boldsymbol{p}_1\boldsymbol{p}_2})^2}\sqrt{1-(z_{\boldsymbol{p}_2\boldsymbol{q}})^2}\cos\phi,\tag{A.27}$$

where ϕ is the relative azimuth angle of $\boldsymbol{q}$ from $\boldsymbol{p}_1$. By using this, we can rewrite the integrand as

$$\frac{u_{\boldsymbol{p}_1}u_{\boldsymbol{q}}\gamma_2(p_2,q,z_{\boldsymbol{p}_2\boldsymbol{q}})}{E-E_{\boldsymbol{p}_1}-E_{\boldsymbol{p}_2}-E_{\boldsymbol{q}}-\varepsilon_{\boldsymbol{p}_1+\boldsymbol{p}_2+\boldsymbol{q}}}=-\frac{u_{\boldsymbol{p}_1}u_{\boldsymbol{q}}\gamma_2(p_2,q,z_{\boldsymbol{p}_2\boldsymbol{q}})}{f+g\cos\phi},\tag{A.28}$$

where

$$f(p_1, p_2, q, z_{\boldsymbol{p}_1\boldsymbol{p}_2}, z_{\boldsymbol{p}_2\boldsymbol{q}}) = E_{p_1} + E_{p_2} + E_q + \frac{1}{2m}\left(p_1^2 + p_2^2 + q^2\right) \\ \frac{1}{m}\left(+p_1 p_2 z_{\boldsymbol{p}_1\boldsymbol{p}_2} + p_2 q z_{\boldsymbol{p}_2\boldsymbol{q}} + p_1 q z_{\boldsymbol{p}_1\boldsymbol{p}_2} z_{\boldsymbol{p}_2\boldsymbol{q}}\right) - E, \tag{A.29}$$

$$g(p_1, q, z_{\boldsymbol{p}_1\boldsymbol{p}_2}, z_{\boldsymbol{p}_2\boldsymbol{q}}) = \frac{p_1 q}{m}\sqrt{1 - (z_{\boldsymbol{p}_1\boldsymbol{p}_2})^2}\sqrt{1 - (z_{\boldsymbol{p}_2\boldsymbol{q}})^2}. \tag{A.30}$$

This makes the ϕ-dependence of the integrand clear, and therefore we can use a formula

$$\int_0^{2\pi} \frac{d\phi}{a + b\cos\phi} = \frac{2\pi}{\sqrt{a^2 - b^2}} \quad (a > b > 0), \tag{A.31}$$

and obtain the following expression:

$$\sum_{\boldsymbol{q}} \frac{u_{\boldsymbol{p}_1} u_{\boldsymbol{q}} \gamma_{\boldsymbol{p}_2\boldsymbol{q}}}{E - E_{\boldsymbol{p}_1\boldsymbol{p}_2\boldsymbol{q}}} = -\frac{1}{4\pi^2}\int \frac{q^2 u_{p_1} u_q \gamma_2(p_2, q, z_{\boldsymbol{p}_2\boldsymbol{q}})\, dq\, dz_{\boldsymbol{p}_2\boldsymbol{q}}}{\sqrt{f(p_1, p_2, q, z_{\boldsymbol{p}_1\boldsymbol{p}_2}, z_{\boldsymbol{p}_2\boldsymbol{q}})^2 - g(p_1, q, z_{\boldsymbol{p}_1\boldsymbol{p}_2}, z_{\boldsymbol{p}_2\boldsymbol{q}})^2}}. \tag{A.32}$$

Substituting this into Eq. (A.20) and doing other angular integrals that can be done, we obtain the third integral equation for states with rotational symmetry:

$$\left[T_{\mathrm{BEC}}^{-1}(E - E_{p_1} - E_{p_2}, |\boldsymbol{p}_1 + \boldsymbol{p}_2|) - \frac{n_0}{E - E_{\boldsymbol{p}_1\boldsymbol{p}_2}}\right]\gamma_2(p_1, p_2, z_{\boldsymbol{p}_1\boldsymbol{p}_2}) \\ = -\frac{u_{p_1} v_{p_2} \gamma_0}{E - E_{p_1} - \varepsilon_{p_1}} + \sqrt{n_0}\left[\frac{u_{p_1}\gamma_1(p_2)}{E - E_{\boldsymbol{p}_1\boldsymbol{p}_2}} - \frac{v_{p_1}\gamma_1(p_2)}{E - E_{p_2} - \varepsilon_{p_2}}\right] \\ + \int \frac{q^2\, dq\, dz_{\boldsymbol{p}_2\boldsymbol{q}}}{4\pi^2}\left(-\frac{u_{p_1} u_q}{\sqrt{f^2 - g^2}} + \frac{v_{p_1} v_q}{E - E_{p_2} - \varepsilon_{p_2}}\right)\gamma_2(p_2, q, z_{\boldsymbol{p}_2\boldsymbol{q}}) + (\boldsymbol{p}_1 \leftrightarrow \boldsymbol{p}_2). \tag{A.33}$$

This is the integral equation for a three-variable function, which can be numerically solved by discretizing the continuous variables.

Appendix B

Perturbative analysis of the r_0-model

In this appendix, we present the details of the perturbation theory within the r_0-model of the Bose polaron. As the properties of the impurity are of our interest, we first discuss the impurity self-energy diagrams up to the order of g_0^4. We then proceed to other quantities that we can derive from the self-energy.

Here is the dictionary of the diagrammatic representation [158]:

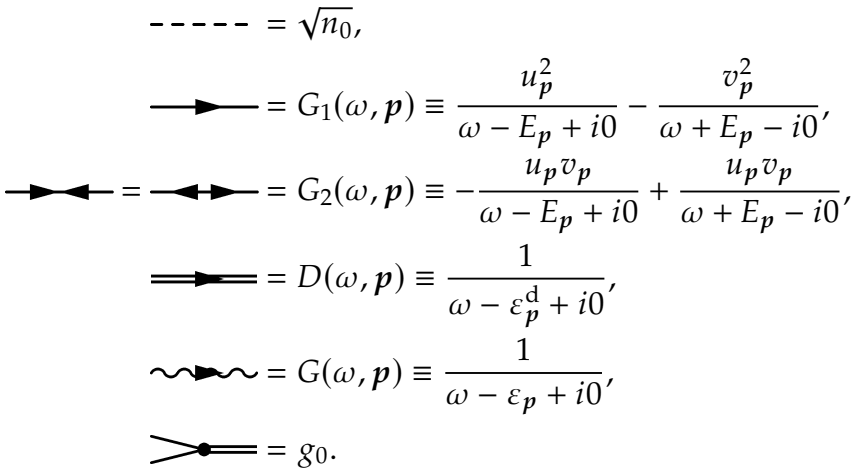

(B.1)

For each loop integral, we attach a factor of i. Here, we assume the unitarity where the dimer has zero detuning (no ν in $D(\omega, \boldsymbol{p})$). Instead of introducing the bare detuning ν_0 as we do in Sec. 2.2.1, we explicitly make the pair propagator finite by subtracting the diverging part (see Sec. B.2). We also note that the impurity and a boson interact only by forming a closed-channel dimer, and that one dimer line always has two vertices at its edge. Thus the self-energy only has terms with the even power of g_0.

(a) (b)

Figure B.1: Self-energy diagrams of $O(g_0^2)$. At this order, the impurity forms a closed-channel dimer and dissociates back into the open channel. This process occurs either (a) by binding a boson in the condensate, or (b) by creating a particle-hole pair, of which the particle binds with the impurity into a closed-channel molecule. The processes represented by (b) have a non-zero contribution only when $\xi \neq 0$ because otherwise the only excitation of the Bose gas is the particle excitation. We denote the corresponding terms by $\Sigma_a^{(2)}$ and $\Sigma_b^{(2)}$.

B.1 Self-energy to $O(g_0^2)$

For a general a_B, there are two diagrams of the impurity self-energy to $O(g_0^2)$, which are shown in Fig. B.1. From Eq. (B.1), they immediately read

$$\Sigma_a^{(2)}(\omega, \boldsymbol{p}) = g_0^2 n_0 D(\omega, \boldsymbol{p}) = \frac{g_0^2 n_0}{\omega - \varepsilon_{\boldsymbol{p}}^\mathrm{d}}, \tag{B.2}$$

$$\Sigma_b^{(2)}(\omega, \boldsymbol{p}) = i g_0^2 \int \frac{d^4 q}{(2\pi)^4} D(\omega + q_0, \boldsymbol{p} + \boldsymbol{q}) G_1(q_0, \boldsymbol{q}) \tag{B.3}$$

$$= i g_0^2 \int \frac{d^4 q}{(2\pi)^4} \frac{1}{\omega + q_0 - \varepsilon_{\boldsymbol{p}+\boldsymbol{q}}^\mathrm{d} + i0} \left(\frac{u_{\boldsymbol{q}}^2}{q_0 - E_{\boldsymbol{q}} + i0} - \frac{v_{\boldsymbol{q}}^2}{q_0 + E_{\boldsymbol{q}} - i0} \right), \tag{B.4}$$

where the 4-momentum q denotes the pair of the frequency q_0 and the 3-momentum $\boldsymbol{q}$. In the frequency integration, one can take the integral contour that encloses the upper half of the complex-q_0 plain. This leads to

$$\Sigma_b^{(2)}(\omega, \boldsymbol{p}) = g_0^2 \int \frac{d^3 \boldsymbol{q}}{(2\pi)^3} \frac{v_{\boldsymbol{q}}^2}{\omega - E_{\boldsymbol{q}} - \varepsilon_{\boldsymbol{p}+\boldsymbol{q}}^\mathrm{d} + i0}, \tag{B.5}$$

which clearly vanishes for $a_\mathrm{B} \to 0$. It is worthwhile to note that the integral does not have a singularity for $\omega \to 0$ and $\boldsymbol{p} \to 0$, and that in this limit, the only scale in the integrand is the coherence length ξ. This implies that for small ω and $\boldsymbol{p}$, apart from a numerical constant,

$$\Sigma_b^{(2)}(\omega, \boldsymbol{p}) \sim -\frac{1}{|r_0|\xi}, \tag{B.6}$$

where $g_0^2 = 8\pi/m^2|r_0|$ is used. In contrast, $\Sigma_a^{(2)}$ is singular for $\omega \to 0$ and $\boldsymbol{p} \to 0$, and therefore is dominant for $g_0 \to 0$.

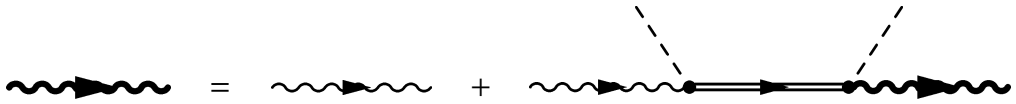

Figure B.2: Dyson equation for the impurity propagator at the lowest order.

The singularity of the leading self-energy $\Sigma_a^{(2)}$ drastically alters the physical picture of the weak-coupling limit from that of the decoupled impurity. This becomes clear if we consider the dressed impurity propagator. It is defined by the Dyson equation shown in Fig. B.2 and has the following analytic expression:

$$\mathcal{G}(\omega, \boldsymbol{p}) = \frac{1}{\omega - \varepsilon_{\boldsymbol{p}} - g_0^2 n_0/(\omega - \varepsilon_{\boldsymbol{p}}^{\mathrm{d}})}. \tag{B.7}$$

For $\boldsymbol{p} = 0$, the pole with the smallest real part, which corresponds to the ground state, is $\omega = -\sqrt{g_0^2 n_0} = -\sqrt{8\pi n_0/|r_0|}/m \equiv E^{(2)}$. Around this point, $\mathcal{G}$ is approximated by

$$\mathcal{G}(\omega, \boldsymbol{p}) \simeq \frac{1}{2} \frac{1}{\omega - E^{(2)} + (\varepsilon_{\boldsymbol{p}} + \varepsilon_{\boldsymbol{p}}^{\mathrm{d}})/2}, \tag{B.8}$$

which implies that the quasi-particle residue is $Z = 1/2$ and the effective mass is $m^* = 4m/3$. The ground state in this limit is in fact the equal-weight superposition state of the decoupled impurity and a closed-channel dimer. For the current perturbative analysis, an important consequence of this consideration is that we need to incorporate this picture from the next order to obtain the correct results. In other word, the impurity propagator in the $O(g_0^4)$ diagrams should be replaced by the dressed one $\mathcal{G}$.

B.2 Self-energy to $O(g_0^4)$

In Figure B.3, we show all the six diagrams to this order. Among them, only $\Sigma_a^{(4)}$ corresponding to Fig. B.3(a) remains finite for $a_{\mathrm{B}} \to 0$. Moreover, we shall show that all the others give smaller corrections, compared with $\Sigma_a^{(4)}$. On the other hand, the quasi-particle residue is subtler because we need to take $\Sigma_b^{(4)}$ to $\Sigma_d^{(4)}$ into account to have a finite result.

Now we can readily write down the self-energies of $O(g_0^4)$. After the frequency integrals, we obtain the following expressions:

$$\Sigma_a^{(4)}(\omega, \boldsymbol{p}) = \frac{g_0^4 n_0}{(\omega - \varepsilon_{\boldsymbol{p}}^{\mathrm{d}})^2} \int \frac{d^3\boldsymbol{q}}{(2\pi)^3} \left[u_{\boldsymbol{q}}^2 \mathcal{G}(\omega - E_{\boldsymbol{q}}, \boldsymbol{p} + \boldsymbol{q}) + \frac{m}{q^2} \right], \tag{B.9}$$

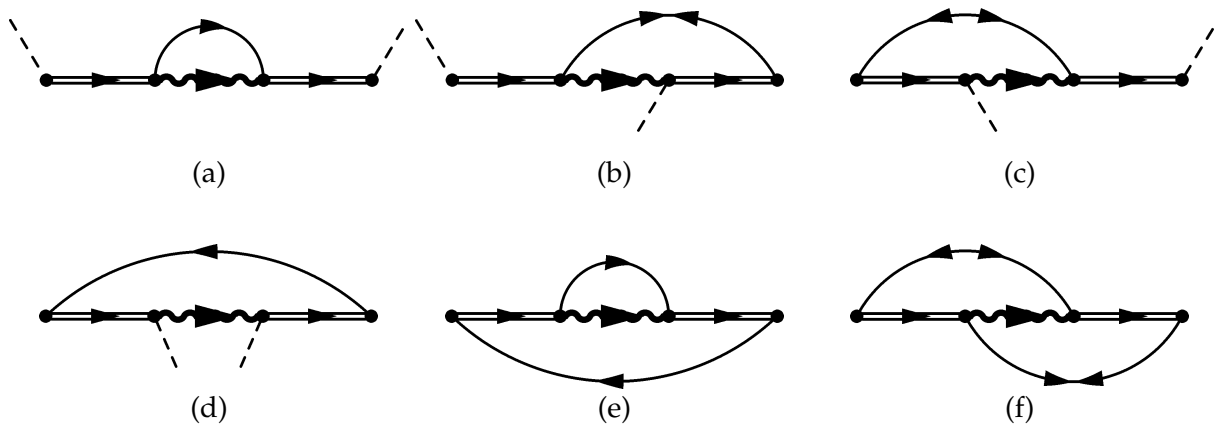

Figure B.3: Self-energy diagrams of $O(g_0^4)$. We denote the diagrams (a-f) by $\Sigma_x^{(4)}$ ($x = a, b, \ldots, f$). We need to use the dressed impurity propagator in order to obtain the correct results to the next-to-the-leading order. Among the six diagrams, only $\Sigma_a^{(4)}$ survives for $a_{\mathrm{B}} \to 0$. For $a_{\mathrm{B}} > 0$, the diagrams (b-f) diminish faster than $\Sigma_a^{(4)}$ in the weak-coupling limit. However, when calculating the derivatives of them, e.g., the residue, we need to take other diagrams into account in order to remove an infrared divergence.

$$\Sigma_b^{(4)}(\omega, \boldsymbol{p}) = \Sigma_c^{(4)}(\omega, \boldsymbol{p}) = -\frac{g_0^4 n_0}{\omega - \varepsilon_{\boldsymbol{p}}^{\mathrm{d}}} \int \frac{d^3\boldsymbol{q}}{(2\pi)^3} \frac{u_{\boldsymbol{q}} v_{\boldsymbol{q}} \mathcal{G}(\omega - E_{\boldsymbol{q}}, \boldsymbol{p} + \boldsymbol{q})}{\omega - E_{\boldsymbol{q}} - \varepsilon_{\boldsymbol{p}+\boldsymbol{q}}^{\mathrm{d}}}, \tag{B.10}$$

$$\Sigma_d^{(4)}(\omega, \boldsymbol{p}) = g_0^4 n_0 \int \frac{d^3\boldsymbol{q}}{(2\pi)^3} \frac{v_{\boldsymbol{q}}^2 \mathcal{G}(\omega - E_{\boldsymbol{q}}, \boldsymbol{p} + \boldsymbol{q})}{(\omega - E_{\boldsymbol{q}} - \varepsilon_{\boldsymbol{p}+\boldsymbol{q}}^{\mathrm{d}})^2}, \tag{B.11}$$

$$\Sigma_e^{(4)}(\omega, \boldsymbol{p}) = g_0^4 \int \frac{d^3\boldsymbol{q}}{(2\pi)^3} \frac{d^3\boldsymbol{k}}{(2\pi)^3} \frac{v_{\boldsymbol{k}}^2 [u_{\boldsymbol{q}}^2 \mathcal{G}(\omega - E_{\boldsymbol{q}} - E_{\boldsymbol{k}}, \boldsymbol{p} + \boldsymbol{q} + \boldsymbol{k}) - m/q^2]}{(\omega - E_{\boldsymbol{k}} - \varepsilon_{\boldsymbol{p}+\boldsymbol{k}}^{\mathrm{d}})^2}, \tag{B.12}$$

$$\Sigma_f^{(4)}(\omega, \boldsymbol{p}) = g_0^4 \int \frac{d^3\boldsymbol{q}}{(2\pi)^3} \frac{d^3\boldsymbol{k}}{(2\pi)^3} \frac{u_{\boldsymbol{q}} v_{\boldsymbol{q}} u_{\boldsymbol{k}} v_{\boldsymbol{k}} \mathcal{G}(\omega - E_{\boldsymbol{q}} - E_{\boldsymbol{k}}, \boldsymbol{p} + \boldsymbol{q} + \boldsymbol{k})}{(\omega - E_{\boldsymbol{q}} - \varepsilon_{\boldsymbol{p}+\boldsymbol{q}}^{\mathrm{d}})(\omega - E_{\boldsymbol{k}} - \varepsilon_{\boldsymbol{p}+\boldsymbol{k}}^{\mathrm{d}})}. \tag{B.13}$$

The subtraction of the ultraviolet divergence in Eqs. (B.9) and (B.12) is equivalent to setting the bare detuning ν_0 to

$$\nu_0(\Lambda) = \frac{m g_0^2}{2\pi^2} \Lambda = g_0^2 \int_{|\boldsymbol{q}|<\Lambda} \frac{d^3\boldsymbol{q}}{(2\pi)^3} \frac{m}{q^2}, \tag{B.14}$$

as we did in Sec. 2.2.1, and to retaining the terms up to $O(g_0^4)$.

Similarly to the discussion in the previous section, we can compare the different diagrams with the help of the dimensional analysis. A naive dimensional analysis for $\omega \to 0$ and $\boldsymbol{p} \to 0$ leads to the following scaling relations:

$$\Sigma_a^{(4)} \sim \frac{1}{|r_0|\xi}, \quad \Sigma_b^{(4)} = \Sigma_c^{(4)} \sim \frac{n_0^{1/2}\xi}{|r_0|^{3/2}}, \quad \Sigma_d^{(4)} \sim \frac{n_0 \xi^3}{|r_0|^2}, \quad \Sigma_e^{(4)} = \Sigma_f^{(4)} \sim \frac{1}{|r_0|^2}. \tag{B.15}$$

This is too simplistic, however, for $\Sigma_b^{(4)} = \Sigma_c^{(4)}$ and $\Sigma_d^{(4)}$ have infrared divergence for $\omega \to 0$ and $\boldsymbol{p} \to 0$. This results in a logarithmic correction to $\Sigma_b^{(4)}$ and $\Sigma_c^{(4)}$ and an additional factor of $|r_0|^{1/2}/(\xi^2 n_0^{1/2})$ for $\Sigma_d^{(4)}$. With these corrections considered, we still see that $\Sigma_a^{(4)}$ is dominant in the weak-coupling limit. Indeed, it has the same scaling as $\Sigma_b^{(2)}$. Therefore, the first correction to $\Sigma_a^{(2)}$ is given by $\Sigma_b^{(2)}$ and $\Sigma_a^{(4)}$ for $a_{\mathrm{B}} \neq 0$ and only by $\Sigma_a^{(4)}$ for $a_{\mathrm{B}} = 0$. Note that this consideration is about the self-energy itself. When we discuss the quasi-particle residue, for example, we consider the derivative of the self-energy, in which more care must be taken to obtain meaningful results.

B.3 Ground-state energy

The energy can be found by solving $E = \Sigma(E, 0)$. From the leading-order self-energy $\Sigma_a^{(2)}$, we obtain the following ground-state energy:

$$E = E^{(2)} = -\frac{1}{m}\sqrt{\frac{8\pi n_0}{|r_0|}}. \tag{B.16}$$

When $\Sigma(\omega, \boldsymbol{p}) = \Sigma^{(2)}(\omega, \boldsymbol{p}) + \delta\Sigma(\omega, \boldsymbol{p})$, the equation for the energy reduces to

$$E = \Sigma_a^{(2)}(E^{(2)} + \delta E, 0) + \delta\Sigma(E^{(2)} + \delta E, 0) \tag{B.17}$$

$$\simeq E^{(2)} - \delta E + \delta\Sigma(E^{(2)}, 0), \tag{B.18}$$

where $\delta E \equiv E - E^{(2)}$ and we have dropped the higher-order corrections. Therefore, the next-to-the-leading-order correction to the ground state energy is obtained by

$$\delta E = \frac{1}{2}\delta\Sigma(E^{(2)}, 0). \tag{B.19}$$

Below, we consider the cases with $a_{\mathrm{B}} = 0$ and $a_{\mathrm{B}} \neq 0$ separately.

Case 1: $a_{\mathrm{B}} = 0$

In this case, only $\Sigma_a^{(4)}$ alone gives the next-to-the-leading-order correction to the ground-state energy. By noting that $u_{\boldsymbol{q}} \to 1$, $E_{\boldsymbol{q}} \to \varepsilon_{\boldsymbol{q}}$, and $(E^{(2)})^2 = g_0^2 n_0$, it is straightforward from Eq. (B.9) to obtain

$$\Sigma_a^{(4)}(E^{(2)}, 0) = \frac{2}{m}\sqrt{\frac{3}{7}}\left(\frac{8\pi n_0}{|r_0|^5}\right)^{1/4}. \tag{B.20}$$

Therefore, the ground-state energy is

$$E \simeq -\frac{1}{m}\sqrt{\frac{8\pi n_0}{|r_0|}} + \frac{1}{m}\sqrt{\frac{3}{7}}\left(\sqrt{\frac{8\pi n_0}{|r_0|^5}}\right)^{1/4}. \tag{B.21}$$

Case 2: $a_{\rm B} > 0$

As shown in the previous sections, the next-to-the-leading-order correction to the self-energy comes from the following two terms:

$$\delta\Sigma(E^{(2)}, 0) = \Sigma_b^{(2)}(E^{(2)}, 0) + \Sigma_a^{(4)}(E^{(2)}, 0). \tag{B.22}$$

By using the expressions for them, we obtain

$$\delta\Sigma(E^{(2)}, 0) = g_0^2 \int \frac{d^3\boldsymbol{q}}{(2\pi)^3}\left[\frac{v_{\boldsymbol{q}}^2}{E^{(2)} - E_{\boldsymbol{q}} - \varepsilon_{\boldsymbol{q}}^{\rm d}} + \frac{u_{\boldsymbol{q}}^2}{E^{(2)} - E_{\boldsymbol{q}} - \varepsilon_{\boldsymbol{q}} - \frac{g_0^2 n_0}{E^{(2)} - E_{\boldsymbol{q}} - \varepsilon_{\boldsymbol{q}}^{\rm d}}} + \frac{m}{q^2}\right]. \tag{B.23}$$

The integral is not singular in the limit of $E^{(2)} \to 0$. Therefore, to obtain the next-to-the-leading-order correction only, we can safely set $E^{(2)} \to 0$,

$$\begin{aligned}
\delta\Sigma(0, 0) &= g_0^2 \int \frac{d^3\boldsymbol{q}}{(2\pi)^3}\left[-\frac{v_{\boldsymbol{q}}^2}{E_{\boldsymbol{q}} + \varepsilon_{\boldsymbol{q}}^{\rm d}} - \frac{u_{\boldsymbol{q}}^2}{E_{\boldsymbol{q}} + \varepsilon_{\boldsymbol{q}}} + \frac{m}{q^2}\right] && \text{(B.24)}\\
&= \frac{8\pi}{m|r_0|\xi}\int \frac{dx}{2\pi^2}\left[-\frac{x^2 + 1 - x\sqrt{x^2+2}}{x^2 + 2 + x\sqrt{x^2+2}/2} - \frac{x^2 + 1 + x\sqrt{x^2+2}}{x^2 + 2 + x\sqrt{x^2+2}} + 1\right] && \text{(B.25)}\\
&= \left(16\sqrt{\frac{\pi}{3}} - \frac{24}{\sqrt{\pi}}\right)\frac{\sqrt{n_0 a_{\rm B}}}{m|r_0|} && \text{(B.26)}\\
&\simeq \frac{2.83268\sqrt{n_0 a_{\rm B}}}{m|r_0|}. && \text{(B.27)}
\end{aligned}$$

Therefore, the ground-state energy to the next-to-the-leading-order correction is

$$E = -\frac{1}{m}\sqrt{\frac{8\pi n_0}{|r_0|}} + \left(8\sqrt{\frac{\pi}{3}} - \frac{12}{\sqrt{\pi}}\right)\frac{\sqrt{n_0 a_{\rm B}}}{m|r_0|}. \tag{B.28}$$

B.4 Quasi-particle residue

In terms of the self-energy, the quasi-particle residue Z is given as

$$Z^{-1} = 1 - \partial_\omega \Sigma(\omega, 0)|_{\omega = E}\,. \tag{B.29}$$

Considering the leading-order self-energy $\Sigma_a^{(2)}$ first, we find that

$$\partial_\omega \Sigma_a^{(2)}(\omega, 0)\Big|_{\omega=E^{(2)}+\delta E} \simeq -1 + \frac{2\delta E}{E^{(2)}}, \tag{B.30}$$

where we retain the next-to-the-leading-order correction to the shift of the ground-state energy. Combining this with the corrections to the self-energy, we obtain

$$Z^{-1} \simeq 2 - \frac{2\delta E}{E^{(2)}} - \partial_\omega \delta\Sigma(\omega, 0)|_{\omega=E^{(2)}}\,, \tag{B.31}$$

where $\delta\Sigma \equiv \Sigma - \Sigma_a^{(2)}$. Clearly, this is consistent with the comment at the end of Sec. B.1. Equivalently, we obtain the leading correction to the quasi-particle residue as follows:

$$Z - \frac{1}{2} \simeq \frac{\delta E}{2E^{(2)}} + \frac{1}{4}\,\partial_\omega \delta\Sigma(\omega, 0)|_{\omega=E^{(2)}}\,. \tag{B.32}$$

Case 1: $a_\mathrm{B} = 0$

In this case, we only need to consider $\Sigma_a^{(4)}$ and set $u_{\boldsymbol{q}} = 1, v_{\boldsymbol{q}} = 0$, and $E_{\boldsymbol{q}} = \varepsilon_{\boldsymbol{q}}$. The frequency derivative of this term is

$$\begin{aligned}\partial_\omega \Sigma_a^{(4)}(\omega, 0) = \left(\partial_\omega \frac{g_0^4 n_0}{\omega^2}\right) \int \frac{d^3\boldsymbol{q}}{(2\pi)^3} \left[\mathcal{G}(\omega - \varepsilon_{\boldsymbol{q}}, \boldsymbol{q}) + \frac{m}{q^2}\right] \\ + \frac{g_0^4 n_0}{\omega^2} \int \frac{d^3\boldsymbol{q}}{(2\pi)^3} \partial_\omega \mathcal{G}(\omega - \varepsilon_{\boldsymbol{q}}, \boldsymbol{q}),\end{aligned} \tag{B.33}$$

and has two contributions, which are distinguished by the part on which the differentiation acts. In the first term, ω outside the integral is differentiated; this leads to the term in $\partial_\omega \Sigma_a^{(4)}(E^{(2)}, 0)$ of the form

$$\frac{-2}{E^{(2)}} \Sigma_a^{(4)}(E^{(2)}, 0) = -\frac{4\delta E}{E^{(4)}}, \tag{B.34}$$

where we use $\delta E = \frac{1}{2}\Sigma_a^{(4)}(E^{(2)}, 0)$ which holds true for $a_\mathrm{B} = 0$. In the other term, ∂_ω acts on $\mathcal{G}$ in the integral, which, in fact, leads to an infrared divergence. For a small $\boldsymbol{q}$ and $a_\mathrm{B} \to 0$, we can use Eq. (B.8) to obtain

$$\partial_\omega \mathcal{G}(\omega - \varepsilon_{\boldsymbol{q}}, \boldsymbol{q})\big|_{\omega=E^{(2)}} \simeq -\frac{1}{2} \frac{1}{[\varepsilon_{\boldsymbol{q}} + (\varepsilon_{\boldsymbol{q}} + \varepsilon_{\boldsymbol{q}}^\mathrm{d})/2]^2} \tag{B.35}$$

$$\sim q^{-4}, \tag{B.36}$$

which makes it clear that the integral diverges linearly around $\boldsymbol{q} = 0$. In total, the inverse of the quasi-particle residue is

$$Z^{-1} \simeq 2 + \frac{2\delta E}{E^{(2)}} + \frac{L}{|r_0|} \tag{B.37}$$

$$= 2 - 2\sqrt{\frac{3}{7}} \frac{1}{(8\pi n_0 |r_0|^3)^{1/4}} + \frac{L}{|r_0|}, \tag{B.38}$$

where L represents the linear divergence. This result implies that the quasi-particle residue is zero within the perturbation theory for $a_\mathrm{B} \to 0$.

We would like to emphasize that the infrared divergence persists even if we take the higher-order self-energy in calculating the dressed propagator. Generally, the low-momentum expansion of $\mathcal{G}$ has the form

$$\mathcal{G}(\omega, \boldsymbol{p}) \simeq \frac{Z}{\omega - E^* - p^2/2m^*}, \tag{B.39}$$

where E^* and m^* are the ground-state energy and the effective mass, respectively, which are determined within the same order of approximation. Then the derivative of $\mathcal{G}$ at low momenta is again

$$\partial_\omega \mathcal{G}(\omega - \varepsilon_{\boldsymbol{p}}, \boldsymbol{p})\big|_{\omega = E^*} \sim p^{-4}. \tag{B.40}$$

Therefore, as long as this expansion applies to $\mathcal{G}$, the integral in Eq. (B.9) inevitably diverges for $a_\mathrm{B} \to 0$.

Case 2: $a_\mathrm{B} > 0$

If we apply the naive counting of the power to each term of $\partial_\omega \Sigma$, we find that $\Sigma_a^{(4)}$ gives the next-to-the-leading-order correction. Similarly to the case with $a_\mathrm{B} = 0$, we can divide $\partial_\omega \Sigma^{(4)}$ into two parts:

$$\begin{aligned} \partial_\omega \Sigma_a^{(4)}(\omega, 0) = \left(\partial_\omega \frac{g_0^4 n_0}{\omega^2}\right) \int \frac{d^3\boldsymbol{q}}{(2\pi)^3} \left[u_{\boldsymbol{q}}^2 \mathcal{G}(\omega - E_{\boldsymbol{q}}, \boldsymbol{q}) + \frac{m}{q^2} \right] \\ + \frac{g_0^4 n_0}{\omega^2} \int \frac{d^3\boldsymbol{q}}{(2\pi)^3} u_{\boldsymbol{q}}^2 \partial_\omega \mathcal{G}(\omega - E_{\boldsymbol{q}}, \boldsymbol{q}). \end{aligned} \tag{B.41}$$

For the term in which ∂_ω acts on ω^{-2} outside the integral, we obtain the following expression:

$$-\frac{2}{E^{(2)}} \Sigma_a^{(4)}(E^{(2)}, 0) \simeq -\frac{2}{E^{(2)}} \Sigma_a^{(4)}(0, 0) \tag{B.42}$$

$$\simeq \frac{4\sqrt{2}}{\pi}\sqrt{\frac{a_{\mathrm{B}}}{|r_0|}}. \tag{B.43}$$

Note that for $a_{\mathrm{B}} \neq 0$, this is not simply $-4\delta E/E^{(2)}$ because δE has a contribution from $\Sigma_b^{(2)}$.

A special care is needed when we consider the term involving the derivative of $\mathcal{G}$, which, for $a_{\mathrm{B}} \to 0$, causes the linear infrared divergence. For a nonzero a_{B}, the Bogoliubov dispersion is linear in momentum, weakening the divergence of $\partial_\omega \mathcal{G}$ around the pole to

$$\partial_\omega \mathcal{G}(\omega - E_{\boldsymbol{q}}, \boldsymbol{q})\big|_{\omega = E^{(2)}} \sim p^{-2}. \tag{B.44}$$

At the same time, a nonzero a_{B} leads to a diverging $u_{\boldsymbol{q}}^2 \sim q^{-1}$ for a small $\boldsymbol{q}$, which, together with the divergence of $\partial_\omega \mathcal{G}$, results in a logarithmic divergence of the integral.

This, however, does not affect the final result because the same divergence occurs in $\partial_\omega \Sigma_b^{(4)}$, $\partial_\omega \Sigma_c^{(4)}$, and $\partial_\omega \Sigma_d^{(4)}$, which have been omitted so far, and they cancel out. To see that this cancellation happens, it is sufficient to consider the terms involving $\partial_\omega \mathcal{G}$. If we look at Eqs. (B.10) and (B.11), we can approximate $\omega - E_{\boldsymbol{q}} - \varepsilon_{\boldsymbol{q}}^{\mathrm{d}}$ by ω and take it out of the integral for $\boldsymbol{p} \to 0$ and $\boldsymbol{q} \to 0$. Then each integral has the logarithmic infrared divergence from the integrands of the form

$$-u_{\boldsymbol{q}} v_{\boldsymbol{q}}\, \partial_\omega \mathcal{G}(\omega - E_{\boldsymbol{q}}, \boldsymbol{q})\big|_{\omega = E^{(2)}} \tag{B.45}$$

and

$$v_{\boldsymbol{q}}^2\, \partial_\omega \mathcal{G}(\omega - E_{\boldsymbol{q}}, \boldsymbol{q})\big|_{\omega = E^{(2)}}\,. \tag{B.46}$$

Here, the sign in Eq. (B.45) is important. Also, Eq. (B.45) is to be doubled because both $\Sigma_b^{(4)}$ and $\Sigma_c^{(4)}$ have the same contribution. Therefore, by summing up these terms, the integrand at low momenta is

$$(u_{\boldsymbol{q}} - v_{\boldsymbol{q}})^2\, \partial_\omega \mathcal{G}(\omega - E_{\boldsymbol{q}}, \boldsymbol{q})\big|_{\omega = E^{(2)}}\,. \tag{B.47}$$

Since for a small $\boldsymbol{q}$, $u_{\boldsymbol{q}} - v_{\boldsymbol{q}} \sim \sqrt{q}$, the resulting integral is infrared finite and can simply be ignored, because after combined with the prefactor, the result scales as $\xi/|r_0|$, decaying faster than $\sqrt{a_{\mathrm{B}}/|r_0|}$ for $g_0 \to 0$.

From the discussion above, we conclude that the quasi-particle residue has a finite value for $a_{\mathrm{B}} \neq 0$ within the perturbation theory up to $O(g_0^4)$. We thus find that

$$Z^{-1} \simeq 2 - \frac{2\delta E}{E^{(2)}} + \frac{2}{E^{(2)}}\Sigma_a^{(4)}(0,0) \tag{B.48}$$

$$\simeq 2 - \left(\frac{10\sqrt{2}}{\pi} - \frac{4\sqrt{2}}{\sqrt{3}}\right)\sqrt{\frac{a_{\mathrm{B}}}{|r_0|}}, \tag{B.49}$$

or equivalently

$$Z \simeq \frac{1}{2} + \left(\frac{5}{\sqrt{2}\pi} - \sqrt{\frac{2}{3}}\right)\sqrt{\frac{a_{\mathrm{B}}}{|r_0|}}, \tag{B.50}$$

which is finite, in contrast to the case for $a_{\mathrm{B}} = 0$.

Appendix C

Effective mass obtained from the variational wave function

The inverse effective mass of the Bose polaron is defined as

$$\frac{1}{m^*}\delta_{uv} \equiv \left.\frac{\partial^2 E(\boldsymbol{p})}{\partial p_u \partial p_v}\right|_{\boldsymbol{p}=0} \quad (u, v = x, y, z), \tag{C.1}$$

where $E(\boldsymbol{p})$ is the energy dispersion of the Bose polaron and the rotational symmetry is assumed. A straightforward way to calculate this quantity is to determine $E(\boldsymbol{p})$ for a small $\boldsymbol{p}$ and differentiate it numerically. However, it is numerically expensive to extend the variational method to finite $\boldsymbol{p}$ states, and thus it is hard to obtain accurate results by this method.

Here, we take an alternative approach based on a perturbative expansion of the variational equation. By regarding the total momentum $\boldsymbol{p}$ as a small parameter, we expand the variational equation in terms of $\boldsymbol{p}$, and evaluate the second derivative of the ground-state energy. A similar method was used to calculate the effective mass of a Fermi polaron by Trefzger and Castin [127].

In the variational method, the integral equation has the following structure:

$$\hat{K}_0(E)\,|\gamma\rangle = 0, \tag{C.2}$$

where $|\gamma\rangle$ is the set of the γ functions to be determined, and $\hat{K}_0(E)$ is a linear integral operator. The ground-state energy is $E = E_0$, where the smallest eigenvalue of $\hat{K}_0(E)$ crosses zero. We can generalize the variational equations for a finite $\boldsymbol{p}$ that implicitly gives $E(\boldsymbol{p})$:

$$\hat{K}[E(\boldsymbol{p}), \boldsymbol{p}]\,|\gamma\rangle = 0. \tag{C.3}$$

Note that this is not a Schrödinger equation, as we have removed the α functions and $\hat{K}$ is no longer of the form $\hat{H} - E$. However, the fact that $\hat{K}$ is a Hermitian matrix allows us to evaluate the eigenvalues perturbatively in a manner similar to the Rayleigh-Schrödinger perturbation theory for Hamiltonians. Once we have a perturbative expression of the lowest eigenvalue, the condition that it vanishes gives the energy $E(\boldsymbol{p})$ for a small $\boldsymbol{p}$, or equivalently, the effective mass.

To this end, we first expand $\hat{K}[E(\boldsymbol{p}), \boldsymbol{p}]$ in terms of $\boldsymbol{p}$:

$$\hat{K}[E(\boldsymbol{p}), \boldsymbol{p}] \simeq \hat{K}_0 + \sum_{u=x,y,z} p_u \hat{K}_u + \sum_{u,v=x,y,z} \frac{p_u p_v}{2} \left(\hat{K}_{uv} + \left. \frac{\partial^2 E(\boldsymbol{p})}{\partial p_u \partial p_v} \right|_{\boldsymbol{p}=0} \hat{K}_E \right) \tag{C.4}$$

$$= \hat{K}_0 + \sum_{u=x,y,z} p_u \hat{K}_u + \sum_{u,v=x,y,z} \frac{p_u p_v}{2} \left(\hat{K}_{uv} + \frac{1}{m^*} \delta_{uv} \hat{K}_E \right), \tag{C.5}$$

where we use $\partial E(\boldsymbol{p})/\partial \boldsymbol{p} = 0$, the definition of the effective mass, $\hat{K}_0 \equiv \hat{K}_0(E_0)$, and the following operators:

$$\hat{K}_u \equiv \left. \frac{\partial \hat{K}[E, \boldsymbol{p}]}{\partial p_u} \right|_{E=E_0, \boldsymbol{p}=0}, \quad \hat{K}_{uv} \equiv \left. \frac{\partial^2 \hat{K}[E, \boldsymbol{p}]}{\partial p_u \partial p_v} \right|_{E=E_0, \boldsymbol{p}=0}, \quad \hat{K}_E \equiv \left. \frac{\partial \hat{K}[E, \boldsymbol{p}]}{\partial E} \right|_{E=E_0, \boldsymbol{p}=0}. \tag{C.6}$$

Owing to rotational symmetry, we can focus on $\boldsymbol{p} = p\boldsymbol{e}_z$ without loss of generality and simplify the expansion as follows:

$$\hat{K}[E(\boldsymbol{p}), \boldsymbol{p}] = \hat{K}_0(E_0) + p\hat{K}_z + \frac{p^2}{2} \left(\hat{K}_{zz} + \frac{1}{m^*} \hat{K}_E \right). \tag{C.7}$$

We use this expansion to obtain the lowest eigenvalue of $\hat{K}[E(\boldsymbol{p}), \boldsymbol{p}]$ for a small p. Suppose the lowest eigenvalue $\lambda_0[E(\boldsymbol{p}), \boldsymbol{p}]$ is expanded as

$$\lambda_0[E(\boldsymbol{p}), \boldsymbol{p}] = \lambda_0^{(0)} + \lambda_0^{(1)} p + \lambda_0^{(2)} p^2 + \dots. \tag{C.8}$$

It should be noted that this is not only an expansion of $\lambda_0[E, \boldsymbol{p}]$ in terms of $\boldsymbol{p}$, but also it contains the information about the expansion of $E(\boldsymbol{p})$. The first coefficient $\lambda_0^{(0)}$ is the lowest eigenvalue of $\hat{K}_0(E_0)$, which is zero from the condition determining the ground-state energy E_0 for $p = 0$. The perturbation coefficients for the higher orders are written as

$$\lambda_0^{(1)} = \left\langle \gamma_0 \middle| \hat{K}_z \middle| \gamma_0 \right\rangle, \tag{C.9}$$

$$\lambda_0^{(2)} = \frac{1}{2} \left\langle \gamma_0 \middle| \left(\hat{K}_{zz} + \frac{1}{m^*} \hat{K}_E \right) \middle| \gamma_0 \right\rangle + \sum_{i>0} \frac{\left| \left\langle \gamma_i \middle| \hat{K}_z \middle| \gamma_0 \right\rangle \right|^2}{\lambda_0^{(0)} - \lambda_i^{(0)}} \tag{C.10}$$

$$= \frac{1}{2}\left\langle \gamma_0 \middle| \left(\hat{K}_{zz} + \frac{1}{m^*}\hat{K}_E \right) \middle| \gamma_0 \right\rangle - \sum_{i>0} \frac{\left| \left\langle \gamma_i \middle| \hat{K}_z \middle| \gamma_0 \right\rangle \right|^2}{\lambda_i^{(0)}}. \tag{C.11}$$

Here, $\lambda_i^{(0)}$ is the i-th lowest eigenvalue of $\hat{K}_0(E_0)$ and $|\gamma_i\rangle$ is the corresponding eigenvector; we count i from zero, which corresponds to the ground state satisfying $\hat{K}_0(E_0)\,|\gamma_0\rangle = 0$. By noting that $\hat{K}_z$ has odd parity while the ground state is an even-parity state, the first-order coefficient $\lambda_0^{(1)}$ automatically vanishes.

Now we return to the condition that determines the ground-state energy, which is

$$\lambda_0[E(\boldsymbol{p}), \boldsymbol{p}] = 0, \tag{C.12}$$

for any given $\boldsymbol{p}$. This means that all the perturbation coefficients in Eq. (C.8) are zero, and that this set of the zero-coefficient conditions determines the low-momentum expansion of $E(\boldsymbol{p})$. In particular, $\lambda_0^{(2)} = 0$ gives the following expression of the effective mass:

$$\frac{1}{m^*} = \frac{1}{\left\langle \gamma_0 \middle| \hat{K}_E \middle| \gamma_0 \right\rangle} \left[2\sum_{i>0} \frac{\left| \left\langle \gamma_i \middle| \hat{K}_z \middle| \gamma_0 \right\rangle \right|^2}{\lambda_i^{(0)}} - \left\langle \gamma_0 \middle| \hat{K}_{zz} \middle| \gamma_0 \right\rangle \right]. \tag{C.13}$$

By introducing a projection operator $\hat{P} \equiv \sum_{i>0} |\gamma_i\rangle \langle\gamma_i|$, we can rewrite the effective mass in the following form:

$$\frac{1}{m^*} = \frac{1}{\left\langle \gamma_0 \middle| \hat{K}_E \middle| \gamma_0 \right\rangle} \left\langle \gamma_0 \middle| \left[2\hat{K}_z \hat{P} \left(\hat{K}_0\right)^{-1} \hat{P}\hat{K}_z - \hat{K}_{zz} \right] \middle| \gamma_0 \right\rangle. \tag{C.14}$$

This is a particularly convenient form, because we do not need to take the numerical derivative of the ground-state energy or calculate the derivative of the γ functions. In this method, we use the derivatives of the integral operator, whose expressions are known, and take the expectation values within $|\gamma_0\rangle$, which is numerically obtained in the calculation of the ground-state energy.

Bibliography

[1] L. D. Landau and L. M. Lifshitz, *Quantum Mechanics: Non-Relativistic Theory*, 3rd ed. (Butterworth-Heinemann, Oxford, 1981).

[2] J. R. Taylor, *Scattering Theory: The Quantum Theory of Nonrelativistic Collisions* (Dover Publications, Mineola, NY, 2006).

[3] V. Efimov, Energy Levels Arising from Resonant Two-Body Forces in a Three-Body System, Phys. Lett. B **33**, 563 (1970).

[4] V. Efimov, Weakly-Bound States of Three Resonantly-Interacting Particles, Sov. J. Nucl. Phys. **12**, 101 (1971).

[5] V. Efimov, Level Spectrum of Three Resonantly Interacting Particles., JETP Lett. **16**, 34 (1972).

[6] V. Efimov, Energy Levels of Three Resonantly Interacting Particles, Nucl. Phys. A **210**, 157 (1973).

[7] R. D. Amado and J. V. Noble, Efimov's Effect: A New Pathology of Three-Particle Systems. II, Phys. Rev. D **5**, 1992 (1972).

[8] E. Braaten and H. W. Hammer, Universality in Few-Body Systems with Large Scattering Length, Phys. Rep. **428**, 259 (2006).

[9] P. Naidon and S. Endo, Efimov Physics: A Review, Rep. Prog. Phys. **80**, 056001 (2017).

[10] C. H. Greene, P. Giannakeas, and J. Pérez-Ríos, Universal Few-Body Physics and Cluster Formation, Rev. Mod. Phys. **89**, 035006 (2017).

[11] O. I. Kartavtsev and A. V. Malykh, Low-Energy Three-Body Dynamics in Binary Quantum Gases, J. Phys. B: At. Mol. Opt. Phys. **40**, 1429 (2007).

[12] Y. Castin, C. Mora, and L. Pricoupenko, Four-Body Efimov Effect for Three Fermions and a Lighter Particle, Phys. Rev. Lett. **105**, 223201 (2010).

[13] S. Endo, P. Naidon, and M. Ueda, Crossover Trimers Connecting Continuous and Discrete Scaling Regimes, Phys. Rev. A **86**, 062703 (2012).

[14] O. I. Kartavtsev and A. V. Malykh, Universal Description of Three Two-Component Fermions, Europhys. Lett. **115**, 36005 (2016).

[15] B. Bazak and D. S. Petrov, Five-Body Efimov Effect and Universal Pentamer in Fermionic Mixtures, Phys. Rev. Lett. **118**, 083002 (2017).

[16] L. Platter, H.-W. Hammer, and U.-G. Meißner, Four-Boson System with Short-Range Interactions, Phys. Rev. A **70**, 052101 (2004).

[17] H.-W. Hammer and L. Platter, Universal Properties of the Four-Body System with Large Scattering Length, Eur. Phys. J. A **32**, 113 (2007).

[18] J. von Stecher, J. P. D'Incao, and C. H. Greene, Signatures of Universal Four-Body Phenomena and Their Relation to the Efimov Effect, Nat. Phys. **5**, 417 (2009).

[19] J. von Stecher, Five- and Six-Body Resonances Tied to an Efimov Trimer, Phys. Rev. Lett. **107**, 200402 (2011).

[20] M. Gattobigio and A. Kievsky, Universality and Scaling in the N-Body Sector of Efimov Physics, Phys. Rev. A **90**, 012502 (2014).

[21] Y. Yan and D. Blume, Energy and Structural Properties of N-Boson Clusters Attached to Three-Body Efimov States: Two-Body Zero-Range Interactions and the Role of the Three-Body Regulator, Phys. Rev. A **92**, 033626 (2015).

[22] Y. Wang, W. B. Laing, J. von Stecher, and B. D. Esry, Efimov Physics in Heteronuclear Four-Body Systems, Phys. Rev. Lett. **108**, 073201 (2012).

[23] D. Blume and Y. Yan, Generalized Efimov Scenario for Heavy-Light Mixtures, Phys. Rev. Lett. **113**, 213201 (2014).

[24] J. Levinsen, N. R. Cooper, and V. Gurarie, Strongly Resonant p-Wave Superfluids, Phys. Rev. Lett. **99**, 210402 (2007).

[25] M. Jona-Lasinio, L. Pricoupenko, and Y. Castin, Three Fully Polarized Fermions Close to a p-Wave Feshbach Resonance, Phys. Rev. A **77**, 043611 (2008).

[26] J. Levinsen, N. R. Cooper, and V. Gurarie, Stability of Fermionic Gases Close to a p-Wave Feshbach Resonance, Phys. Rev. A **78**, 063616 (2008).

[27] Y. Nishida, S. Moroz, and D. T. Son, Super Efimov Effect of Resonantly Interacting Fermions in Two Dimensions, Phys. Rev. Lett. **110**, 235301 (2013).

[28] A. G. Volosniev, D. V. Fedorov, A. S. Jensen, and N. T. Zinner, Borromean Ground State of Fermions in Two Dimensions, J. Phys. B: At. Mol. Opt. Phys. **47**, 185302 (2014).

[29] D. K. Gridnev, Three Resonating Fermions in Flatland: Proof of the Super Efimov Effect and the Exact Discrete Spectrum Asymptotics, J. Phys. A: Math. Theor. **47**, 505204 (2014).

[30] C. Gao, J. Wang, and Z. Yu, Revealing the Origin of Super Efimov States in the Hyperspherical Formalism, Phys. Rev. A **92**, 020504 (2015).

[31] E. Tiesinga, B. J. Verhaar, and H. T. C. Stoof, Threshold and Resonance Phenomena in Ultracold Ground-State Collisions, Phys. Rev. A **47**, 4114 (1993).

[32] S. Inouye *et al.*, Observation of Feshbach Resonances in a Bose–Einstein Condensate, Nature **392**, 151 (1998).

[33] P. Courteille, R. S. Freeland, D. J. Heinzen, F. A. van Abeelen, and B. J. Verhaar, Observation of a Feshbach Resonance in Cold Atom Scattering, Phys. Rev. Lett. **81**, 69 (1998).

[34] C. Chin, R. Grimm, P. Julienne, and E. Tiesinga, Feshbach Resonances in Ultracold Gases, Rev. Mod. Phys. **82**, 1225 (2010).

[35] T. Kraemer *et al.*, Evidence for Efimov Quantum States in an Ultracold Gas of Caesium Atoms, Nature **440**, 315 (2006).

[36] M. Zaccanti *et al.*, Observation of an Efimov Spectrum in an Atomic System, Nat. Phys. **5**, 586 (2009).

[37] S. E. Pollack, D. Dries, and R. G. Hulet, Universality in Three- and Four-Body Bound States of Ultracold Atoms, Science **326**, 1683 (2009).

[38] F. Ferlaino *et al.*, Evidence for Universal Four-Body States Tied to an Efimov Trimer, Phys. Rev. Lett. **102**, 140401 (2009).

[39] P. Dyke, S. E. Pollack, and R. G. Hulet, Finite-Range Corrections near a Feshbach Resonance and Their Role in the Efimov Effect, Phys. Rev. A **88**, 023625 (2013).

[40] A. Zenesini *et al.*, Resonant Five-Body Recombination in an Ultracold Gas of Bosonic Atoms, New J. Phys. **15**, 043040 (2013).

[41] G. Barontini *et al.*, Observation of Heteronuclear Atomic Efimov Resonances, Phys. Rev. Lett. **103**, 043201 (2009).

[42] R. S. Bloom, M.-G. Hu, T. D. Cumby, and D. S. Jin, Tests of Universal Three-Body Physics in an Ultracold Bose-Fermi Mixture, Phys. Rev. Lett. **111**, 105301 (2013).

[43] S.-K. Tung, K. Jiménez-García, J. Johansen, C. V. Parker, and C. Chin, Geometric Scaling of Efimov States in a ^{6}Li–^{133}Cs Mixture, Phys. Rev. Lett. **113**, 240402 (2014).

[44] R. A. W. Maier, M. Eisele, E. Tiemann, and C. Zimmermann, Efimov Resonance and Three-Body Parameter in a Lithium-Rubidium Mixture, Phys. Rev. Lett. **115**, 043201 (2015).

[45] L. J. Wacker *et al.*, Universal Three-Body Physics in Ultracold KRb Mixtures, Phys. Rev. Lett. **117**, 163201 (2016).

[46] T. B. Ottenstein, T. Lompe, M. Kohnen, A. N. Wenz, and S. Jochim, Collisional Stability of a Three-Component Degenerate Fermi Gas, Phys. Rev. Lett. **101**, 203202 (2008).

[47] J. H. Huckans, J. R. Williams, E. L. Hazlett, R. W. Stites, and K. M. O'Hara, Three-Body Recombination in a Three-State Fermi Gas with Widely Tunable Interactions, Phys. Rev. Lett. **102**, 165302 (2009).

[48] A. N. Wenz *et al.*, Universal Trimer in a Three-Component Fermi Gas, Phys. Rev. A **80**, 040702 (2009).

[49] T.-L. Ho, Universal Thermodynamics of Degenerate Quantum Gases in the Unitarity Limit, Phys. Rev. Lett. **92**, 090402 (2004).

[50] G. F. Bertsch, MBX Challenge Competition.

[51] G. A. Baker, The Mbx Challenge Competition: A Neutron Matter Model, Int. J. Mod. Phys. B **15**, 1314 (2001).

[52] S. Tan, Energetics of a Strongly Correlated Fermi Gas, Ann. Phys. **323**, 2952 (2008).

[53] S. Tan, Large Momentum Part of a Strongly Correlated Fermi Gas, Ann. Phys. **323**, 2971 (2008).

[54] S. Tan, Generalized Virial Theorem and Pressure Relation for a Strongly Correlated Fermi Gas, Ann. Phys. **323**, 2987 (2008).

[55] E. Braaten and L. Platter, Exact Relations for a Strongly Interacting Fermi Gas from the Operator Product Expansion, Phys. Rev. Lett. **100**, 205301 (2008).

[56] F. Werner, L. Tarruell, and Y. Castin, Number of Closed-Channel Molecules in the BEC-BCS Crossover, Eur. Phys. J. B **68**, 401 (2009).

[57] S. Zhang and A. J. Leggett, Universal Properties of the Ultracold Fermi Gas, Phys. Rev. A **79**, 023601 (2009).

[58] R. Combescot, F. Alzetto, and X. Leyronas, Particle Distribution Tail and Related Energy Formula, Phys. Rev. A **79**, 053640 (2009).

[59] F. Werner and Y. Castin, General Relations for Quantum Gases in Two and Three Dimensions: Two-Component Fermions, Phys. Rev. A **86**, 013626 (2012).

[60] E. Braaten, Universal Relations for Fermions with Large Scattering Length, in *The BCS-BEC Crossover and the Unitary Fermi Gas*, edited by W. Zwerger, , Lecture Notes in Physics No. 836, pp. 193–231, Springer-Verlag, Heidelberg, 2012.

[61] H. Bethe and R. Peierls, Quantum Theory of the Diplon, Proc. R. Soc. London, Ser. A **148**, 146 (1935).

[62] K. Huang and C. N. Yang, Quantum-Mechanical Many-Body Problem with Hard-Sphere Interaction, Phys. Rev. **105**, 767 (1957).

[63] T. D. Lee, K. Huang, and C. N. Yang, Eigenvalues and Eigenfunctions of a Bose System of Hard Spheres and Its Low-Temperature Properties, Phys. Rev. **106**, 1135 (1957).

[64] P. Pieri, A. Perali, and G. C. Strinati, Enhanced Paraconductivity-like Fluctuations in the Radiofrequency Spectra of Ultracold Fermi Atoms, Nat. Phys. **5**, 736 (2009).

[65] W. Schneider, V. B. Shenoy, and M. Randeria, Theory of Radio Frequency Spectroscopy of Polarized Fermi Gases, arXiv:0903.3006 [cond-mat] (2009).

[66] W. Schneider and M. Randeria, Universal Short-Distance Structure of the Single-Particle Spectral Function of Dilute Fermi Gases, Phys. Rev. A **81**, 021601 (2010).

[67] E. Braaten, D. Kang, and L. Platter, Short-Time Operator Product Expansion for Rf Spectroscopy of a Strongly Interacting Fermi Gas, Phys. Rev. Lett. **104**, 223004 (2010).

[68] D. T. Son and E. G. Thompson, Short-Distance and Short-Time Structure of a Unitary Fermi Gas, Phys. Rev. A **81**, 063634 (2010).

[69] E. Taylor and M. Randeria, Viscosity of Strongly Interacting Quantum Fluids: Spectral Functions and Sum Rules, Phys. Rev. A **81**, 053610 (2010).

[70] J. Hofmann, Current Response, Structure Factor and Hydrodynamic Quantities of a Two- and Three-Dimensional Fermi Gas from the Operator-Product Expansion, Phys. Rev. A **84**, 043603 (2011).

[71] W. D. Goldberger and I. Z. Rothstein, Structure-Function Sum Rules for Systems with Large Scattering Lengths, Phys. Rev. A **85**, 013613 (2012).

[72] T. Enss, R. Haussmann, and W. Zwerger, Viscosity and Scale Invariance in the Unitary Fermi Gas, Ann. Phys. **326**, 770 (2011).

[73] F. Werner and Y. Castin, General Relations for Quantum Gases in Two and Three Dimensions. II. Bosons and Mixtures, Phys. Rev. A **86**, 053633 (2012).

[74] E. Braaten, D. Kang, and L. Platter, Universal Relations for Identical Bosons from Three-Body Physics, Phys. Rev. Lett. **106**, 153005 (2011).

[75] Y. Nishida, Probing Strongly Interacting Atomic Gases with Energetic Atoms, Phys. Rev. A **85**, 053643 (2012).

[76] S. Tan, S-Wave Contact Interaction Problem: A Simple Description, arXiv:cond-mat/0505615 (2005).

[77] M. Barth and W. Zwerger, Tan Relations in One Dimension, Ann. Phys. **326**, 2544 (2011).

[78] M. Valiente, N. T. Zinner, and K. Mølmer, Universal Relations for the Two-Dimensional Spin-1/2 Fermi Gas with Contact Interactions, Phys. Rev. A **84**, 063626 (2011).

[79] S. M. Yoshida and M. Ueda, Universal High-Momentum Asymptote and Thermodynamic Relations in a Spinless Fermi Gas with a Resonant p-Wave Interaction, Phys. Rev. Lett. **115**, 135303 (2015).

[80] Z. Yu, J. H. Thywissen, and S. Zhang, Universal Relations for a Fermi Gas Close to a p-Wave Interaction Resonance, Phys. Rev. Lett. **115**, 135304 (2015).

[81] S.-G. Peng, X.-J. Liu, and H. Hu, Large-Momentum Distribution of a Polarized Fermi Gas and p-Wave Contacts, Phys. Rev. A **94**, 063651 (2016).

[82] M. He, S. Zhang, H. M. Chan, and Q. Zhou, Concept of a Contact Spectrum and Its Applications in Atomic Quantum Hall States, Phys. Rev. Lett. **116**, 045301 (2016).

[83] P. Zhang, S. Zhang, and Z. Yu, Effective Theory and Universal Relations for Fermi Gases near a d-Wave-Interaction Resonance, Phys. Rev. A **95**, 043609 (2017).

[84] G. A. Baker, Neutron Matter Model, Phys. Rev. C **60**, 054311 (1999).

[85] S. Nascimbène, N. Navon, K. J. Jiang, F. Chevy, and C. Salomon, Exploring the Thermodynamics of a Universal Fermi Gas, Nature **463**, 1057 (2010).

[86] M. Horikoshi, S. Nakajima, M. Ueda, and T. Mukaiyama, Measurement of Universal Thermodynamic Functions for a Unitary Fermi Gas, Science **327**, 442 (2010).

[87] M. J. H. Ku, A. T. Sommer, L. W. Cheuk, and M. W. Zwierlein, Revealing the Superfluid Lambda Transition in the Universal Thermodynamics of a Unitary Fermi Gas, Science **335**, 563 (2012).

[88] C. Cao *et al.*, Universal Quantum Viscosity in a Unitary Fermi Gas, Science **331**, 58 (2011).

[89] Y. A. Liao *et al.*, Metastability in Spin-Polarized Fermi Gases, Phys. Rev. Lett. **107**, 145305 (2011).

[90] A. Sommer, M. Ku, G. Roati, and M. W. Zwierlein, Universal Spin Transport in a Strongly Interacting Fermi Gas, Nature **472**, 201 (2011).

[91] M. Koschorreck, D. Pertot, E. Vogt, and M. Köhl, Universal Spin Dynamics in Two-Dimensional Fermi Gases, Nat. Phys. **9**, 405 (2013).

[92] A. B. Bardon *et al.*, Transverse Demagnetization Dynamics of a Unitary Fermi Gas, Science **344**, 722 (2014).

[93] J. T. Stewart, J. P. Gaebler, T. E. Drake, and D. S. Jin, Verification of Universal Relations in a Strongly Interacting Fermi Gas, Phys. Rev. Lett. **104**, 235301 (2010).

[94] E. D. Kuhnle *et al.*, Universal Behavior of Pair Correlations in a Strongly Interacting Fermi Gas, Phys. Rev. Lett. **105**, 070402 (2010).

[95] E. D. Kuhnle *et al.*, Temperature Dependence of the Universal Contact Parameter in a Unitary Fermi Gas, Phys. Rev. Lett. **106**, 170402 (2011).

[96] Y. Sagi, T. E. Drake, R. Paudel, and D. S. Jin, Measurement of the Homogeneous Contact of a Unitary Fermi Gas, Phys. Rev. Lett. **109**, 220402 (2012).

[97] S. Hoinka *et al.*, Precise Determination of the Structure Factor and Contact in a Unitary Fermi Gas, Phys. Rev. Lett. **110**, 055305 (2013).

[98] D. B. Kaplan, More Effective Field Theory for Non-Relativistic Scattering, Nucl. Phys. B **494**, 471 (1997).

[99] C. A. Bertulani, H. W. Hammer, and U. van Kolck, Effective Field Theory for Halo Nuclei: Shallow p-Wave States, Nucl. Phys. A **712**, 37 (2002).

[100] P. F. Bedaque, H. W. Hammer, and U. van Kolck, Narrow Resonances in Effective Field Theory, Phys. Lett. B **569**, 159 (2003).

[101] C. Ticknor, C. A. Regal, D. S. Jin, and J. L. Bohn, Multiplet Structure of Feshbach Resonances in Nonzero Partial Waves, Phys. Rev. A **69**, 042712 (2004).

[102] Y. Cui *et al.*, Observation of Broad d-Wave Feshbach Resonances with a Triplet Structure, Phys. Rev. Lett. **119**, 203402 (2017).

[103] V. Gurarie, L. Radzihovsky, and A. V. Andreev, Quantum Phase Transitions across a p-Wave Feshbach Resonance, Phys. Rev. Lett. **94**, 230403 (2005).

[104] C.-H. Cheng and S.-K. Yip, Anisotropic Fermi Superfluid via p-Wave Feshbach Resonance, Phys. Rev. Lett. **95**, 070404 (2005).

[105] V. Gurarie and L. Radzihovsky, Resonantly Paired Fermionic Superfluids, Ann. Phys. **322**, 2 (2007).

[106] M.-G. Hu *et al.*, Bose Polarons in the Strongly Interacting Regime, Phys. Rev. Lett. **117**, 055301 (2016).

[107] N. B. Jørgensen *et al.*, Observation of Attractive and Repulsive Polarons in a Bose-Einstein Condensate, Phys. Rev. Lett. **117**, 055302 (2016).

[108] J. Levinsen, M. M. Parish, and G. M. Bruun, Impurity in a Bose-Einstein Condensate and the Efimov Effect, Phys. Rev. Lett. **115**, 125302 (2015).

[109] C. H. Schmickler, H.-W. Hammer, and E. Hiyama, Tetramer Bound States in Heteronuclear Systems, Phys. Rev. A **95**, 052710 (2017).

[110] L. A. P. Ardila and S. Giorgini, Impurity in a Bose-Einstein Condensate: Study of the Attractive and Repulsive Branch Using Quantum Monte Carlo Methods, Phys. Rev. A **92**, 033612 (2015).

[111] F. M. Cucchietti and E. Timmermans, Strong-Coupling Polarons in Dilute Gas Bose-Einstein Condensates, Phys. Rev. Lett. **96**, 210401 (2006).

[112] J. Tempere *et al.*, Feynman Path-Integral Treatment of the BEC-Impurity Polaron, Phys. Rev. B **80**, 184504 (2009).

[113] S. P. Rath and R. Schmidt, Field-Theoretical Study of the Bose Polaron, Phys. Rev. A **88**, 053632 (2013).

[114] W. Li and S. Das Sarma, Variational Study of Polarons in Bose-Einstein Condensates, Phys. Rev. A **90**, 013618 (2014).

[115] A. Shashi, F. Grusdt, D. A. Abanin, and E. Demler, Radio-Frequency Spectroscopy of Polarons in Ultracold Bose Gases, Phys. Rev. A **89**, 053617 (2014).

[116] R. S. Christensen, J. Levinsen, and G. M. Bruun, Quasiparticle Properties of a Mobile Impurity in a Bose-Einstein Condensate, Phys. Rev. Lett. **115**, 160401 (2015).

[117] F. Grusdt, Y. E. Shchadilova, A. N. Rubtsov, and E. Demler, Renormalization Group Approach to the Fröhlich Polaron Model: Application to Impurity-BEC Problem, Scientific Reports **5**, srep12124 (2015).

[118] F. Grusdt and E. Demler, New Theoretical Approaches to Bose Polarons, arXiv:1510.04934 [cond-mat] (2015).

[119] L. A. P. Ardila and S. Giorgini, Bose Polaron Problem: Effect of Mass Imbalance on Binding Energy, Phys. Rev. A **94**, 063640 (2016).

[120] Y. E. Shchadilova, R. Schmidt, F. Grusdt, and E. Demler, Quantum Dynamics of Ultracold Bose Polarons, Phys. Rev. Lett. **117**, 113002 (2016).

[121] F. Grusdt, R. Schmidt, Y. E. Shchadilova, and E. Demler, Strong-Coupling Bose Polarons in a Bose-Einstein Condensate, Phys. Rev. A **96**, 013607 (2017).

[122] M. Sun, H. Zhai, and X. Cui, Visualizing the Efimov Correlation in Bose Polarons, Phys. Rev. Lett. **119**, 013401 (2017).

[123] A. Lampo, S. H. Lim, M. Á. García-March, and M. Lewenstein, Bose Polaron as an Instance of Quantum Brownian Motion, Quantum **1**, 30 (2017).

[124] N.-E. Guenther, P. Massignan, M. Lewenstein, and G. M. Bruun, Bose Polarons at Finite Temperature and Strong Coupling, arXiv:1708.08861 [cond-mat] (2017).

[125] J. Levinsen, M. M. Parish, R. S. Christensen, J. J. Arlt, and G. M. Bruun, Finite-Temperature Behavior of the Bose Polaron, arXiv:1708.09172 [cond-mat] (2017).

[126] F. Chevy, Universal Phase Diagram of a Strongly Interacting Fermi Gas with Unbalanced Spin Populations, Phys. Rev. A **74**, 063628 (2006).

[127] C. Trefzger and Y. Castin, Impurity in a Fermi Sea on a Narrow Feshbach Resonance: A Variational Study of the Polaronic and Dimeronic Branches, Phys. Rev. A **85**, 053612 (2012).

[128] W. Yi and X. Cui, Polarons in Ultracold Fermi Superfluids, Phys. Rev. A **92**, 013620 (2015).

[129] I. Tamm, Relativistic Interaction of Elementary Particles, J. Phys. (USSR) **9**, 449 (1945).

[130] S. M. Dancoff, Non-Adiabatic Meson Theory of Nuclear Forces, Phys. Rev. **78**, 382 (1950).

[131] U. Fano, Sullo spettro di assorbimento dei gas nobili presso il limite dello spettro d'arco, Nuovo Cim **12**, 154 (1935).

[132] H. Feshbach, Unified Theory of Nuclear Reactions, Ann. Phys. **5**, 357 (1958).

[133] U. Fano, Effects of Configuration Interaction on Intensities and Phase Shifts, Phys. Rev. **124**, 1866 (1961).

[134] H. Feshbach, A Unified Theory of Nuclear Reactions. II, Ann. Phys. **19**, 287 (1962).

[135] E. Timmermans, P. Tommasini, M. Hussein, and A. Kerman, Feshbach Resonances in Atomic Bose–Einstein Condensates, Phys. Rep. **315**, 199 (1999).

[136] R. A. Duine and H. T. C. Stoof, Microscopic Many-Body Theory of Atomic Bose Gases near a Feshbach Resonance, J. Opt. B: Quantum Semiclass. Opt. **5**, S212 (2003).

[137] E. Timmermans, K. Furuya, P. W. Milonni, and A. K. Kerman, Prospect of Creating a Composite Fermi–Bose Superfluid, Phys. Lett. A **285**, 228 (2001).

[138] M. Holland, S. J. J. M. F. Kokkelmans, M. L. Chiofalo, and R. Walser, Resonance Superfluidity in a Quantum Degenerate Fermi Gas, Phys. Rev. Lett. **87**, 120406 (2001).

[139] S. J. J. M. F. Kokkelmans, J. N. Milstein, M. L. Chiofalo, R. Walser, and M. J. Holland, Resonance Superfluidity: Renormalization of Resonance Scattering Theory, Phys. Rev. A **65**, 053617 (2002).

[140] Y. Ohashi and A. Griffin, BCS-BEC Crossover in a Gas of Fermi Atoms with a Feshbach Resonance, Phys. Rev. Lett. **89**, 130402 (2002).

[141] Y. Ohashi and A. Griffin, Superfluid Transition Temperature in a Trapped Gas of Fermi Atoms with a Feshbach Resonance, Phys. Rev. A **67**, 033603 (2003).

[142] A. O. Gogolin, C. Mora, and R. Egger, Analytical Solution of the Bosonic Three-Body Problem, Phys. Rev. Lett. **100**, 140404 (2008).

[143] M. Jona-Lasinio and L. Pricoupenko, Three Resonant Ultracold Bosons: Off-Resonance Effects, Phys. Rev. Lett. **104**, 023201 (2010).

[144] J. Levinsen and D. S. Petrov, Atom-Dimer and Dimer-Dimer Scattering in Fermionic Mixtures near a Narrow Feshbach Resonance, Eur. Phys. J. D **65**, 67 (2011).

[145] C. J. Pethick and H. Smith, *Bose-Einstein Condensation in Dilute Gases*, 2nd ed. (Cambridge University Press, New York, 2008).

[146] L. Pricoupenko, Modeling Interactions for Resonant p-Wave Scattering, Phys. Rev. Lett. **96**, 050401 (2006).

[147] L. Pricoupenko, Pseudopotential in Resonant Regimes, Phys. Rev. A **73**, 012701 (2006).

[148] H. W. Hammer and D. Lee, Causality and Universality in Low-Energy Quantum Scattering, Phys. Lett. B **681**, 500 (2009).

[149] H. W. Hammer and D. Lee, Causality and the Effective Range Expansion, Ann. Phys. **325**, 2212 (2010).

[150] Y. Nishida, Impossibility of the Efimov Effect for p-Wave Interactions, Phys. Rev. A **86**, 012710 (2012).

[151] C. Luciuk *et al.*, Evidence for Universal Relations Describing a Gas with p-Wave Interactions, Nat. Phys. **12**, 599 (2016).

[152] Y. Ohashi, BCS-BEC Crossover in a Gas of Fermi Atoms with a p-Wave Feshbach Resonance, Phys. Rev. Lett. **94**, 050403 (2005).

[153] L. H. Thomas, The Interaction Between a Neutron and a Proton and the Structure of H^3, Phys. Rev. **47**, 903 (1935).

[154] P. F. Bedaque, H. W. Hammer, and U. van Kolck, The Three-Boson System with Short-Range Interactions, Nucl. Phys. A **646**, 444 (1999).

[155] M. R. Hadizadeh, M. T. Yamashita, L. Tomio, A. Delfino, and T. Frederico, Scaling Properties of Universal Tetramers, Phys. Rev. Lett. **107**, 135304 (2011).

[156] A. Deltuva, Shallow Efimov Tetramer as Inelastic Virtual State and Resonant Enhancement of the Atom-Trimer Relaxation, EPL **95**, 43002 (2011).

[157] K. M. Watson, J. Nuttall, and J. S. R. Chisholm, *Topics in Several Particle Dynamics* (Holden-Day, San Francisco, 1967).

[158] A. L. Fetter, J. D. Walecka, and Physics, *Quantum Theory of Many-Particle Systems* (Dover Publications, Mineola, N.Y, 2003).

[159] P. W. Anderson, Localized Magnetic States in Metals, Phys. Rev. **124**, 41 (1961).

[160] H.-J. Lee and R. Bulla, Quantum Phase Transitions in the Bosonic Single-Impurity Anderson Model, Eur. Phys. J. B **56**, 199 (2007).

[161] H.-J. Lee, K. Byczuk, and R. Bulla, Numerical Renormalization Group for the Bosonic Single-Impurity Anderson Model: Dynamics, Phys. Rev. B **82**, 054516 (2010).

[162] A. J. Leggett *et al.*, Dynamics of the Dissipative Two-State System, Rev. Mod. Phys. **59**, 1 (1987).

[163] U. Weiss, *Quantum Dissipative Systems*, 4th ed. (World Scientific Publishing, New Jersey, 2012).

[164] L. D. Landau, Über Die Bewegung Der Elektronen in Kristallgitter, Phys. Z. Sowjet. **3**, 644 (1933).

[165] S. Pekar, Local Quantum States of Electrons in an Ideal Ion Crystal, Zh. Eksp. Teor. Fiz. **16**, 341 (1946).

[166] L. Landau and S. Pekar, Effective Mass of a Polaron, Zh. Eksp. Teor. Fiz. **18**, 419 (1948).

[167] J. T. Devreese, Fr\"ohlich Polarons. Lecture Course Including Detailed Theoretical Derivations, arXiv:1012.4576 [cond-mat] (2010).

[168] H. Fröhlich, H. Pelzer, and S. Zienau, XX. Properties of Slow Electrons in Polar Materials, Phil. Mag. **41**, 221 (1950).

[169] H. Fröhlich, Electrons in Lattice Fields, Adv. Phys. **3**, 325 (1954).

[170] P. Massignan, Polarons and Dressed Molecules near Narrow Feshbach Resonances, Europhys. Lett. **98**, 10012 (2012).

[171] P. Törmä and K. Sengstock, *Quantum Gas Experiments: Exploring Many-Body States* (Imperial College Press, London, 2015).

[172] E. Braaten, D. Kang, and L. Platter, Universal Relations for a Strongly Interacting Fermi Gas near a Feshbach Resonance, Phys. Rev. A **78**, 053606 (2008).

[173] X. Cui, Universal One-Dimensional Atomic Gases near Odd-Wave Resonance, Phys. Rev. A **94**, 043636 (2016).

[174] Y.-C. Zhang and S. Zhang, Strongly Interacting p-Wave Fermi Gas in Two Dimensions: Universal Relations and Breathing Mode, Phys. Rev. A **95**, 023603 (2017).

[175] P. Zhang and Z. Yu, Signature of the Universal Super Efimov Effect: Three-Body Contact in Two-Dimensional Fermi Gases, Phys. Rev. A **95**, 033611 (2017).

[176] P. Naidon, Two Impurities in a Bose-Einstein Condensate: From Yukawa to Efimov Attracted Polarons, arXiv:1607.04507 [cond-mat] (2016).